Thesis for the Degree of Doctor of Philosophy

COERCIVITY STUDY OF THERMALLY PROCESSED Nd-Fe-B-TYPE HDDR-TREATED MATERIAL

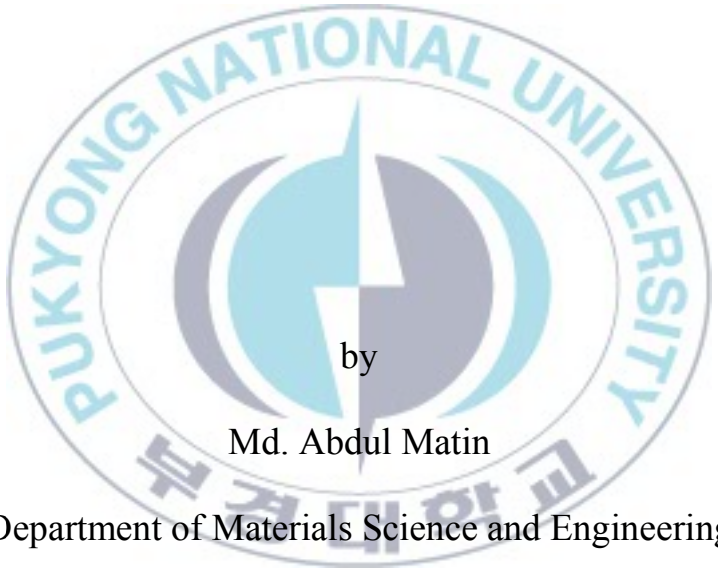

by

Md. Abdul Matin

Department of Materials Science and Engineering

The Graduate School

Pukyong National University

February 2014

COERCIVITY STUDY OF THERMALLY PROCESSED Nd-Fe-B-TYPE HDDR-TREATED MATERIAL

열적으로 가공한 Nd-Fe-B 계 HDDR 처리 재료의 보자력에 관한 연구

Advisor: Professor Hae-Woong Kwon

by

Md. Abdul Matin

A thesis submitted in partial fulfillment of the requirements for the degree of

Doctor of Philosophy

in the Department of Materials Science and Engineering, The Graduate School, Pukyong National University

February 2014

COERCIVITY STUDY OF THERMALLY PROCESSED Nd-Fe-B-TYPE HDDR-TREATED MATERIAL

A dissertation

by

Md. Abdul Matin

Approved by:

(Chairman) Chan Park

(Member) Hae-Woong Kwon

(Member) Hae Yong Jeong

(Member) Byung-Hyun Ahn

(Member) Ji-Hun Yu

February 2014

Acknowledgement

I would like to express my deepest gratitude to ALMIGHTY ALLAH who has generously given me mental, physical ability to carry on my research activities in an entirely new atmosphere.

I also express my earnest gratefulness to my honorable supervisor **Professor Hae-Woong Kwon** for his hospitality and all out support on academic and financial perspectives. His valuable discussion and instructions help me much throughout my research for pursuing doctoral degree. My sincere thanks to all the Professors of the Department of Materials Science and Engineering, Pukyong National University, Busan, South Korea who have enriched my academic knowledge as well as way of life. Especially I am very grateful to Kim Kyong Min who has helped me much through the most difficult and challenging times on my research. I would like to thanks my other lab mates Kim Jha Young, Kim Seong Yong, Jung Hee-do, Park Seul-gi and Kim Shinwoo for their co-operation.

I state my appreciation to the authority of Pukyong National University, Busan, South Korea for considering me to be enrolled as a Ph. D student. I am also highly grateful to the Ministry of Knowledge Economy, Republic of Korea and Korea Institute of Materials Science (KIMS) for their grant throughout my study here. I am indebted to the authorities of University of Rajshahi, Bangladesh who have paved the way for my higher study granting study leave.

Sincere thanks to my family members wife Sufia, son Ayon, daughter Arin who have faced lot of challenges maintaining their daily life in absence of me throughout three-years of my Ph. D tenure. I also express my deepest gratitude to my elderly parents and brother in law engineer Sharfuddin for their encouragement and mental support. I specially acknowledge the role of Dr. Masud and Dr Dipty for introducing me to the Prof Kwon. I also thanks to the PKNU Bangladeshi students for their all out support who were or are on studying here namely Dr. Rafiq, Dr. Tanvir, Dr. Tofazzal, Dr Tareq, Dr. Nurul, Mr. Mustafiz, Mr Mizan, Mr. Eng. Mizan, Mr. Asad, Mr. Rafiquzzaman, Tanbir, Eusuf, Mrs Eshita and Bipul.

Md Abdul Matin
February 2014

COERCIVITY STUDY OF THERMALLY PROCESSED
Nd-Fe-B-TYPE HDDR-TREATED MATERIAL

Md. Abdul Matin

Department of Materials Science and Engineering, The Graduate School,
Pukyong National University

Abstract

This project focused on the coercivity behavior of thermally processed $Nd_{12.5}Fe_{80.6}B_{6.4}Ga_{0.3}Nb_{0.2}$ HDDR-treated material. The research was carried out emphasizing on the following three categories: the residual hydrogen in the Nd-Fe-B-type HDDR-treated material, the effect of residual hydrogen on the coercivity of heated HDDR-treated material, and the coercivity of hot-pressed compacts of HDDR-treated material. The HDDR-treated material contained significant amount of residual hydrogen (1500 ppm). The presence of hydrogen in the HDDR-treated material was examined by hydrogen analysis and desorption behavior on heating. The effect of residual hydrogen on coercivity of the heated Nd-Fe-B-type HDDR-treated material was investigated. The material was heated in Ar atmosphere or in vacuum with distinctively different evacuation speed. The coercivity of the HDDR-treated material was radically reduced around 650 °C or above when the material was heated in Ar or in vacuum with slow pumping speed. The coercivity reduction was much more profound for the material heated in Ar atmosphere or in vacuum with slow pumping speed than in vacuum with high pumping speed heating chamber. This fact can be explained that the residual hydrogen was desorbed more effectively in the course of heating in vacuum with high pumping speed than in Ar or vacuum with slow pumping speed. The coercivity reduction in the HDDR-treated material on heating is believed to be attributed to the disproportionation of $Nd_2Fe_{14}BH_x$ hydride formed by the residual hydrogen in it. The residual hydrogen is considered as a technical barrier for the thermal process of HDDR-treated material without losing magnetic performance. It was witnessed that coercivity loss in the HDDR material was inconsiderable despite heating at elevated temperature if the residual hydrogen could be desorbed effectively on heating. The HDDR-treated material was compacted by hot-pressing in the closed and open-type die in terms of different evacuation system. The coercivity loss in the compact prepared in the closed-type die above

650 °C was more radical than in the compact prepared in the open die. Residual hydrogen in the HDDR-treated material was desorbed more effectively in the open die compared to the closed-type die on heating for hot-pressing. The coercivity retaining rate was 80 % (10.8 out of 13.5 kOe) in the full dense compact prepared in the open die. The rate was only 28 % (3.8 out of 13.5 kOe) in the full dense compact prepared in the closed die. The present findings suggest that the coercivity of the HDDR-treated material is affected radically by the residual hydrogen if it is not desorbed effectively on thermal processing.

열적으로 가공한 Nd-Fe-B 계 HDDR 처리 재료의 보자력에 관한 연구

Md. Abdul Matin

부경대학교, 대학원, 재료공학과

초록

본 연구는 조성이 $Nd_{12.5}Fe_{80.6}B_{6.4}Ga_{0.3}Nb_{0.2}$ 인 HDDR 처리한 재료를 가지고 열적처리를 했을때 보자력의 거동에 대해 초점을 맞추었다. 본 연구는 세가지 내용에 대해서 강조한다: HDDR 처리한 재료의 잔류 수소, 가열한 HDDR 처리 재료 보자력에 대한 잔류수소의 효과, 그리고 HDDR 처리재료를 Hot-pressed compact 를 만들었을 때의 보자력. HDDR 처리한 재료는 상당량의 잔류수소가 포함되어 있다 (1500ppm). HDDR 처리한 재료내의 잔류수소존재는 수소분석 및 가열 시 탈착의 거동에 의하여 조사하였다. 가열한 Nd-Fe-B-type HDDR 처리된 재료의 보자력에 대한 잔류수소의 효과를 조사하였다. HDDR 처리한 재료는 Ar 분위기나 또는 진공 분위기에서 가열을 하였다. HDDR 처리한 재료의 보자력은 느린 pumping 속도로 Ar분위기나 진공분위기에서 가열을 했을 때650℃ 근방이나 그보다 높은 온도에서 급격히 감소한다. 이 사실은 잔류수소가 가열 중 진공상태 또는 Ar 상태에서의 느린 pumping 속도보다 진공 상태에서의 높은 pumping 속도가 더욱 더 효과적으로 탈착하는 것을 설명 할 수 있다. 가열하에 있는 HDDR 재료의 보자력 감소는 그 안에 있는 잔류수소에 의해서 형성된 $Nd_2Fe_{14}BH_x$ 의 분해결과라고 생각한다. 잔류수소는 자기적 성능을 잃지 않는 HDDR 처리 분말의 열적공정에 대한 기술적인 장애물로 생각한

다. 가열 중 잔류수소가 효과적으로 탈착이 된다면, HDDR 재료에서의 보자력 손실은 온도가 증가함에도 불구하고 아주 미미할 것 이라는것이 설명된다. HDDR 처리된 재료는closed die 와 open die 라는 배출방식이 다른 두가지 방식에서 Hot-pressing 을 하여 compact 를 만들었다. 650 ℃ 이상의 온도에서 closed die 방법을 이용하여 compact 를 만들 었을 때의 보자력 손실은 open die 방법보다 더욱 더 손실이 크다. HDDR 처리한 재료내의 잔류수소는 Hot pressing 을 할 때 open die 방법이 closed die 방법보다 효과적으로 탈착된다. Open die 에서 100% 밀도의 compact 를 만들 었을 때 보자력 유지비율은 80 % (13.5 kOe 중 10.8 kOe) 이다. Closed die 에서 100 % 밀도의 compact 를 만들 었을 때 보자력 유지비율은 28 % (13.5 kOe 중3.8 kOe) 이다. 본 연구 결과는 이 열처리에 효율적으로 탈착되지 않는 경우 HDDR 처리된 재료의 보자력은 잔여수소에 의해 영향을 받는 것을 시사한다.

Content

CHAPTER ONE GENERAL INTRODUCTION PAGE No.

1.1 Development of Nd-Fe-B-type Permanent Magnet…..... 1
1.2 Applications and Prospects of Permanent Magnet.....……. 3
1.3 Processing Routes of Nd-Fe-B-type Permanent Magnet..... 5
1.4 Excellence of HDDR Process ……..…….....……. 8
1.5 Objectives of this Thesis……..…….....…… 9
1.6 Scopes of the Thesis…….....……..... 11
1.7 References…….....……..... 12

CHAPTER TWO MAGNETISM AND MAGNETIC MATERIALS

2.1 Magnetism.....……..... 15
2.2 Classification of Magnetism and Magnetic Materials 15
2.2.1 Diamagnetism…….....…….. 16
2.2.2 Paramagnetism…….....……..... 17
2.2.3 Ferromagnetism…….....……..... 18
2.2.4 Antiferromagnetism…….....…….. 19
2.2.5 Ferrimagnetism…….....…….. 20
2.3 Electronic Configuration of Rare Earth-Transition Metal Compounds
2.3.1 In the Rare-Earth (R) Series…….....……... 21
2.3.2 In the Transition-Metal (T) Elements: Fe, Co and Ni..... 22
2.3.3 Rare Earth-Transition Metal Compounds..... 23

2.4 Some Properties of Ferromagnetic Materials
2.4.1 Curie Temperature: Tc..... 24
2.4.2 Magnetic Anisotropy..... 25
2.4.3 Magnetic Domain..... 26
2.4.4 Domain Wall Process..... 28
2.4.5 Origin of Coercivity..... 29
2.4.6 Hysteresis Loop and Magnetization Process..... 32
2.4.7 Maximum Energy Product 35
2.5 Units of Magnetism..... 36
2.6 References..... 37

CHAPTER THREE APPARATUS AND EXPERIMENTAL PROCEDURE

3.1 Experimental Procedure..... 38
3.2 HDDR Process..... 39
3.3 Consolidation of HDDR-treated Material..... 41
3.4 Heat Treatment of HDDR-treated Material..... 44
3.5 Magnetic Characterization..... 46
3.6 Microstructure Analysis
3.6.1 Scanning Electron Microscopy (SEM)..... 49
3.6.2 Transmission Electron Microscopy (TEM) 50
3.6.3 X-ray Diffraction (XRD)..... 53
3.6.4 Crystal Lattice Parameters by XRD..... 56
3.7 Differential Thermal Analysis (DTA)..... 57
3.8 Thermopiezic Analyser (TPA)..... 59
3.9 References..... 61

CHAPTER FOUR A STUDY OF RESIDUAL HYDROGEN IN Nd-Fe-B-TYPE HDDR-TREATED MATERIAL

Abstract……..……..... 62
4.1 Introduction.....……..... 63
4.2 Experimental Work…….....……..... 64
4.3 Results and Discussion….....……..... 65
4.4 Conclusion…….....……..... 71
4.5 References…….....……..... 71

CHAPTER FIVE EFFECT OF RESIDUAL HYDROGEN ON COERCIVITY OF HEATED Nd-Fe-B-TYPE HDDR-TREATED MATERIAL

Abstract……..……..... 73
5.1 Introduction…….....……..... 74
5.2 Experimental Work…….....……..... 75
5.3 Results and Discussion.....……..... 75
5.4 Conclusion…….....……..... 85
5.5 References….....……..……..... 86

CHAPTER SIX COERCIVITY OF HOT-PRESSED COMPACTS OF Nd-Fe-B-TYPE HDDR-TREATED MATERIAL

Abstract ……..….....……..……..... 88

6.1 Introduction…….....…….. 89
6.2 Experimental Work…….....…….. 90
6.3 Results and Discussion.....…… 91
6.4 Conclusion…….....…… 102
6.5 References.....…….. 103

CHAPTER SEVEN

SUMMERY…..…….. 105

APPENDIX: Publications……... 109

Chapter One

GENERAL INTRODUCTION

1.1 Development of Nd-Fe-B-Type Permanent Magnet

Despite being used of magnets for more than one thousand years, a boom only occurred in the mid-1960s with the development of rare earth permanent magnets based on inter-metallic compounds of rare earths and the transition metals Fe or Co [1]. The auspicious combination of properties of the rare earths sub-lattice (4f) and the transition metals sub-lattice (3d) led to the spectacular development in the energy density, or also energy product, $(BH)_{max}$ of hard magnetic materials [2, 3]. By the mid 1960's, $LnCo_5$ compounds (Ln being any lanthanide) had been recognized as excellent candidates for permanent magnet materials, due to their high magnetocrystalline anisotropy, moderate saturation magnetization and electronic configuration. The first $SmCo_5$ magnets appeared in the late 1960's and early 1970's, due to the research and development efforts of several organizations, most notably: General Electric, Raytheon, Bell Telephone Laboratories, Wright Patterson Air Force Base, N. V. Philips and Brown Boveri. As soon as $SmCo_5$ became a commercially viable permanent magnet and research began in two directions. One direction was to replace or reduce the amount of samarium in the alloy, by substituting one or more of the more abundant and less expensive lanthanides: Ce, La, Nd, Pr and MM, where MM is mischmetal. The other direction was to replace the cobalt with iron, since iron is less expensive and has a slightly larger magnetic moment per atom than cobalt. In both cases, the goal was to reduce the cost of the

magnet, by reducing the raw material cost, without adversely affecting the magnetic properties.

Four distinct alloys have evolved from this research. The first material is $MMCo_5$. Mischmetal is far less expensive than samarium. However, the magnetic properties of $MMCo_5$ magnets are drastically poorer than $SmCo_5$ magnets, to the point that the tradeoff of magnetic properties versus alloy cost is unfavorable for $MMCo_5$. Similar behavior was also observed for $CeCo_5$, $LaCo_5$ and $NdCo_5$ [4-7]. The main fault is that the anisotropy is much lower for these compounds, making difficult to obtain acceptable coercivity (iHc) levels [8].

The second material is $Sm_xPr(1-x)Co_5$. Praseodymium is more abundant, less expensive and has a slightly larger magnetic moment than samarium. A partial substitution of Pr for Sm actually improves Br and $(BH)_{max}$. However, as the Pr/Sm ratio increases above 1, the stability of the alloy above room temperature is reduced and it is difficult to keep iHc as high as it is in $SmCo_5$. Therefore, most commercial materials have a Pr/Sm under 0.5, for a good combination of magnetic properties and raw material cost.

The third material is the Sm_2(Co, Fe, Cu, Zr or Hf)17 alloy system, here after referred to a 2-17 magnets. This is a metallurgically complicated alloy system, with high iHc based on precipitation hardening. In these alloys, both the samarium and the cobalt levels are reduced, while the magnetic properties are generally superior to $SmCo_5$. The major drawback to 2-17 magnets is their complicated processing; the heat treatments are much longer and more complicated than the heat treatment of $SmCo_5$. The limited availability of 2-17 magnets stem from these complications [9].

The fourth material is $Nd_2Fe_{14}B$, which achieves the original goals of replacing Sm and Co in $SmCo_5$ magnets. The magnetic properties of the binary lanthanide-iron compounds, including Nd-Fe, were examined at about the same time as the lanthanide-cobalt systems, in the 1960's and early 1970's. However, all the binary lanthanide-iron alloys have at least one of the following problems, making them unsuitable as permanent magnets. The problems are:

(i) A Curie temperature near or below room temperature,

(ii) Unfavorable anisotropy, usually an easy cone or an easy plane, or

(iii) Antiferromagnetic coupling between the lanthanide and the iron magnetic moments, resulting in low saturation magnetization.

The critical addition of the metalloid element boron to the Nd-Fe alloy, results in a slightly expanded crystal structure, overcoming the above mentioned drawbacks of the lanthanide-iron alloys. At almost the same time in 1983, several groups including the Sumitomo Special Metal Company in Japan reported independently, excellent permanent magnet properties based on the Nd-Fe-B alloy system [10-14]. The Sumitomo Special Metal Company marked “Neomax” as trade name of the Nd-Fe-B based permanent magnet. Commercial production of these materials started almost immediately thereafter. These magnets were continuously improved and instituted a new era in permanent magnet technology due to their advantageous magnetic properties and relatively low costs of manufacturing.

1.2 Application and Prospects of Permanent Magnet

A new energy paradigm, consisting of greater reliance on renewable energy sources and increased concern for energy efficiency in the total energy life-cycle, has accelerated research into energy-related technologies. Permanent

magnets are now playing significant role on improving the efficiency of electricity transmission and utilization providing strong magnetic flux for saving electric power. The production and application of Nd-Fe-B magnets have been incredible growth in recent years. It has been predicted that the total Nd-Fe-B permanent magnet market will grow by around 9 % accelerated growth after 2016 from a current value of 6 to $ 12 billion over the next 8 years shown in Fig.1 [15].

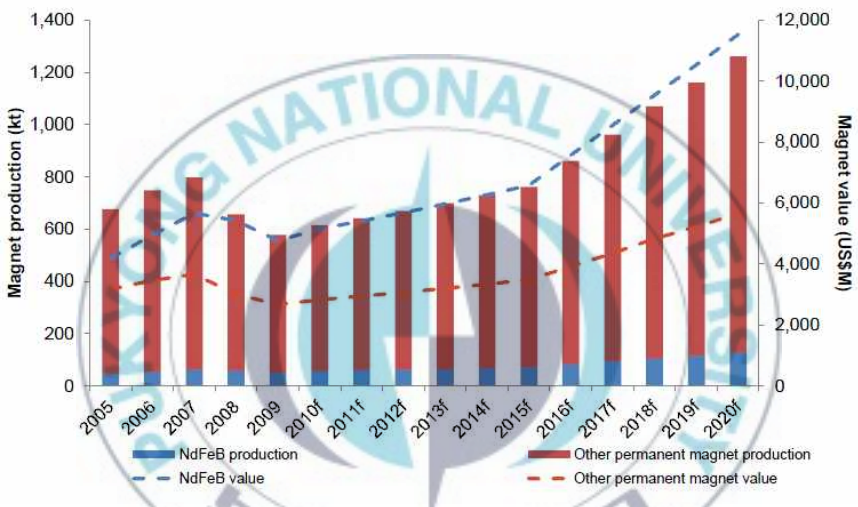

Fig. 1.1 Current and future prediction of world permanent magnet production and value by type, 2005 to 2020 (copied from Ref. 15).

The spectacular growth of Nd-Fe-B-type magnet production has been predominantly due to the rapid growth in the PC market over the last 10 years [16]. The remarkable increase in motor applications also started in 1995, where Nd-Fe-B-type permanent magnets have been applied to servo motors, compressor motors, lifting motors, electric power steering (EPS) motors of automobiles and driving motors of hybrid-type automobiles. The

widespread use of hybrid electric vehicles (HEV) and electric vehicles (EV), which are highly anticipated for their qualities regarding air pollution and global environmental problems, promotes the increase in the use of Nd-Fe-B magnets. Therefore, Nd-Fe-B permanent magnets have been actively applied in these driving motors and electric generators [17]. In developed countries such as the USA, nearly 30 % of this electricity is consumed by the industrial sector and, of that; nearly 65 % is consumed by electric motor drives [18]. Thus the consumption of electricity energy by motors, both big and small, in the USA alone, accounts for nearly 750 billion kWh or, at an average price of $0.06 per kWh, nearly 45 billion US dollars. A 1% improvement in efficiency would result in the savings of hundreds of millions of dollars and a reduction in CO 2 emissions of nearly 2.2 million metric tons of carbon equivalent [19]. Even a small improvement in energy efficiency for electric motors can have a large economical and environmental savings.

1.3 Processing Routes of Nd-Fe-B-Type Permanent Magnet

Several research efforts have been approached to the development of Nd-Fe-B-type permanent magnets manufacturing. The processing routes of Nd-Fe-B magnets play an important role in determining the microstructure and thus their magnetic performance. The common processes for producing these magnets are conventional powder metallurgy methods and melt spinning followed by hot pressing of nanocrystalline powders [20, 21]. Other techniques are inert gas atomization, mechanical alloying and the Hydrogenation Disproportionation Desorption Recombination (HDDR) process [22-24]. In the powder metallurgy route, first microcrystalline alloys of Nd-rich composition are produced by induction melting of Nd, Fe and Fe-B in the form of cast ingots. The ingots are milled to fine powder composed

of particles of 3-5 μm size to allow perfect alignment in an external magnetic field. The fine powder is then pressed, sintered and finally heat treated. Dense bulk magnets can be prepared by taking advantage of the low-melting Nd-rich intergranular phase. This intergranular phase is not ferromagnetic and acts as decoupling layer between the $Nd_2Fe_{14}B$ ferromagnetic grains and blocks the reverse domain propagation [25]. The major advantage of the powder metallurgy process is that a wide variety of sintered shapes can be produced and machined to their tolerances but a disadvantage is the high reactivity and oxidation tendency, even at room temperature. The presence of the pro-peritectic soft magnetic α-Fe phase in the microstructure is detrimental for the hard magnetic properties of Nd-Fe-B magnets [20]. The melt spinning process is based on rapid solidification [26]. A stream of molten alloy is directed and quenched on the surface of a rotating water cooled copper wheel where the liquid solidifies at a cooling rate of the order of one million °C/s. This leads to an ultrafine grain size of typically 20-50 nm depending on the wheel speed. The different parameters in this quenching process (e.g. wheel speed, ejection condition and melt temperature) govern the microstructure of the ribbon. It was reported that high quench rates produce essentially amorphous ribbons (i.e. no crystal grains), on the other hand optimum cooling rates produce roughly spherical nano crystalline $Nd_2Fe_{14}B$ grains [27]. If the ribbons are amorphous, low temperature quick annealing treatment is employed for making crystallization form. Subsequently the ribbons are pulverized into powder with particle size around 100-150 μm. Each particle contains many randomly oriented grains that's why it is not possible to align and resultant powder will be isotropic [22, 23]. A larger remanence can be achieved by hot pressing the crushed ribbons to full density followed by hot deformation. Mechanical alloying is a solid-state reaction process and is used for the

preparation of metastable alloys. This method was originally established for super alloys [28]. The alloying can take place either during milling or during a subsequent heat treatment process depending on the thermodynamics of the alloy system, the energy input during milling and the mechanical workability of the starting powders. Schultz et al. [24, 29] reported that a layered microstructure of Fe and Nd is formed with B particles remaining undeformed and being embedded in the interfaces during ball milling. When these powders are annealed at low temperatures (600 ºC-700 ºC), the ferromagnetic $Nd_2Fe_{14}B$ phase is formed within a short reaction time of 10-30 minutes due to the extremely fine distribution of the reactants. Thus, an isotropic powder of randomly oriented nanocrystallites in the size range of 10 to 50 nm is obtained. The discovery of the Hydrogenation Disproportionation Desorption Recombination (HDDR) process was a significant progress to achieve higher energy density magnets [30, 31]. The HDDR process is in principle a strikingly simple method for producing magnetically high coercive rare-earth transition metal powders by utilizing a fully reversible hydrogen gas induced chemical reaction. Although, the phase transformation is reversible, the grain size drastically decreased by about three orders of magnitude (from over 100 μm to 0.3 μm), resulting high coercivity (13.5 kOe) of the HDDR-treated materials [32-33]. An optimum microstructure, which is favorable for good magnetic decoupling of hard magnetic phases, is essential having desired magnetic performance of the magnet. The hard magnetic properties of Nd-Fe-B-type magnets depend on the processing parameters of different production routes. The achievement of desired microstructure is very important in determining hard magnetic properties. Hence, in order to obtain $Nd_2Fe_{14}B$-based permanent magnets with high remanence, coercivity and energy product, the optimization of the processing parameters is very important.

1.4 Excellence of HDDR Process

In spite of several processing routes the hydrogenation, disproportionation, desorption and recombination, (HDDR) process developed by Takeshita and Nakyama in 1989 is established as an effective technique for producing high coercive ultra fine Nd-Fe-B powders [34]. HDDR process is in principle a strikingly simple method by utilizing a fully reversible hydrogen gas induced chemical reaction. It consists of two stages. At the first stage, alloy ingot of Nd-Fe-B is heated between the temperature range 750 ℃-850 ℃ for 3-4 hour under hydrogen atmosphere called hydrogenation and disproportionation (HD) process. On absorbing the hydrogen, alloy ingot becomes extremely friable and disproportionates into an intimate mixture of α-Fe, $NdH_{2\pm x}$ (with x as a function of hydrogen pressure) and Fe_2B. The second stage was followed by desorption and recombination (DR) at the same or little bit higher temperature for ½-1 hour under vacuum. On desorbing the hydrogen, the disproportionated unstable phase mixture of α-Fe, $NdH_{2\pm x}$ and Fe_2B recombine to form the thermodynamically more stable $Nd_2Fe_{14}B$ phases. Although, the phase transformation is reversible, the grain size drastically decreased by about three orders of magnitude (from over 100 μm to 0.3 μm), resulting high coercivity (13.5 kOe) of the HDDR-treated materials [32, 33]. Finally the treated material was rapidly cooled to prevent the grain coarsening at an elevated temperature. The principal advantage of HDDR process is that highly coercive fine Nd-Fe-B magnetic powder with size comparable to single domain size (~300 nm for $Nd_2Fe_{14}B$) can be produced simply without much processing steps. In addition, controlling the HDDR process variables, the end product of the HDDR process could be prepared either isotropic or anisotropic form. Particularly the disproportionation kinetic influenced by temperature, hydrogen pressure and additives plays an

important role to make the final form of HDDR-treated material [35-39]. The recombined grains are oriented orderly (texture) in such a manner that the magnetization easy axis (c-axis) of the neighboring recombined Nd-Fe-B grains is parallel to each other maintaining the crystallographic orientation of their mother grains resultant of the anisotropic powder. Over the past years, HDDR process has attracted much attention because of easy preparation of high coercive ultra-fine powder with grain structure comparable to single domain size (~300 nm for $Nd_2Fe_{14}B$). Another advantage of HDDR process is that anisotropic powder can be prepared without following much steps.

1.5 Objectives of this Thesis

Human development has caused a depletion of natural energy resources and climate changes with unpredictable consequences. New energy concepts are required for an ever-increasing industrial society. Permanent magnets are now playing significant role to improve the efficiency of electricity transmission and utilization providing strong magnetic flux resulting saving electric power. A major part of the electricity is being consumed by motor whatever it is small or big. A 1% improvement in efficiency for electric motors would result in the savings of hundreds of millions of dollars and a huge reduction in CO_2 emissions [19]. The key requirement for the permanent magnet used in motor is the temperature stability for safe operation. Temperature stability is dependent upon a number of factors for the various types of Nd-Fe-B-type magnet. Nd-Fe-B-type magnets show a low Curie temperature and their temperature dependence of coercivity is large. Therefore, the coercivity decreases drastically with increasing temperature and Nd-Fe-B-type magnets cannot operate at high temperatures. To meet this requirement, permanent magnets require significant amounts of

dysprosium substitution for the neodymium, which results in a substantial increase in the cost of the magnet, as Dy is less plentiful and cost ~8 times as much as Nd metal [17, 38]. In addition, the magnetic moment of Dy is coupled anti-parallel to that of Fe in $R_2Fe_{14}B$ compounds (R: rare earth), which leads to a decrease in their energy product. Therefore, the development of Dy-free or Dy-lean Nd-Fe-B magnets with a high coercivity is strongly in demand. The coercivity is a complex phenomena still there is no straight forward theory or experimental result to explain that. The final suitability concerning corercivity can only be assessed from a favorable chemical composition adequate microstructures and processing variables fulfilling certain criteria. There are two methods for increasing coercivity, one of the methods is decreasing the possibility of multi-domain structure in magnets by decreasing the grain size of the $Nd_2Fe_{14}B$ phase. The other method is controlling the interfacial microstructure between a $Nd_2Fe_{14}B$ phase and a Nd-rich phase. It is generally accepted that the Nd-rich phase in grain boundary region plays an important role for magnetic isolation of each hard $Nd_2Fe_{14}B$ grains, hence enhancing the coercivity in $Nd_2Fe_{14}B$ magnets.

The hydrogenation, disproportionation, desorption and recombination (HDDR) process has been established as an effective technique for producing highly coercive fine isotropic and anisotropic Nd-Fe-B-type magnetic powder [34]. In spite of the anisotropy field ~73 kOe of the $Nd_2Fe_{14}B$ phase, the typical coercivity reported for Nd-Fe-B-type HDDR-treated powder is ranges from 10 to 13 kOe which is only about 20 % of the anisotropy field of $Nd_2Fe_{14}B$. The coercivity iHc of sintered magnets follows $iHc=24–2.6\ \ln(D^2)$, where D stands for average grain size, from which a coercivity of around 32 kOe is expected for D=200 nm if good magnetic isolation is kept [33, 39]. The coercivity of HDDR powder for the grain size

close to a single domain size (~300 nm for $Nd_2Fe_{14}B$) is much too low and has long been a mystery. Therefore, the possibility of increasing the coercivity is still left. That's why the HDDR process and the HDDR-treated material have received much attention in the permanent magnet research community. It has been generally accepted that one of the key requirements for achieving high performance of Nd-Fe-B-type magnet is having a fine $Nd_2Fe_{14}B$ grain structure with appreciable magnetic decoupling of grains. As the HDDR-treated material consists of very fine grains and usually in powder form. Therefore, it would be expected that consolidation of the HDDR-treated powder into high density bulk magnet keeping the grain structure in the powder state could lead to high coercivity. Our research project has been carried out aiming the thermal process of Nd-Fe-B-type HDDR-treated material and followed by coercivity investigation in the processed material.

1.6 Scopes of the Thesis

Historical background, development of Nd-Fe-B-type permanent magnet with its applications and prospects are discussed in chapter one, together with the different processing routes and objectives of the thesis. Theories of magnetism emphasizing to the coercivity is discussed in chapter two. Apparatus and experimental procedures used in the project are placed in chapter three. A study of residual hydrogen in the HDDR-treated material and its effect on the coercivity of heated Nd-Fe-B-type HDDR-treated material are appeared respectively in chapter four and five. Chapter six is covered with coercivity of hot-pressed compacts of Nd-Fe-B-type HDDR-treated material. Finally summary of this project is briefed in chapter seven.

1.7 References

1. O Gutfleisch, J. Phys. D: Appl. Phys. vol. 33, pp.157-172, 2000.
2. Strnat K, Hoffer G, Olson J, Ostertag W and Becker J. J., J. Appl. Phys. vol. 38, p. 1001, 1967.
3. M. Sagawa, S. Hirosawa, H. Yamamoto, S. Fujimura and Y. Matsuura J., J. Appl. Phys., vol. 26 (6), pp. 785-800, 1987.
4. E. A. Nesbitt and J. H. Wernick, Rare Earth Permanent Magnets, Academic Press, New York, 1973.
5. K. Nassau, L. V. Cherry and W. E. Wallace, J. Phys. Chem. Solids, vol. 16, p. 123, 1960.
6. G. Hoffer and K. J. Strnat, IEEE Trans. Magnetics vol. 2, p. 487, 1966.
7. W. E. Wallace, R. S. Craig, H. O. Gupta, S. Hirosawa, A Pedziwiatr, E. Oswald and E. Schwab, IEEE Trans. Magnetics, vol. 20, p. 1599, 1984.
8. H. Nagel and A. Menth, Goldschmidt Informiert, vol. 35, p. 42, 1975.
9. A. E. Ray, W. A. Soffa, J. R. Blachere and B. Zhang, IEEE Trans. Magnetics, vol. 23, p. 2714, 1987.
10. M. Sagawa, S. Fujimura, N. Togawa, H. Yamamoto and Y. Matsuura, J. Appl. Phys., vol. 55, p. 2083, 1984.
11. J. J. Croat, J. F. Herbst, R. W. Lee and F. E. Pinkerton, J. Appl. Phys., vol. 55, p. 2079, 1984.
12. G. C. Hadjipanayis, R. C. Hazelton and K. R. Lawless, J. Appl. Phys., vol. 55, p. 2073, 1984.
13. Joseph J. Becker, J. Appl. Phys., vol. 55, p. 2067, 1984.
14. N. C. Koon and B. N. Das, J. Appl. Phys., vol. 55, p. 2063, 1984.

15. Suzanee Shaw, “8th International Rare Earths Conferences,” November, 2012, Hong Kong.
16. M. H. Walmer, J. F. Liu, and P. C. Dent, “Proceedings of 20th International Workshop on Rare Earth Permanent Magnets and Thier Application,” Sept. 8-10, 2008, Crete, Greece.
17. S. Sugimoto, J. Phys. D: Appl. Phys., vol. 44, p. 064001, 2011.
18. M. Lowe, R. Golini, and G. Gereffi “U. S. Adoption of High-Efficiency Motors and Drives: Lessons Learned,” published by Center on Globalization, Governance and Competitiveness, February 2010.
19. Oliver Gutfleisch, Matthew A. Willard , Ekkes Brück, Christina H. Chen, S. G. Sankar, and J. Ping Liu, Adv. Mater., vol. 23, pp. 821-842, 2011.
20. J. M. D. Coey, Rare-Earth Iron Permanent Magnets, Oxford University Press, New York, USA, 1996.
21. B.M. Ma, J. W. Herchenroeder, B. Smith, M. Suda, D. N. Brown, and Z. Chen, J. Magn. Magn. Mater. vol. 239, pp. 418-423, 2002.
22. G. C. Hadjipanayis and W. Gong., J. Appl. Phys., vol. 64, pp. 5559-5563, 1988.
23. A. Manaf, R. A. Buckley, H. A. Davies, and M. Leonowicz, J. Magn. Magn. Mater, vol. 101, pp. 360-362, 1991.
24. L. Schultz, K. Schnitzke, and J. Wecker, J. Appl. Phys., vol. 64, pp. 5302-5304, 1988.
25. W. Rodewald, B. Wall, and W. Fernengel, IEEE Trans. Magnetics, vol. 33 pp. 3841-3843, 1997.
26. J. J. Croat, J. F. Herbst, R. W. Lee, and F. E. Pinkerton, J. Appl. Phys., vol. 55, pp. 2078-2082, 1984.

27. R. Lee, E. Brewer, and N. Schaffel, IEEE Trans. Magnetics, vol. 21, pp. 1958-1963, 1985.
28. J. S. Benjamin, Metallurgical Transactions, vol. 1, pp. 2943-2951, 1970.
29. L. Schultz, K. Schnitzke, J. Wecker, M. Katter, and C. Kuhrt, J. Appl. Phys., vol. 70, pp. 6339-6344, 1991.
30. P. J. McGuiness, X. J. Zhang, X. J. Yin, and I. R. Harris, J. Less-Common Metals, vol. 158, pp. 359-365, 1990.
31. P. J. McGuiness, X. J. Zhang, X. J. Yin, and I. R. Harris, J. Less-Common Metals, vol. 158, pp.379–387, 1990.
32. T. Takeshita, J. Alloys Comp., vol. 231, pp. 51-59, 1995.
33. W. F. Li, T. Ohkubo, K. Hono, T. Nishiuchi and S. Hirosawa, Appl. Phys. Lett., vol. 93, p. 052505, 2008.
34. T. Takeshita and R. Nakayama, "Proceedings 10th International Workshop on Rare Earth Magnets and Their Applications," Kyoto, vol. 1, p. 551, 1989, unpublished.
35. H. W. Kwon and J. H. Yu, J. Alloys Comp., vol. 487, pp. 138-141, 2009.
36. T. Tomida, P. Choi, Y. Maehara, M. Uhera, H. Tomizawa, S. Hirosawa, J. Alloys Comp., vol. 242, pp. 129-135, 1996.
37. Zhong Lin, Jingzhi Han, Meiying Xing, Shunquan Liu, Rui Wu, Changsheng Wang, Yan Zhang, Yingchang Yang, and Jinbo Yang, Appl. Phys. Lett., vol. 100, p. 052409, 2012.
38. Metal Pages Homepage, www.metal-pages.com (accessed September 2010).
39. K. Hono, H. Sepehri-Amin, Scripta Materialia, vol. 67, p. 530, 2012.

Chapter Two

MAGNETISM AND MAGNETIC MATERIALS

2.1 Magnetism

Magnetism and magnetic materials have been known to mankind since ancient times. From magnetite (Fe_3O_4), the first magnetic material ever known to mankind, to elementary magnetic metals Fe, Co and Ni, to more complex magnetic compounds and alloys, magnetic materials have been widely used in our daily life and in industry for a long time. Magnetism is a phenomenon by which materials assert an attractive or repulsive force on other materials which originates from the electrons' spin motion and their orbital motion around the nucleus. These motions produce the spin magnetic moment and the orbital magnetic moment of an electron, respectively. The total magnetic moment of an atom is the resultant magnetic moments from these two contributions together with a small contribution from the nucleus, taking into account the magnetic moments cancellations due to the electrons being grouped in pairs. The best way, however, to define of magnetism of a materials how it responds to magnetic fields. The main distinction is that in some materials there is no collective interaction of atomic magnetic moments, whereas in other materials there is a very strong interaction between atomic moment [1, 2].

2.2 Classification of Magnetism and Magnetic Materials

Every substance can be regarded as magnetic. The magnetic response to a magnetic field differs for different materials depending on the collective

interaction of atomic magnetic moments. Magnetic materials which show collective interaction of atomic magnetic moments appear to be magnetic whereas other groups appear as non magnetic [3]. The magnetic behavior of materials can be classified into the following five major groups:

2.2.1 Diamagnetism

2.2.2 Paramagnetism

2.2.3 Ferromagnetism

2.2.4 Antiferromagnetism

2.2.5 Ferrimagnetism

Materials in the first two groups are those that exhibit no collective magnetic interactions and are not magnetically ordered. Materials in the last three groups exhibit long-range magnetic order below a certain critical temperature. Ferromagnetic and ferrimagnetic materials are usually what we consider as being magnetic (i.e., behaving like iron).

2.2.1 Diamagnetism

Diamagnetism is a fundamental property of all matter, it is the general tendency of a material to oppose an applied field and therefore, to be repelled by a magnetic field. Diamagnetic substances are composed of atoms which have no net magnetic moments (i.e., all the orbital shells are filled and there are no unpaired electrons). When an external magnetic field H is applied, a negative magnetization M in the opposite direction to that of the applied field will be produced. Thus the susceptibility χ, which is defined as the variation in magnetization M of a material with applied magnetic field H, will be negative for diamagnetic materials. The value of susceptibility for diamagnetic materials is independent of temperature. Examples of diamagnetic materials are Cu, He, Au.

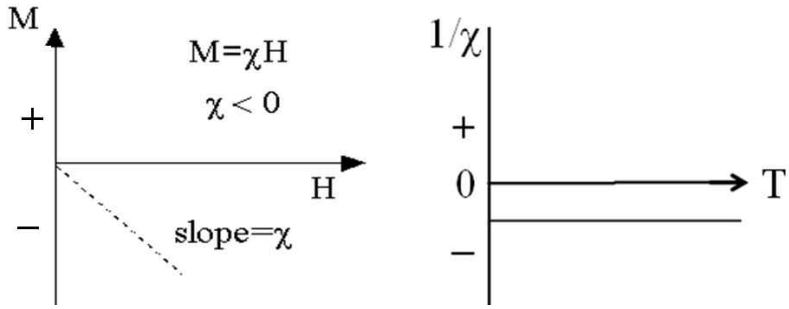

Fig. 2.1 Susceptibility and effect of temperature on diamagnetic materials.

2.2.2 Paramagnetism

In a paramagnetic material there are unpaired electrons, thus atomic or molecular orbitals have net magnetic moments with exactly one electron in them. Afterwards, paramagnetic material does not exhibit net magnetic moments without an applied field like diamagnetism due to random orientation of the individual magnetic moments. When an external magnetic field is applied, these magnetic moments will tend to align themselves in the same direction as the applied field, thus reinforce it resulting in a net positive magnetization and positive susceptibility. In addition, the susceptibility is temperature dependent. As the temperature increases, the thermal agitation will also increase and so the atomic magnetic moments will become harder to align to the direction of the applied magnetic field. The susceptibility of paramagnets is often inversely proportional to the temperature following the Curie-Weiss law. Some examples of paramagnetic materials are Na, Al and Mn.

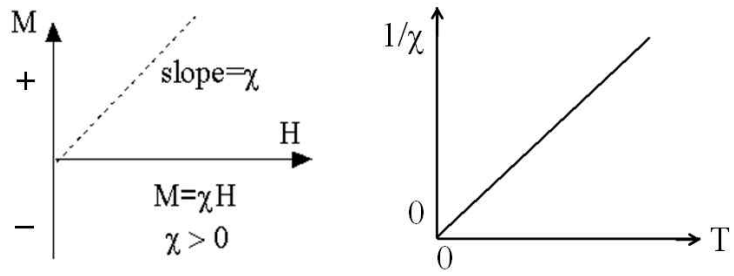

Fig. 2.2 Susceptibility and effect of temperature on paramagnetic materials.

2.2.3 Ferromagnetism

Ferromagnetism is one of the strongest forms of magnetism. A ferromagnet, like a paramagnetic substance, has unpaired electrons. In ferromagnetic materials, the atoms are arranged in a lattice and the atomic magnetic moments coupled to align parallel to each other to maintain a lowered-energy state. Thus, even when the applied field is removed, the electrons in the material maintain a parallel orientation. The susceptibilities of ferromagnetic materials are positive and large. Every ferromagnetic substance has its own individual temperature, called the Curie temperature, or Curie point, above which it loses its ferromagnetic properties. This is because the thermal tendency to disorder overwhelms the energy-lowering due to ferromagnetic order. Above the Curie temperature Tc, ferromagnets becomes the paramagnetic and the susceptibility will be inversely proportional to the temperature following the Curie-Weiss law. Common ferromagnetic materials include Fe, Co and Ni.

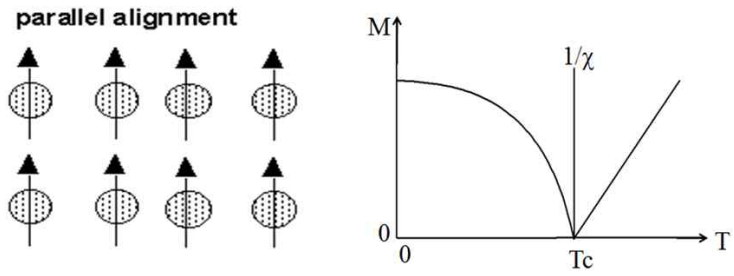

Fig. 2.3 Susceptibility and effect of temperature on ferromagnetic materials.

2.2.4 Antiferromagnetism

Antiferromagnetic materials are very similar to ferromagnetic materials but the exchange interaction between neighboring atoms results in antiparallel alignment of the atomic magnetic moments. The magnetic moments of opposing directions cancel each other leading to zero net magnetization of the materials. But the material appears slightly different to behave from that of ferromagnetic and paramagnetic materials in terms of susceptibility. As the temperature increases, the susceptibility increases and goes through a maximum at a critical temperature T_N called the **Néel temperature.**

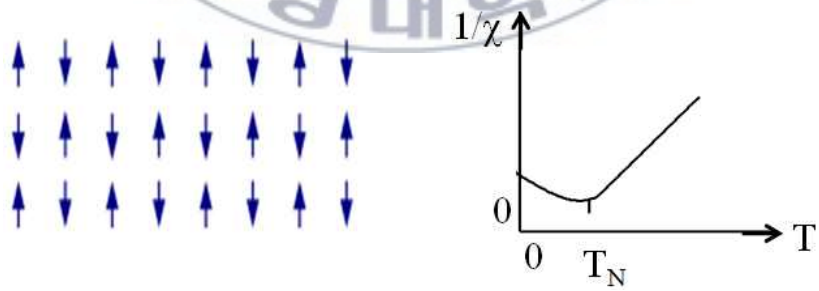

Fig. 2.4 Susceptibility and effect of temperature on antiferromagnetic materials.

As the temperature increases, contrary to the paramagnetic behavior, the susceptibility of antiferromagnetics increases with increasing temperature. Above the T_N, spin arrangement becomes random, the susceptibility decreases with increasing the temperature obeying the Curie-Weiss law for paramagnets. Examples of antiferromagnetic materials are Cr, MnO and FeO.

2.2.5 Ferrimagnetism

Ferrimagnetism is another type of magnetic ordering and is only observed in compounds. In a ferromagnetic material, atomic magnetic moments are arranged in an antiparallel manner, but the magnitude of the moments pointing in one direction does not equal that pointing in the opposite direction, so that a spontaneous magnetization corresponding to the difference between the some of the moments is produced. As the temperature increases, the arrangement of the spins is disturbed by thermal agitation, thus resulting in a decrease of the spontaneous magnetization. The arrangement of the spins becomes completely random at the Curie point above which the material shows paramagnetic behavior. Susceptibility decreases with increasing the temperature following the Curie-Weiss law for paramagnets. The example of ferrimagnetic materials is magnetite Fe3O4. MnZn and NiZn.

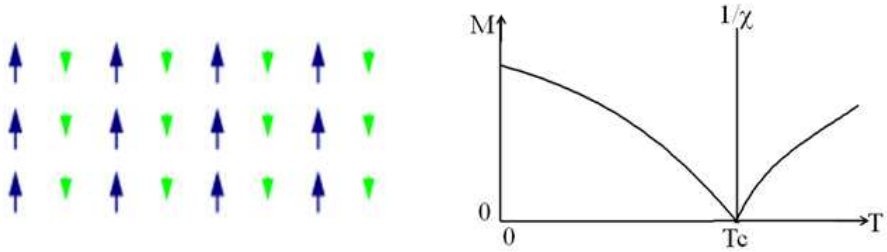

Fig. 2.5 Susceptibility and effect of temperature on ferrimagnetic materials.

2.3 Electronic Configuration of Rare Earth-Transition Metal Compounds

2.3.1 In the Rare-Earth (R) Series

In searching for Rare Earth elements as constituents of the permanent magnet, it obviously needs to know the electronic configurations of those. As the origin of magnetism lies in the orbital and spin motions of electrons and how the electrons interact with one another. The rare earth metals are the fifteen elements which ranges from lanthanum (La), atomic number 57, to lutetium (Lu), atomic number 71. The electron structure of these metals is given

$(4f)^n (5s)^2 (5p)^6 (5d)^1 (6s)^2$

where n increases from 0 to14 as atomic number increases from 57 to71.

However the 4f shell is not the outermost shell of the atom. The incomplete 4f shell has a close relation to the magnetic properties of this series of elements as does the 3d shell for the iron group transitional metals.

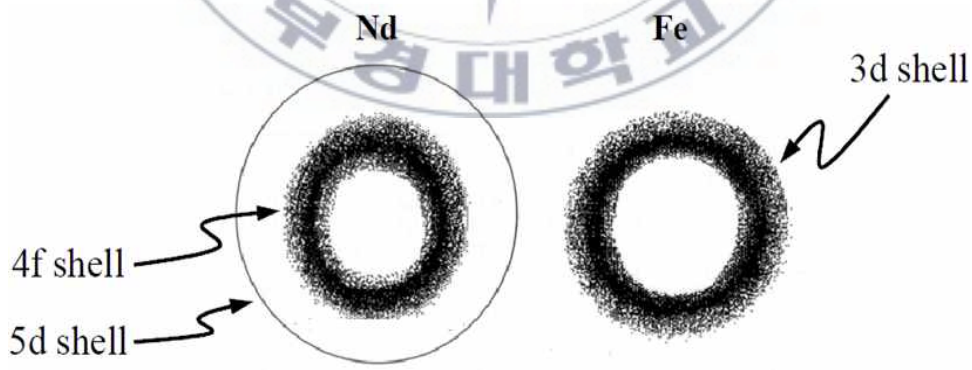

Fig. 2.6 Positions of the unpaired electron shells in Nd and Fe atoms (copied from Ref. 4).

The only difference is that in the rare earth metals, the 4f shell is enclosed by an outer electron shell composed of $(5s)^2$, $(5p)^6$, even if the atoms are ionized by the loss of three electrons. Figure 2.6 illustrates the position of the 4f shell for Nd (Z = 60) and 3d shell of iron group transition metals. Therefore the orbital angular momentum of 4f electrons remains unquenched by the crystalline field of neighboring ions and the total magnetic moment has both orbital and spin components.

The similarity of the magnetic of the rare earth metals in the ionic and metallic states indicates that, even in the metallic states, 4f electrons are well localized in an inner core of each atom. Most of the rare earth metals with a more than half-filled 4f shell show forms of ferromagnetism at low temperature. On the other hand, rare earth metals with a less than half-filled 4f shell exhibit anti-ferromagnetism. The R-R exchange-coupling between two R atoms in a solid is indirect because the direct overlap between the 4f shells of adjacent rare-earth atoms is negligible. The resulting weak magnetic interaction with the 4f electrons of neighbouring atoms, results in low Curie temperatures of the ferromagnetic rare-earth metals; in fact, all of them have a T_C below room temperature (only Gd has a Curie temperature as high as ambient temperature, $T_C = 20°C$).

2.3.2 In the Transition-Metal (T) Elements: Fe, Co and Ni

There are three ferromagnetic transition elements: Fe, Co and Ni which have partially filled 3d, 4d and 5d shells. These orbits tend to project out to the atoms periphery and can be easily affected by crystalline fields resulting from surrounding atoms or ions in the solid. Therefore these orbits cannot contribute to the magnetic moments, and electron spin is the only

contribution to the magnetic moment of the transitional metals. The 3d electrons of these atoms are localized in the outer shell (see Fig. 2.6). Hence in solids the 3d electrons are considerably less localized than the 4f electrons of the rare earths. Therefore the orbital momentum of T atoms or ions is nearly completely removed ("quenched") by the interaction in the solid.

The origin of the magnetic moment of transition metals showing forms of ferromagnetism can be explained by considering the state of the d-shell. In 3d transition metals, the energy levels from 1s to 3p have been filled completely, but the 3d and 4s bands show a different situation; the 4s band is filled with 2 electrons and the 3d band remains partially filled. This incomplete 3d band is responsible for the magnetic moment of 3d transition metals. Fe is classified as a weak ferromagnet (despite its relatively large moment) because the majority spins 3d↑ levels are not completely occupied, whereas the other two are strong ferromagnets because there are no 3d ↑ holes. Fe is the 3d element with largest spin moment per atom (2.22 μ B) followed by Co (1.72 μ B). In a description of 3d magnetism by localised moments the strong overlap of the 3d wave functions results in a strong direct exchange interaction between these moments and, consequently, they exhibit high Curie temperatures: T_C (Fe) = 770 °C, T_C (Co) = 1127 °C and T_C (Ni) = 362 °C.

2.3.3 Rare Earth-Transition Metal Compounds

By combining rare-earth elements with one of the ferromagnetic 3d elements, it is possible to marry the best features of 4f and 3d magnetism. In the 3d magnetic elements such Fe, Co and Ni large 3d exchange interactions stabilize ferromagnetic ordering well above room temperature, but the orbital

angular momentum is mostly quenched, so that the magnetic anisotropy is generally very small thus limiting the coercivity of the 3d transition elements, and the contribution to the total magnetic moment comes essentially from the electron spin of the unpaired 3d electrons. The 4f electrons in the rare earth, on the contrary, are shielded by the electrons in the 5s and 5p, so that the orbital angular momentum of 4f electrons is not quenched and shows large values and the total observed magnetic moment is a composite of both the orbital and the spin contributions. The magnetic interaction of 4f electrons is much smaller than that of 3d electrons, and the ordered magnetic state of rare earths is attained only below room temperature.

R-R interactions in the rare earth transition-metal intermetallic compounds are generally quite small by comparison with R-T and T-T interactions, and are often neglected. The R-T interaction is indirect because there is almost no overlap between 4f shells of R atoms and 3d shells of T atoms. The 5d electrons are involved as the intermediary. Then, the coupling between the transition-metal spin and the rare-earth spin will be different depending on the rare-earth element involved. The 4f-5d interaction is invariably ferromagnetic, but the 5d-3d interaction will be antiferromagnetic when the 5d band is less than half full and the 3d band is more than half full. In this way, the magnetisations of rare-earth and transition metal sub-lattices couple parallel for the light rare-earths and antiparallel for the heavy rare-earths.

2.4 Some Properties of Ferromagnetic Materials

2.4.1 Curie Temperature: Tc

Curie temperature Tc, is the temperature above which thermal energy

overcomes the electronic exchange forces in ferromagnets and produces a randomizing effect. This occurs at a particular temperature for each type of ferromagnetic material. Below the Curie temperature, the ferromagnet is ordered and above it, disordered. The saturation magnetization goes to zero at the Curie temperature. The Curie temperature is treated an intrinsic property and used for the diagnostic purpose for mineral identification. However, it is not foolproof because different magnetic minerals, in principle, can have the same Curie temperature.

2.4.2 Magnetic Anisotropy

Magnetic anisotropy simply means that the magnetic properties of ferromagnetic materials depend on the direction in which they are measured. The magnetization tends to align along certain preferred directions, which are called easy axes since it is easier to magnetize a demagnetized ferromagnetic material to saturation if the external magnetic field is applied along a preferred direction. The energy difference between magnetizations along the easy and hard axes is called magnetic anisotropy energy. There are several kinds of magnetic anisotropy, including magnetocrystalline anisotropy, shape anisotropy, stress anisotropy, exchange anisotropy and anisotropy induced by material processing. Only magnetocrystalline anisotropy is intrinsic to the ferromagnetic material and all the others are extrinsic. The magnitude and type of magnetic anisotropy affect magnetization and hysteresis loop in ferromagnetic properties. In this section, I will only introduce magnetocrystalline anisotropy and shape anisotropy since these are the properties we will investigate in our study. Magnetocrystalline anisotropy is the tendency of the magnetization to align itself along the easy axis. The origin of magnetocrystalline anisotropy mainly

comes from the spin-orbit coupling, which is the interaction between the spin and the orbital motion of an electron. When an external applied field tries to reorient the spin of an electron, the orbit of that electron also tends to be reoriented because of this spin-orbital coupling. However, the orbit is strongly coupled to the crystal lattice and therefore resists the attempt to rotate the spin axis. The energy required to rotate the spin system of a domain away from the easy axis to the hard axis, which is defined as magnetocrystalline anisotropy energy, is actually just the energy required to overcome the spin-orbit coupling. Shape anisotropy is another kind of magnetic anisotropy which origins in the non-spherical shape of a ferromagnetic sample. If it is spherical in shape, the same applied magnetic field will magnetize it to the same extent in every direction. However if it is not spherical, it will be easier to magnetize it along a long axis than along a short axis because the demagnetizing field along a short axis is stronger than along a long axis. The applied field along a short axis then has to be stronger to produce the same magnitude of magnetization inside the sample.

2.4.3 Magnetic Domain

As the ferromagnetic and ferrimagnetic materials are aligned in the same direction, causing an internal magnetic field even in the absence of an applied field. This brings up another question from our practical experience. In spite of having internal magnetic fields, how can we obtain the ferromagnetic and ferrimagnetic materials in the demagnetized condition? The formation of a small region within the crystal allows the materials to minimize its magnetostatic energy caused by internal magnetic field. This small region is called a magnetic domain, which possesses a spontaneous magnetization in easy direction. In the absence of an applied field the

magnetization of each region points randomly with respect to each other, so that there is no net magnetic moment as a whole. The boundaries between neighboring domains are called domain walls in which the magnetization has different directions. Domain walls have a finite width that is determined principally by exchange and magnetocrystaline energy [5]. The origin of magnetic domains can be explained by considering the structure of a large single crystal. For uniaxial crystal, magnetic free poles are formed on the ends when the single crystal is compose of one domain spontaneously magnetized and parallel to the easy axis. These free poles are the source of a demagnetizing field resulting in magnetostatic energy.

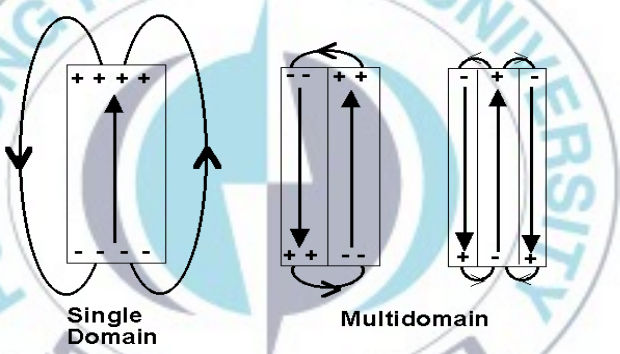

Fig. 2.7 Domain formation in ferromagnetic materials (copied from Ref. 3).

This energy can be reduced by one-half by dividing the crystal into two domains magnetized in opposite directions because this division brings north and south poles closer to one another, thus decreasing the spatial extent of the demagnetizing field shown in Fig.2.7. This division process will continue until an equilibrium domain size is reached, where the domain wall energy produced by the splitting of a domain is balanced by the magnetostatic energy. Thus an equilibrium number of domains will be reached for a given particle size.

2.4.4 Domain Wall Process

The exchange energy tends to make the wall as wide as possible whereas the anisotropy tends to make the wall as thin as possible. As a result of this competition between exchange and anisotropy energies, the domain wall has a finite width (on the order of 100 nm) and surface energy. When a domain wall bisects an inclusion, the wall area will decrease by πr^2, the surface area of a spherical inclusion with a radius r, and the wall energy will decrease $\pi r^2\gamma$, where γ is the total domain wall energy per unit area. In other words, the wall energy will increase if the domain wall moves to leave the inclusion behind. This increase in the domain wall energy may impede wall movement. Meanwhile an inclusion within a domain would have free poles on it and have an associated magnetostatic energy which forms a greater source of internal energy. This magnetostatic energy can be halved by redistribution of free poles when the domain wall moves to bisect the inclusion. Therefore the magnetostatic energy will increase if the domain wall moves from a position bisecting the inclusion to a position away from the inclusion. This increase in the magnetostatic energy opposes domain wall movement. Domain wall motion is hindered by microstess due to crystal imperfection of crystal. As a domain wall moves through a stressed region, it exerts a mgnetostrictive force on the immediate surrounding area. This mgnetostrictive force introduces extra uniaxial anisotropy which will impede the domain wall motion. Therefore a domain wall trends to move away from a high stress region and the wall becomes curved. If the wall is curved, a free pole must form on the wall and extra magnetostatic energy is introduced. This situation is not energetically favorable. On the other hand, if the wall remains straight in order to avoid free poles, part of it must have a high energy because it is located in the region where the stress is not a minimum. The domain wall

therefore assumes the shape which minimizes the sum of the magnetostatic and the wall energies.

For a multi domain particle, a favorable domain becomes dominant and others almost disappear when saturation magnetization is gained. In the case of demagnetization after certain level a reverse domain is nucleated on the surface. The spin on the surface atom is rotated by the applied field, and this rotation in turns tends to rotate the spin on the next atom because of exchange coupling. A complete wall is formed and moved inward, producing a new domain magnetized antiparallel to the original domain. In real crystal, the most favourable sites for nucleation of reverse domains are surface irregularities with large demagnetizing fields and chemical or physical defect where the magnetocrystalline anisotropy is lowered locally.

2.4.5 Origin of Coercivity

Coercivity is the required field to demagnetize the materials completely from its magnetizing state attributed to the saturation magnetization after removing applied field. The coercivity is a complex phenomena still there is no straight forward theory or experimental result to explain that. The final suitability concerning corercivity can only be assessed from a favorable chemical composition adequate microstructures and processing variables fulfilling certain criteria. In spite of quite similar microstructure, coercivity displays peculiar behavior. For example sintered magnet shows high coercivity than Nd-Fe-B type HDDR-treated powder despite almost same-sized grains. Afterwards microstructure is considered as a single most influential parameter to lead the coercivity of materials.

Once the magnetic domains are aligned along the direction of an applied magnetic field, the formation of reversed domains is necessary in order to demagnetize the material. The process of magnetization reversal involves the nucleation and wall motion of reverse domains. The coercivty of ferromagnetic can be determined by a process predominantly dependent on the nucleation of reverse domain walls, or it can be dependent on domain wall movement, where “pinning” plays a major role. These two routes have been theoretically developed to produce a wall nucleation dominated model [6] or a wall pinning dominated model [7]. Single domain particle has spontaneous magnetic orientation called EMD, when its direction is changed from EMD to magnetic hard direction, it needs to change atomic magnetic moment with much energy. If it is once changed need to much demagnetization field for taking the initial state because of absence reverse domain nucleation. That’s why single domain particles are favorable for high coercivity. For a spherical, single domain and saturated crystal of any size, the total reversal field acting on the crystal given by:

$H_a+H_d=2K/M_s$

Where H_a is the applied field, H_d demagnetizing field and K anisotropy constant; both H_a and H_d opposing the direction of magnetization [1]. In multi domain particle there will be domain wall which can be rotated easily using less energy than changing the atomic moment in single domain particle. A favorable domain becomes dominant and others almost disappear when saturation magnetization is gained after applying required field. In the case of demagnetization after certain level reverse domain nucleated and very rapidly it becomes demagnetized. That’s why the field required to reverse magnetization decrease as the particle size increases. However, the coercivity values of real materials are much less than the corresponding theoretical maximum values. This discrepancy between experiment and

theory, which is known as “Browon’s paradox” can be explained by, magnetization reversal by the nucleation and wall movement of the nucleated reverse domain. The condition for wall nucleation in a single particle is given by

$H_a+H_d>2K/M_s$

Nucleation of reverse domains, originating at imperfections or at irregularities at the grain boundaries, is one of the main factors that reduces the coercivity. Nucleation of reverse domains is most likely (a) at surface irregularities such as pits, bumps, steps, cracks and scratches with large demagnetization fields, and (b) at chemical or physical defects such as dislocation, solute atoms, interstitials, vacancies and second phase precipitates, where the anisotropy energy is lowered locally. Nucleation-controlled coercivity can be increased by minimizing the density and size of nucleating defects. Easy-axis anisotropy is indispensable for maintaining the metastable domain configuration required for a permanent magnet. Modern high performance magnets are, therefore, based on compounds of a magnetic light rare earth (Pr, Nd, Sm) for anisotropy and a 3d element (Fe, Co) for magnetisation and high Curie temperature [8]. The particular rare earth needed for uniaxial anisotropy is determined by the symmetry of the site it occupies in the crystal structure.

As alternatives to the nucleation of reverse domains, the coercivity can also be controlled by the growth of small residual (or nucleated) reverse domains [9] or by pinning of domain walls by inhomogeneities. Necessary conditions for having a nucleation-controlled coercivity are a defect-free microstructure and smooth grain boundaries. High coercivity is obtained in this type of magnets because it is difficult to nucleate reverse domains [10-12]. This can be easily understood considering that the typical grain size of these magnets

is much larger than the critical single domain size, so that once a domain wall is created, it will easily run across the grain. Shtrikman and Treves [13], however, have postulated that the reverse domains are not nucleated but are already present at defects, so that the nucleation process is one of "unpinning" walls that already exist.

Wall movement of reverse domains may be impeded by defects such as second phase precipitates which pin domain walls by locally altering wall energy. For materials with very large anisotropy K, the wall becomes very thin, and even points defects may acts as pinning sites. It is worthwhile, however, to note that defects may lower coercivity by serving as nucleation sites or raise coercivity by pinning domains walls. Large defects are most effective for nucleation, small defects for pinning. The difference between pinning controlled and nucleation controlled behavior can be seen clearly by observing the "virgin" magnetization curve. In the two phase pinning controlled magnet, the existing domain walls cannot move easily and the permeability remains low until the applied field approaches the coercivity, whereas for the single phase nucleation-controlled magnet the domain walls can move easily and initial permeability is high.

2.4.6 Hysteresis Loop and Magnetization Process

In the initial demagnetized state, the domains are arranged randomly so there is no net magnetization as a whole in a ferromagnetic material. When an external magnetic field is applied, the domain whose magnetization is closest to the direction of the applied field starts to grow through domain wall motion, at the expense of shrinking of other domains that are unfavorably oriented. Usually the moving domain walls will encounter imperfections

such as defects or dislocations in the ferromagnetic crystal. When a domain boundary intersects the imperfection, the magnetostatic energy associated with the imperfection will be eliminated. The intersection of the domain boundary with the imperfection is a local energy minimum [14]. As a result the domain boundary will tend to stay pinned at the imperfection, and energy is required to move it past the imperfection. The external applied magnetic field provides this energy. Eventually, all domain walls in the ferromagnetic material are eliminated with sufficient high applied field. This leads to a single domain, with its magnetization pointing to the easy axis oriented most closely to the external magnetic field. Further increase of the applied field will rotates the magnetization of the single domain from the easy axis to the direction of the applied field. At this stage the magnetization can be increased no more with increasing applied field and the saturation is reached. This magnetization is called **saturation magnetization**; **Ms**.

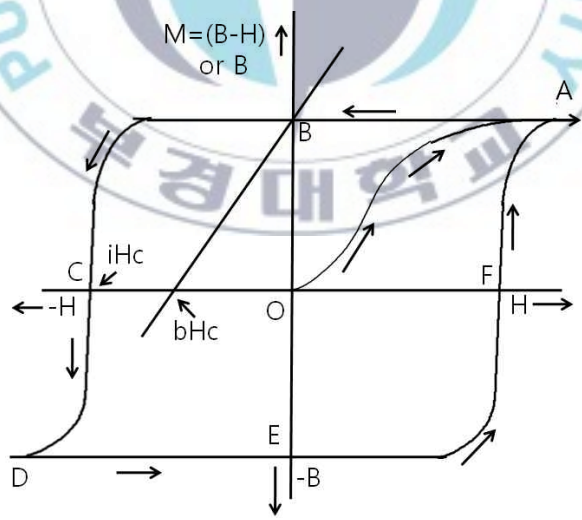

Fig. 2.8 A typical hysteresis loop for a ferromagnetic material.

It measures the maximum amount of field that a ferromagnetic material can generate. The curve from the demagnetization state (where H=0 and M=0) to saturation is called the **initial magnetization curve** or "**virgin**" magnetization curve (OA in Fig.2.8). When the applied field is reduced after saturation has been reached, the magnetization first rotates back to the easy axis. Next reverse magnetic domains grow to allow the material to be partially demagnetized, initiated by the demagnetizing field inside the ferromagnetic material. However, the domain walls are unable to fully reverse their motion back to their original positions. This is because the demagnetizing field, not the applied magnetic field, drives the demagnetization process, and the demagnetizing field is not strong enough to overcome the energy barriers encountered when the domain walls intersect the imperfections. As a result, some magnetization, called **residual magnetization, Mr** (B in Fig.2.8), remains in the ferromagnetic material even when the field is completely removed. If the applied field is then reversed and increased in the negative direction, the magnetization of the materials will decrease and reach zero at a certain negative applied field. This value of applied field is called the **coercivity, Hc** (C in Fig.2.8). If the applied field is further increased in the negative direction magnetization in the reverse direction will reach saturation again (CD in Fig.2.8). If the field is reversed after saturation and increased in the positive direction the magnetization will go through E and F then reach saturation (DEFA in Fig.2.8). Cycling of this magnetization curve results in a symmetrical loop (ABCDEFA in Fig.2.8); this is called **hysteresis loop**. The second quadrant of the hysteresis loop corresponding to the demagnetizing curve (BC in Fig. 2.8.) is important in describing the quality of permanent magnetic materials.

It would be worthwhile to introduce the magnetic induction B versus field H curve because magnetic induction is more popular than magnetization M in the engineering area. The relationship between B, M and H is as below:

$B=4\pi M+H$

The B vs H curve, therefore, can be plotted from the M vs H curve by adding H in the positive field region and subtracting H in the negative field region. The magnetic induction at zero applied field is called the **remanence (Br)**, which corresponds to the residual magnetization (Mr) in the M vs H curve. The value of the coercivity in the B vs H curve should be different from that in the B-H versus H curve. The coercivity in the B vs H curve and B-H vs H curve are called the**, induction coercivity, bHc** and **intrinsic coercivity, iHc** respectively.

2.4.7 Maximum Energy Product

The maximum energy product $(BH)_{max}$ is one of a few measures of quality of a ferromagnetic material, representing the energy required to demagnetize the material. It is defined as the maximum value of the product of B and H, corresponding to the area of the largest rectangular that can be constructed in the second quadrant of the B-H loop. In the permanent magnet application, even if the magnets do not have a magnetic gap in them, a demagnetizing field due to magnetic free poles necessarily exists in the magnet. This demagnetization field leaves the magnets not in the state of residual magnetization but in a slightly demagnetized state even without an external applied field. Similarly permanent magnet in application always have magnetic gap in the magnetic circuit because they are used to produce an external field in the gap. This external magnetic field in the gap acts as a demagnetizing field for the magnet and the state of the magnet is not at Br

but at some point on the demagnetization curve. The magnetic energy in the gap is proportional to the product of B and H, and this is why the maximum energy product $(BH)_{max}$ is used as a parameter describing the performance of a permanent magnet. As can be expected, there is one point on the demagnetization curve for which the product B and H has a maximum value, this is called **maximum energy product $(BH)_{max}$.** Having a well designed shape and thus being operated at the $(BH)_{max}$ point in an application, the permanent magnet can produce its maximum magnetic energy.

2.5 Units of Magnetism

Despite the popularity of the SI system in such fields of electricity and physics, the majority of data on magnetic materials are given in the C.G.S system in both the material laboratory and plant. The problem of the acceptance of the SI system by workers in magnetism is in part due to the wide difference between numerical values of flux density B, and magnetizing field H. In this thesis, magnetic quantities are presented in the C.G.S system.

Quantity	CGS unit	SI unit	Relation
Induction	B Gauss (G)	B_o Tesla (T)	$1G = 10^{-4}$ T
Magnetic field	H Oersted (Oe)	H (Am^{-1})	1 Oe=79.58 Am^{-1}
Maximum energy product	(BH)max (MGOe)	(BH)max(KJm^{-3})	1 MGOe=7.958 KJm^{-3}

2.6 References

1. B. D. Cullity, Introduction to magnetic materials, Addison-Wesley Pub. Co., Reading, Massachusetts, 1972.
2. Nicola A. Spaldin, Magnetic materials: fundamentals and device applications, Cambridge University Press, Cambridge, U.K., 2003.
3. http://www.irm.umn.edu/hg2m/hg2m_b/hg2m_b.html
4. J.M.D. Coey (Editor), Rare Earth Iron Permanent Magnets, Clarendon Press Oxford, 1996.
5. http://www.aacg.bham.ac.uk/magnetic_materials/history.htm.
6. J. J. Becker, J. Appl. Phys. vol. 39, p. 1270, 1968.
7. H. Zijlstra, J. Appl. Phys. vol. 41, p. 4881, 1970.
8. D. Eckert, A. Kirchner, O. Gutfleisch, W. Grünberger, B. Gebel, K. Arnold, A.Handstein, M. Wolf and K.-H. Müller, "Procedings 10th Int. Symp. Magn. Anisotropy and Coercivity in RE-TM Alloys," Dresden, Germany, p. 297, 1998.
9. D. Givord and M.F. Rossignol, Rare Earth Iron Permanent Magnets, J.M.D. Coey (Editor), Clarendon Press Oxford , pp. 218-285, 1996.
10. E. Adler and P. Hamann, "Procedings 4th Int. Symp. Magn. Anisotropy and Coercivity in RE-TM Alloys," Dayton, pp. 747-760, 1985.
11. K. Schnitzke, L. Schultz, J. Wecker and M. Katter, Appl. Phys. Lett. vol. 57, p. 2853, 1990.
12. M. Sagawa, S. Fujimori, M. Togawa and Y. Matsuura, J. Appl. Phys. vol. 55, p. 2083 1984.
13. S. Shtrikman and D Treves, J. Appl. Phys. vol. 31, p. 729, 1960.
14. http://www.aacg.bham.ac.uk/magnetic_materials/hysteresis.htm.

Chapter Three

APPARATUS AND EXPERIMENTAL PROCEDURE

3.1 Experimental Procedure

Alloy ingot was prepared by Arc melting with the composition of $Nd_{12.5}Fe_{80.6}B_{6.4}Ga_{0.3}Nb_{0.2}$. Alloy ingot was crashed into coarse particle followed by hydrogenation disproportionation desorption and recombination (HDDR) treatment. $Nd_{12.5}Fe_{80.6}B_{6.4}Ga_{0.3}Nb_{0.2}$ HDDR-treated

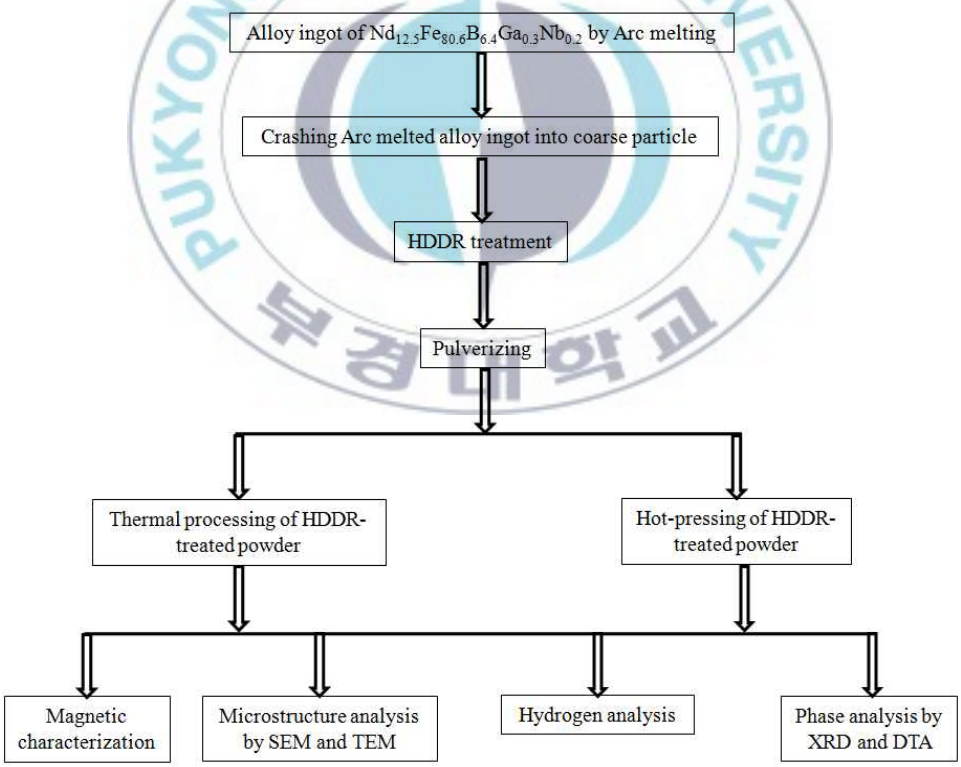

Fig. 3.1 Schematic representation of the experimental procedure.

material was pulverized into fine particle with size on an average 100-150 μm. The HDDR-treated fine powder was thermally processed by heating without load or hot-pressing with load. The thermally processed material was characterized by several means. Magnetic characterization was performed by vibrating sample magnetometer (VSM). Microstructure was analyzed by scanning electron microscopy (SEM) and transmission electron microscopy (TEM). Hydrogen in the HDDR-treated material was determined by Hydrogen Determinator (LECO, RH-600). Phase evolution in the HDDR-treated material on thermal processing was verified by XRD and DTA. Each and every experimental procedure is described in details to this chapter individually. The overall schematic of experimental procedure is shown in the Fig.3.1.

3.2 HDDR Process

Alloy ingot with the composition of $Nd_{12.5}Fe_{80.6}B_{6.4}Ga_{0.3}Nb_{0.2}$ was prepared by arc melting process. The alloy ingot was homogenized at 1100 ℃ for 20 h and then crashed into coarse particle with size of approx. over 3 mm. Coarse alloy particle were exposed to hydrogen (P_{H_2}=1 bar) from room temperature. Hydrogen was absorbed at or close to room temperature by Nd-rich phases and then the second stage absorption was occurred by the $Nd_2Fe_{14}B$ matrix phases at temperature (~200 ℃). This process is called hydrogen decrepitation (HD) and the resulting material becomes extremely friable. The friable ingots were then hold at 740 ℃ in hydrogen (P_{H_2} = 0.35 bar) for 3 hr for accomplishing the hydrogenation and disproportionation (HD) step where Nd-Fe-B-type phase transformed into an intimate mixture of α-Fe, $NdH_{2\pm x}$ (with x as a function of hydrogen pressure) and Fe_2B. The reaction was as follows [1]:

$Nd_2Fe_{14}B + 2 \pm xH_2 \longrightarrow 2NdH_{2\pm x} + 12Fe + Fe_2B$

The second step desorption and recombination (DR) process was accomplished at 820 ℃ for 40 min under vacuum. Schematic diagram of heat treatment and cooling for HDDR process is shown in Fig.3.2. On desorbing the hydrogen, the disproportionated unstable phases recombine to form the thermodynamically more stable $Nd_2Fe_{14}B$ phases. Although, the phase transformation is reversible, the grain size drastically decreased by about three orders of magnitude (from over 100 μm to 0.3 μm), resulting high coercivity (13.5 kOe) of the HDDR-treated materials. Recombination reaction was as follows:

$2NdH_{2\pm x} + 12Fe + Fe_2B \longrightarrow Nd_2Fe_{14}B + 2 \pm xH_2$

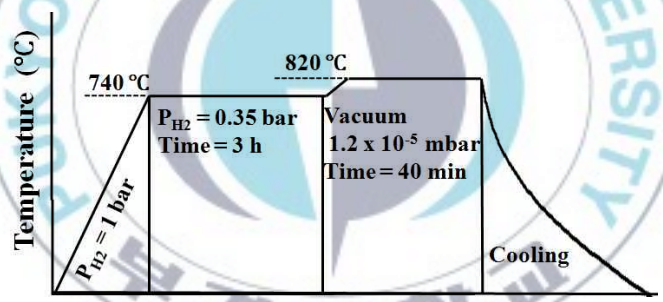

Fig. 3.2 Schematic diagram showing the heat treatment under various atmospheres applied for HDDR experiment.

It is generally accepted that the control of the HDDR process variables, particularly in the disproportionation step, can provide either isotropic or anisotropic powder. Temperature, hydrogen pressure and additives like Ga, Nb and Zr play an important role to produce anisotropic powder influencing the disproportionation kinetic [2]. The main beauty of HDDR process is that an anisotropic powder with a strong crystallographic texture aligned to the

same orientation of the easy axis of the original mother grain of $Nd_2Fe_{14}B$ can be obtained directly by applying right processing conditions. After completion of the recombination stage, the extremely friable material was rapidly cooled to prevent the grain coarsening. Following the HDDR procedure, the friable but magnetically coercive material were pulverized into a fine powder with a size around 100-150 μm.

3.3 Consolidation of HDDR-treated Material

HDDR-treated powder was compacted by hot pressing using different types of die configuration as well as different heating medium. The heating system equipped with high frequency induction coil existing in our laboratory is shown in Fig. 3.3 (a) real set-up, and schematic diagram of (b) closed-type, and (c) open-type die. The induction heating was used for high heating rate. When high-frequency current flows through the induction coil, eddy current is induced in the material and the charge is heated very rapidly as fast as 200 ℃/min. Another heating system used for slow heating rate is nicrome wire based resistance heating. Resistance heating system available in our lab is shown in Fig. 3.4 (a) real set-up and schematic diagram of (b) closed-type, and (c) open-type die. The term resistance heating is self explanatory when current flows through the wire it generates heat due to high resistance. Two types of die configuration namely closed and open-type were used in terms of effectiveness of pumping out the desorbed gas from the sample position on heating. The sample powder was placed in a graphite bushing and inserted to the pressing die for closed-type die shown in Fig. 3.3 (b) and Fig. 3.4 (b). In contrast, the sample powder was kept in copper ring without any pressing die in the open-type die resulting effective evacuation of desorbed gas from the sample area on heating shown in Fig. 3.3 (c) and Fig. 3.4 (c).

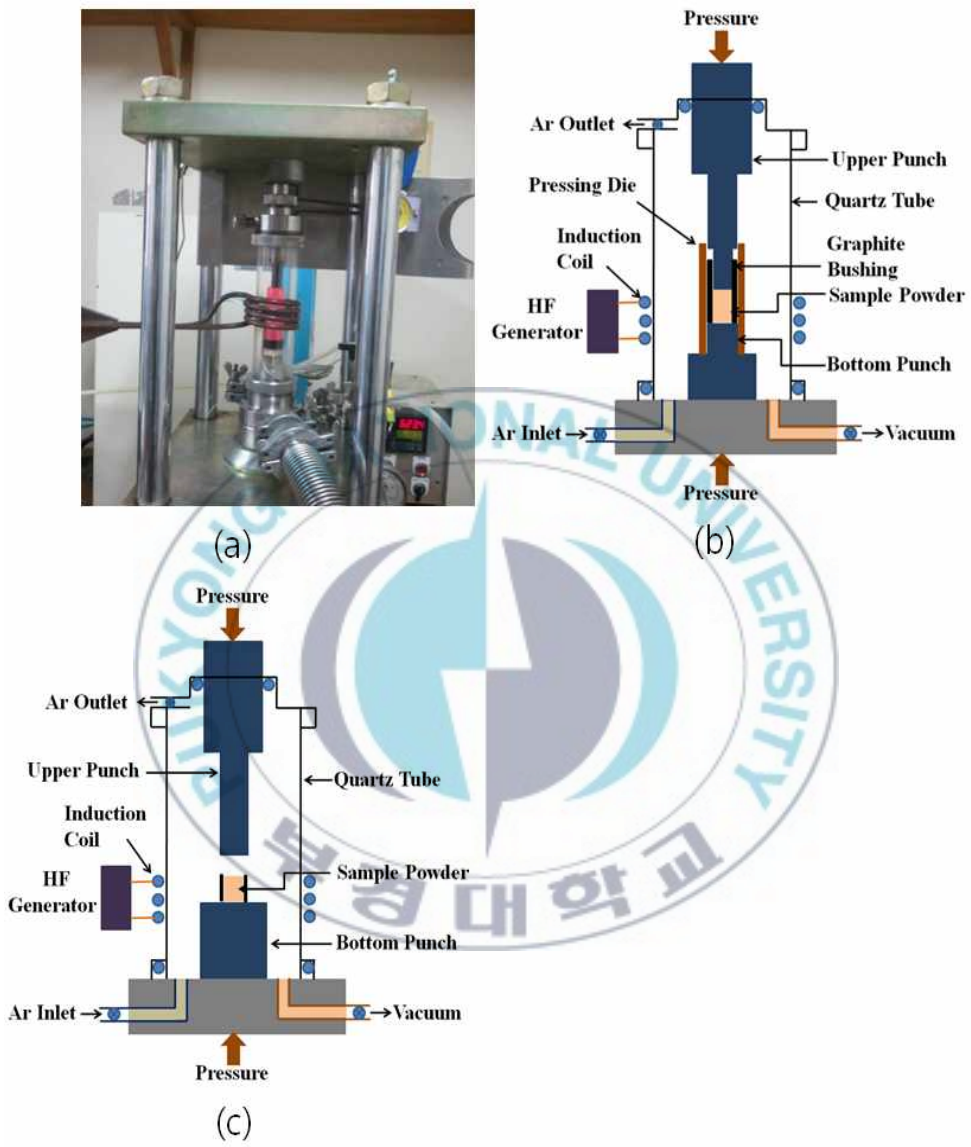

Fig. 3.3 (a) Real set-up and schematic diagram of (b) closed-type, and (c) open-type die equipped with high frequency induction heating system.

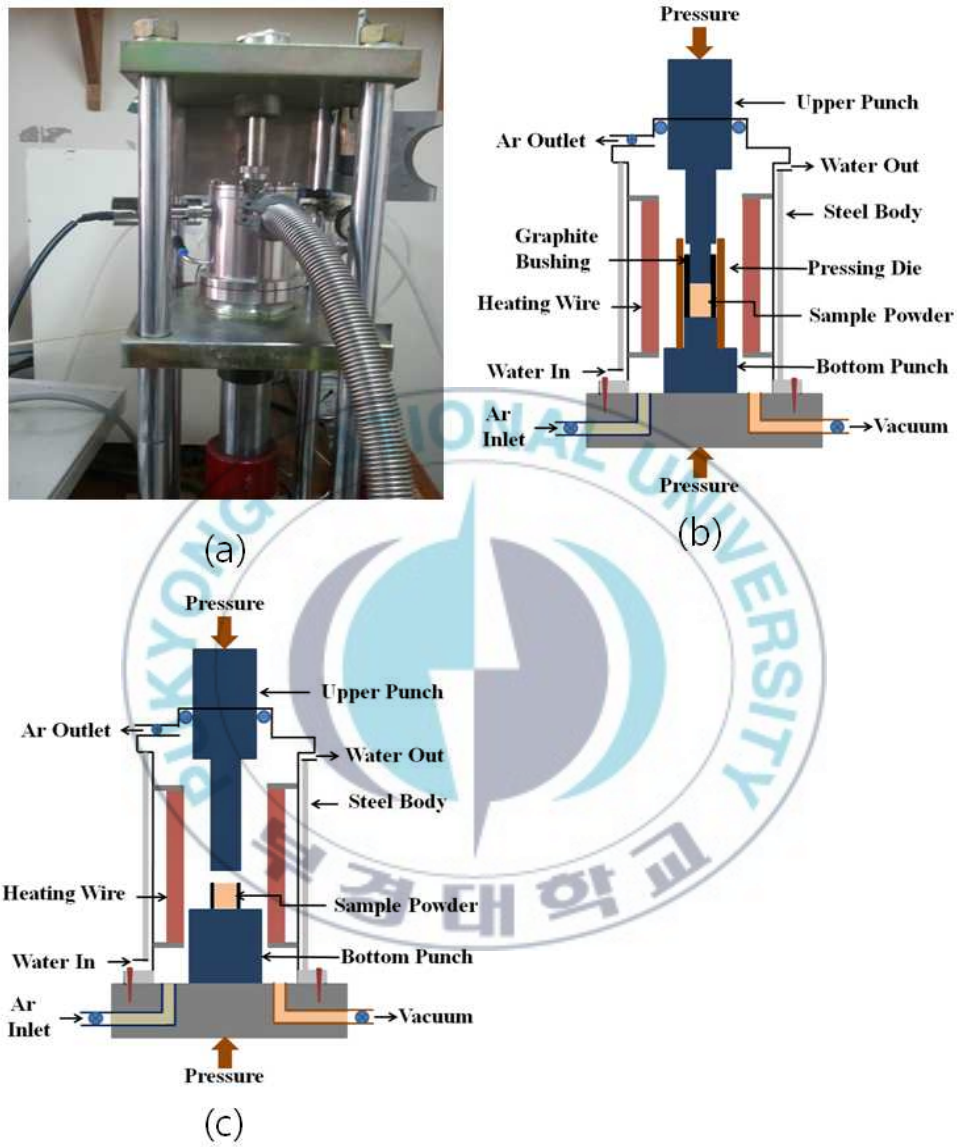

Fig. 3.4 (a) Real set-up and schematic diagram of (b) closed-type, and (c) open-type die equipped with resistance heating system.

The induction coil was wrapped around the quartz tube and connected to the high-frequency power supply. In the resistance heater, the heating wire was coiled allowing the gap for placing the sample. The system was covered by water cooled steel body equipped with vacuum and Ar blowing system. For both type's induction and resistance heating, systems were evacuated to 1.2 $x10^{-5}$ mbar at room temperature. Residual hydrogen in the HDDR-treated powder was desorbed effectively in the open type-die compared to the closed-type die on heating for hot-pressing. Because closed-type die was consisted of many stuffs rather than open-type die. Hot-pressing was performed at different heating rates with applying load 1 Ton/cm^2.

3.4 Heat Treatment of HDDR-treated Material

The furnace was a "Fercalloy" wire wound high temperature type, capable of maximum temperature of 1200 ℃. The furnace could be moved over the nimonic tube which was connected via rubber O-ring seal and a crosspiece to the stainless steel tubing. The seal was water cooled via copper tubing to prevent the O-ring overheating. A gas inlet valve and pressure gauge were installed to introduce the required gas and monitor the pressure of the system. There were also penning gauge and temperature controller in the system. The heating facility existing in our laboratory is shown in Fig. 3.5 (a) real set-up, and (b) schematic diagram. The samples were placed into the nimonic tube with wrapping stainless steel foil or baffle. For rapid quenching after heat treatment, sample would be magnet pull out to the water cooled zone. Stainless steel foil or baffle was attached to the nicrome wire and other end of the wire was connected to iron bolt which could then be easily push out or push back the samples by moving the magnet placing the outside of the

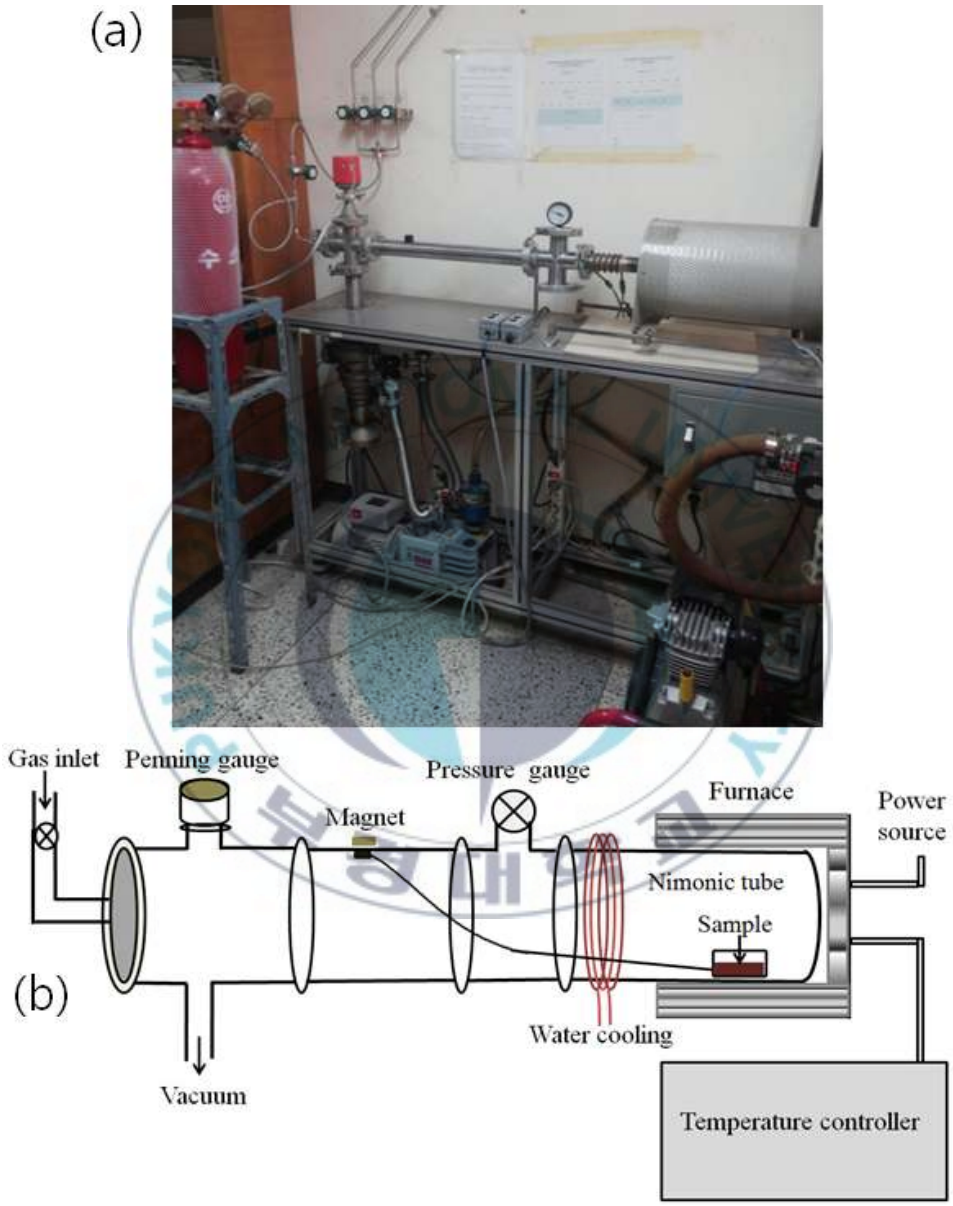

Fig. 3.5 (a) Real set-up, and (b) schematic diagram of heat treatment system.

stainless steel tube. System was evacuated with rotary-diffusion combined vacuum system as best 1.2 x10^{-5} mbar. To get the required temperature for the specific time periods, modes were set using temperature controller.

3.5 Magnetic Characterization

Magnetic properties of the HDDR-treated powder, hot-pressed compacts and other specimen used for the experiments purpose were measured by vibrating sample magnetometer (VSM) with a maximum field of 12 kOe. Prior to the VSM measurement, the samples were wax bonded and then magnetized in 4.5 T pulsing field. The vibrating sample magnetometer invented in 1956 by Simon Foner, a scientist of the MIT, has become a widely used instrument for determining magnetic properties of materials. It has a flexible design and combines high sensitivity with easy of sample mounting and exchange. Samples may be interchange rapidly even at any operating temperature. Measurements of magnetic moments as small as 5 x 10^{-5} emu are possible in magnetic fields from zero to 9 Tesla (or higher). Vibrating sample magnetometers normally operate over a temperature range of 2.0 to 1050 K. Powders, bulk and thin films can be measured and studied. The real set-up and schematic diagram of VSM consisting of basic parts are shown in Fig. 3.6. (a) and (b) respectively. A VSM operates on Faraday's Law of induction, which tells us that a changing magnetic field will produce an electric field. This electric field can be measured and can tell us information about the changing magnetic field. The sample to be studied is placed in a constant magnetic field with a sample holder fixed at the end of a sample rod mounted in a electromechanical transducer. The transducer is driven by a power amplifier which itself is driven by an oscillator at about 85-90 Hertz with an amplitude of about 0.1 mm in direction of right angles to the magnetic field.

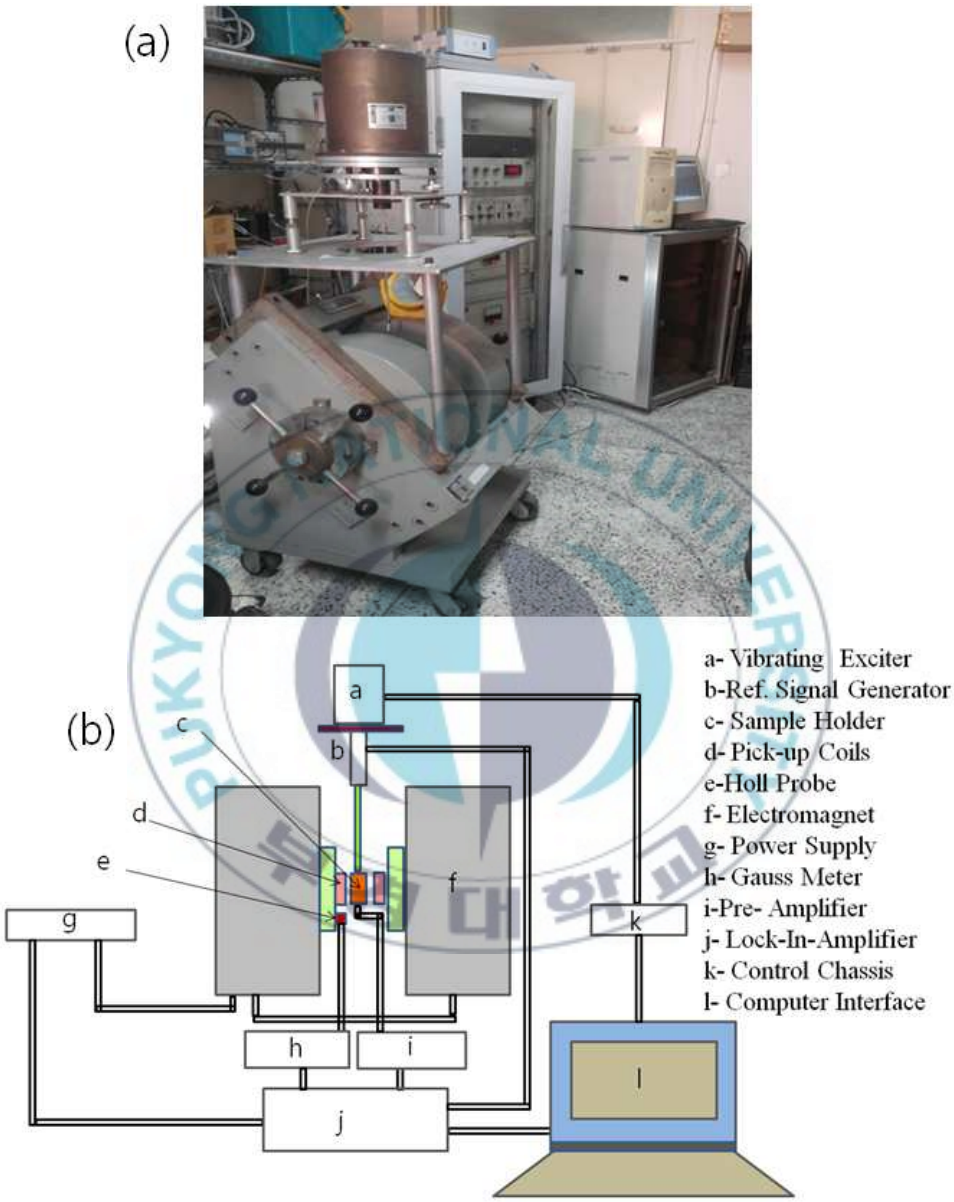

Fig. 3.6 (a) Real set-up, and (b) schematic diagram of VSM consisting of basic parts.

So, the sample vibrates along the Z axis perpendicular to the magnetizing field. If the sample is magnetic the constant magnetic field will magnetize the sample. The magnetic dipole moment of the sample will create a magnetic field around the sample, sometimes called the magnetic stray field. The oscillating magnetic field of the samples as a function of time induces an alternating emf in the pick-up coil placed near the sample. The latter induced a signal in the pick-up coil system that is fed to a differential amplifier. The output of the differential amplifier is subsequently fed into a tuned amplifier and an internal lock-in amplifier. The vibrating rod also carries a reference specimen, in the form of a small permanent magnet, near its upper end. The oscillating field of the reference induces another emf into reference coils. Lock-in amplifier also receives the signal supplied by the reference specimen. The output of the lock-in amplifier is a DC signal proportional to the magnetic moment of the sample being studied. The electromechanical transducer can move along X, Y and Z directions in order to find the saddle point (which calibration of the vibrating sample magnetometer is done by measuring the signal of a pure Ni standard of known the saturation magnetic moment placed in the saddle point).The hall probe placed between the pole pieces of the electromagnet forms a part of the Gauss meter which measures the external magnetic field strength at the sample site. The various components are hooked up to a computer interface. Using controlling and monitoring software the system can tell how much the sample is magnetized and how its magnetization depends on the strength of the constant magnetic field. And a plot of magnetization (M) versus magnetic field strength (H) is generated which provide the magnetic performance of the samples being studied.

3.6 Microstructure Analysis

3.6.1 Scanning Electron Microscopy (SEM)

Morphology of the HDDR-treated powder subjected for thermal treatments was analyzed using scanning electron microscope of TESCAN Co. Model No. VEGA-II-LSU combined with energy-dispersive X-ray spectroscopy (EDS) of HORIBA-6074H. Electrons are used in SEM rather than visible light, to produce magnified images, especially of objects having dimensions smaller than the wavelengths of visible light, with linear magnification approaching or exceeding a million (10^6). An electron beam is produced at the top of the microscope by heating the Tungsten filament. The electron beam follows a vertical path through electromagnetic lenses which focus and direct the beam down towards the sample. The specimen is hit by an electron beam and data on the specimen are delivered by secondary electrons coming from the surface layer. Secondary electrons and backscattered electrons are commonly used for imaging samples: secondary electrons are most valuable for showing morphology and topography on samples and backscattered electrons are most valuable for illustrating contrasts in composition in multiphase samples. The schematic block diagram of SEM is shown in Fig. 3.7 indicating the interaction of the electron beam with a sample producing secondary, reflected electrons, X-rays, etc. Detectors collect the electrons, and convert them to a signal that is sent to a viewing screen to produce a magnified image which allows the examination of the structure, and morphology of materials. Useful magnifications in excess of 100,000 times are obtainable, which translate to a resolution of 3.5 nm at an accelerating voltage of 30 kV.

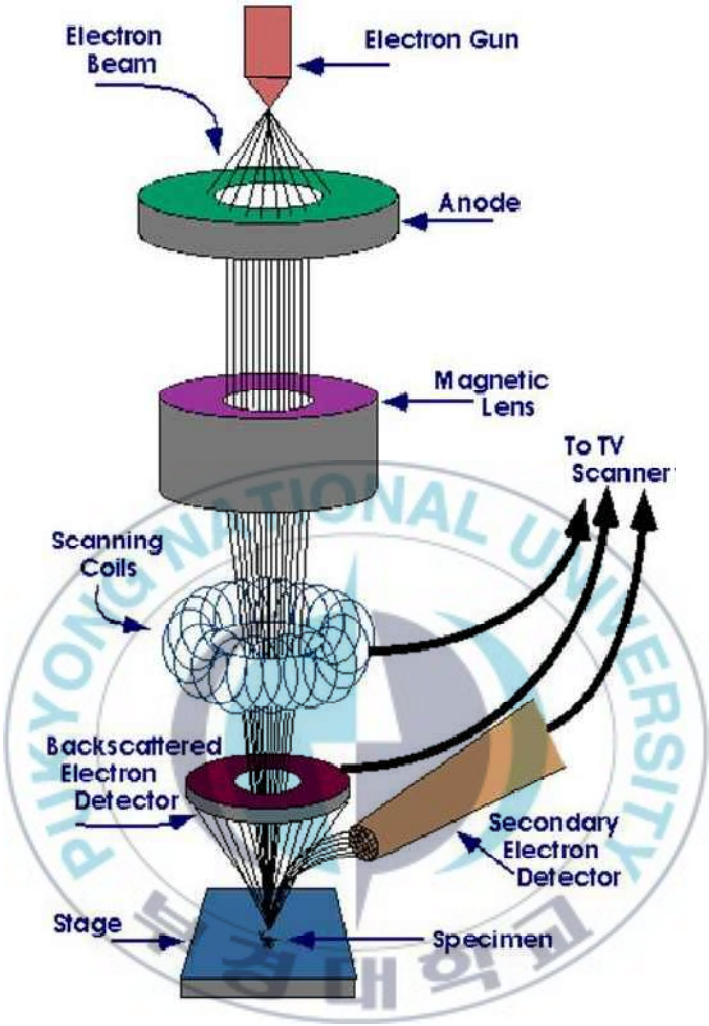

Fig. 3.7 Schematic diagram of Scanning Electron Microscopy (SEM) (copied from Ref. 3).

3.6.2 Transmission Electron Microscopy (TEM)

Microstructure of the hot-pressed compacts prepared in various conditions was also analyzed using JEOL-JEM 2100F TEM. The TEM is suitable for studying the inside of objects.

Sample Preparation for TEM:

A low speed diamond saw (Buehler isomet low speed saw, Model 11-1180) was used for slicing the specimens. Sample was attached with crystal bond to the aluminum sheet as a specimen holder. The holder was fixed to a specimen arm, which could be raised or lowered with respect to the diamond-wafering blade. Micrometer of the saw was used to obtain desired thickness of the specimen. The specimens were cut into thin slices with thickness of the order of 250 μm. The slice obtained from diamond saw was cut by ultrasonic disc cutter with a size of diameter (~3 mm). The disc was then attached to copper grid and grinded using emery paper (grit No. 2000) to reduce the thickness from 250 μm to below 100 μm. Afterwards, the disc was focused for Ion Beaming. Ion Beaming is a sputtering process in which energetic (~ 5 keV) neutral atoms and ions (typically argon) from a cathode impinge on the disc (or target), at an angle. As a result, the atoms of the sample are knocked off. Ion beaming continued until the sample became transparent to electrons for TEM studies.

TEM Studies:

The transmission electron microscope is basically composed of two or more condenser lenses, an electron gun, a specimen holder and a viewing screen. A schematic diagram of TEM showing the basic components is shown in Fig. 3.8. TEM must be operated under very high vacuum to avoid collisions between electrons of the beam and stray molecules. An electron gun produces a stream of electrons those are condensed more than one time by the magnetic condenser lens and focused on the object being studied. The specimen thinned by Ion Beaming allows electrons to pass through in it. The condensed beam and transmitted

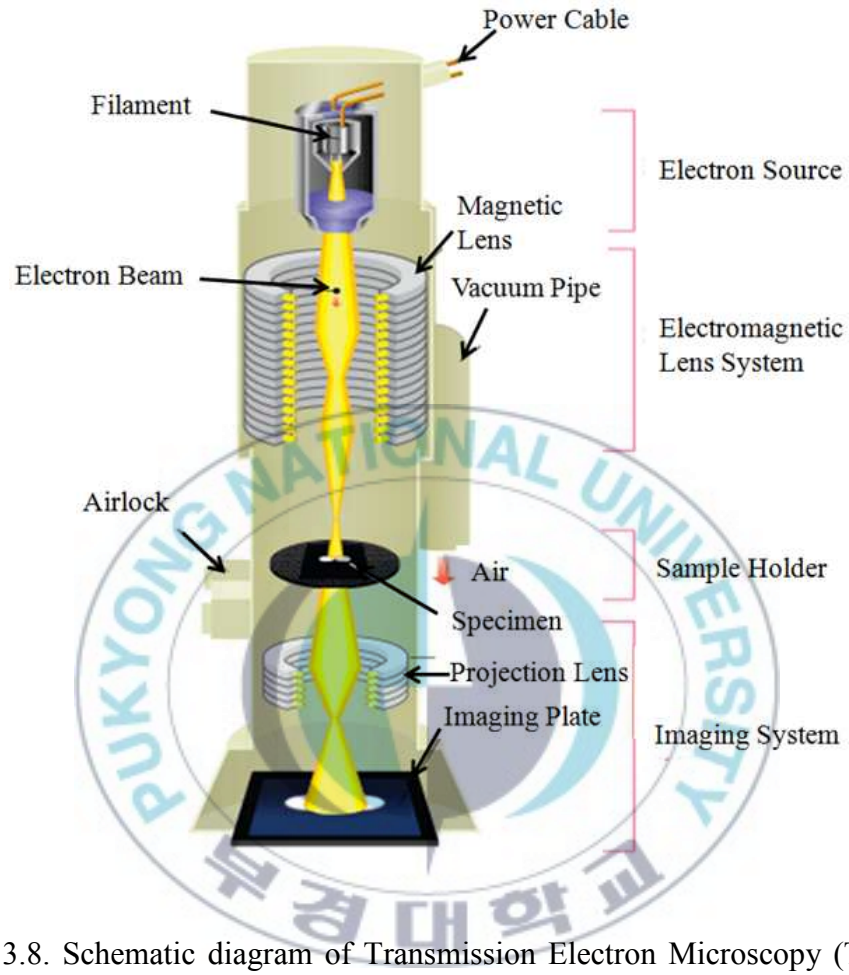

Fig. 3.8. Schematic diagram of Transmission Electron Microscopy (TEM) showing basic parts (copied from Ref. 4).

electrons are focused by an objective lens into an image on a phosphor image screen. The TEM builds an image by way of differential contrast. Those electrons that pass through the sample go on to form the image while those that are stopped or deflected by dense atoms in the specimen are subtracted from the image. In this way a black and white image is formed. Some electrons pass close to a heavy atom and are thus only slightly deflected. In order to eliminate these scattered electrons from the image an aperture is

placed in the objective lens that will stop all those electrons that have deviated from the optical path. The image is then projected with higher magnification onto either the fluorescent screen or onto the photographic film. Image contrast can tell the internal structure and phase composition of the materials being studied.

3.6.3 X-ray Diffraction (XRD)

X-ray diffraction (XRD) (Cu-K_α radiation) was used for studying the phase and lattice parameters of the specimen subjected for various thermal processing. X-ray Diffractometer of RIGAKU Co. Model no. Ultima-IV was used for the experiment. X-ray diffraction (XRD) is a rapid analytical technique primarily used for phase identification of a crystalline materials and can provide information on unit cell dimension. The analyzed materials is finely ground and homogenized. X-ray crystallography can determine the atomic and molecular structure of a crystal, in which the crystalline atoms cause a beam of X-rays to diffract into many specific directions. From this diffraction, electron density, the mean positions of the atoms in the crystal can be determined, as well as their chemical bonds, their disorder and various other information. The schematic representation of x-ray diffractometer is shown in Fig. 3.9. Crystals are regular arrays of atoms, and X-rays can be considered waves of electromagnetic radiation. Atoms scatter X-ray waves, primarily through the atoms' electrons. Just as an ocean wave striking a lighthouse produces secondary circular waves emanating from the lighthouse, so an X-ray striking an electron produces secondary spherical waves emanating from the electron. This phenomenon is known as elastic scattering, and the electron (or lighthouse) is known as the scatterer. A regular array of scatterers produces a regular array of spherical waves.

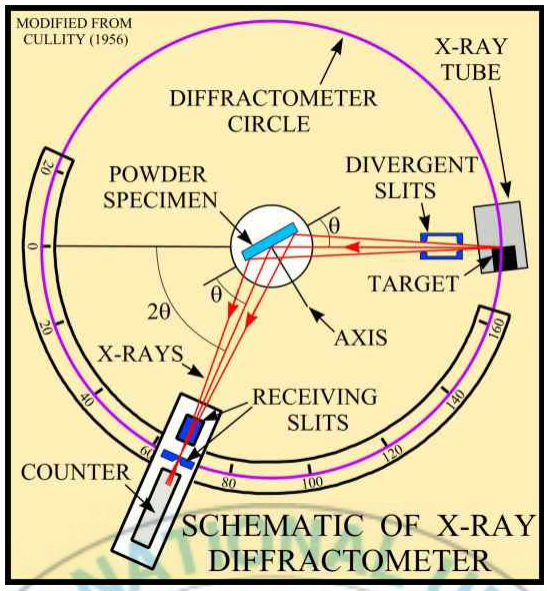

Fig. 3.9 Schematic representation of X-ray diffractometer (copied from Ref. 3).

Although these waves cancel one another out in most directions through destructive interference, they add constructively in a few specific directions, determined by Bragg's law:

$2d \sin\theta = n\lambda$

Here *d* is the inter-planar spacing between diffracting planes, θ is the incident angle, *n* is any integer, and λ is the wavelength of the beam. These specific directions appear as spots on the diffraction pattern called reflections. Thus, X-ray diffraction results from an electromagnetic wave (the X-ray) impinging on a regular array of scatterers (the repeating arrangement of atoms within the crystal) shown in Fig. 3.10. The incoming beam (coming from upper left) causes each scatterer to re-radiate a small portion of its intensity as a spherical wave. If scatterers are arranged symmetrically with

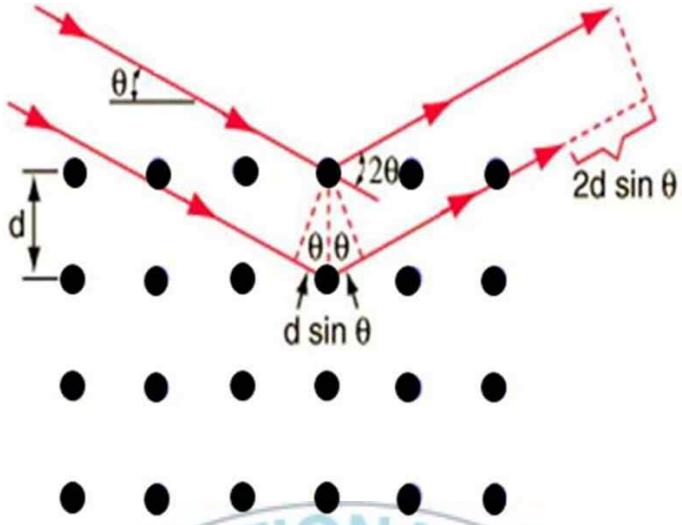

Fig. 3.10 Schematic representation of diffraction of X-rays by crystallographic plane (Bragg's Law) (copied from Ref. 3).

a separation *d*, these spherical waves will be constructively only in directions where their path-length difference 2*d* sinθ equals an integer multiple of the wavelength λ. In that case, part of the incoming beam is deflected by an angle 2θ, producing a reflection spot in the diffraction pattern. The constructive diffracted X-rays are then detected, processes and counted. By scanning the samples through a range of 2θ angles, all possible diffraction directions of the lattice should be attained due to the random orientation of the powdered materials. Conversion of the diffraction peaks to interplanar *d*-spacing allows identification of phase because each phase has a set of unique interplanar *d*-spacing. Typically this is achieved by comparison of *d*-spacing with standard reference patterns. It is noteworthy to mention that crystallinity and density of atoms make sharper and higher intensity of reflection peck respectively.

3.6.4 Crystal Lattice Parameters by XRD

From the diffraction patterns of XRD, inter-planar spacing *d* of planes of crystalline materials can be easily calculated using Bragg's law. All detectable peaks also indexed as par planes from the standard reference data. At least two suitable planes from peak should be chosen as at least one of Miller indices *h, k,* and *l* value is fitted to zero for convenient calculation the value of lattice parameters. Then the values put in Lattice Geometry Equation according to the crystal structure of the studied materials. Lattice Geometry Equation of cubic, tetragonal and hexagonal crystal structures are shown below:

Cubic: $\frac{1}{d^2} = \frac{h^2 + k^2 + l^2}{a^2}$

Tetragonal: $\frac{1}{d^2} = \frac{h^2 + k^2}{a^2} + \frac{l^2}{c^2}$

Hexagonal: $\frac{1}{d^2} = \frac{4}{3}\left(\frac{h^2 + hk + k^2}{a^2}\right) + \frac{l^2}{c^2}$

The value of λ is 1.54056 Å for CuK_α radiation, θ is taken from the diffraction angle 2θ. During the calculation, angles should be precisely measured otherwise lattice values greatly vary. Putting the required values to the Bragg's law: $2d \sin\theta = n\lambda$

Inter-planar spacing *d* is calculated from the two chosen planes as at least one of Miller indices *h, k*, and *l* value of each plane is fitted to zero. Then obtaining two equations co-relate each other to find out the lattice parameters.

3.7 Differential Thermal Analysis (DTA)

Differential Thermal Analysis (DTA) of $Nd_{12.5}Fe_{80.6}B_{6.4}Ga_{0.3}Nb_{0.2}$ HDDR-treated powder was carried out to investigate the phase change during heating under different atmospheres with heating rate 7 °C/min. DTA is a technique in which the temperature change of the studied material is compared with a thermally inert material such as α-alumina on heating or cooling. The principle of method consists of measuring the change in temperature associated with physical or chemical changes indicated by endothermic or exothermic departure from the base line during the gradual heating of the substance. Thermal changes due to fusion, crystalline structure inversions, boiling, dissociation or decomposition reactions, oxidation and reduction reactions, destruction of crystalline lattice structure and other chemical reactions are generally accompanied by an appreciable rise or fall in temperature. Hence, all these are accounted in DTA. Generally speaking, phase transitions, dehydration, reduction and some decomposition reactions produce endothermic effects whereas crystallization, oxidation and some decomposition reactions produce exothermic effects. The real set-up and schematic diagram of DTA consisting of basic parts are shown in Fig. 3.11 (a) and (b) respectively. As can be seen that DTA consists of the several units; detection unit comprising furnace, thermocouple, sample holder and reference, temperature control unit with a specified program to control the furnace temperature as par requirement and data recording unit composed with amplifier, data recorder and programmed computer. The sample and the reference are placed symmetrically. Thermocouple is set for each of the sample and reference. A differential thermocouple is set to detect the temperature difference between the sample and reference. Also, the sample

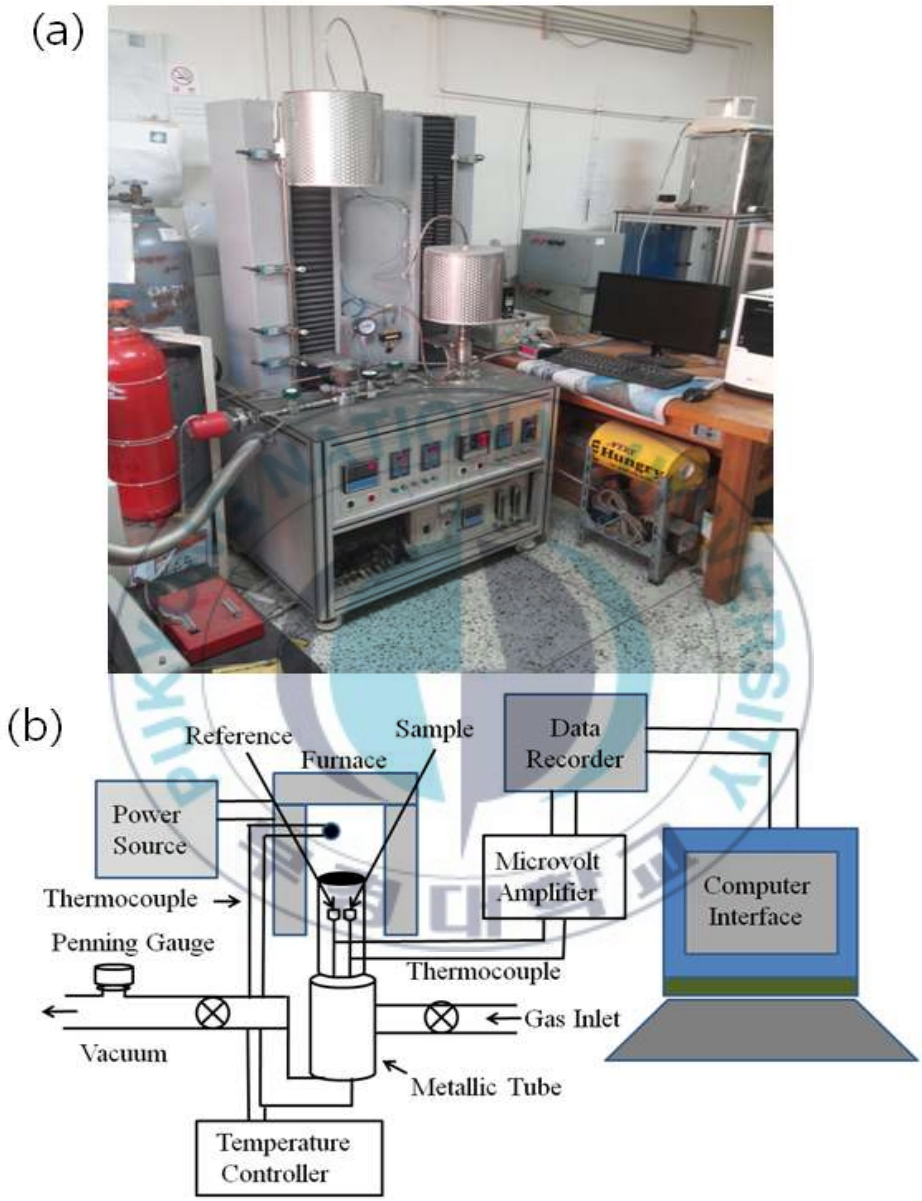

Fig. 3.11 (a) Real set-up and (b) schematic diagram of differential thermal analysis (DTA) showing the basic parts.

temperature is detected from the thermocouple on the sample area. The sample is contained in a small crucible made of materials such as alumina, Pyrex, silica, nickel or platinum and reference is also made of same materials for identical conditions. The furnace is connected to the temperature controller via thermocouple in order to obtain constant heating rate with a setting program. Samples holders with thermocouple are encompassed by a metallic tube with the connection of gas inlet and vacuum outlet line for making the desired atmosphere in the sample chamber. The differential thermocouple is connected to the microvolt amplifier to detect the small difference of ΔT. After suitable voltage amplification then ΔT signal is referred to the data recorder followed by programmed computer interface. ΔT is plotted on y-axis against time or temperature T on x-axis. The temperature of the sample is greater for an exothermic reaction, than that of the reference, for endothermic the sample temperature lags behind that of the reference. When no reaction occurs in the sample material, the temperature of the sample remains similar to that of reference substance. This is because both are being heated exactly under identical condition i.e. temperature difference ΔT (Ts–Tr) will be zero for no reaction. But as soon as reaction starts, the sample becomes either hot or cool depending upon whether the reaction is exothermic or endothermic.

3.8 Thermopiezic Analyser (TPA)

Desorption and absorption behavior of HDDR-treated materials was examined by thermopiezic analyser (TPA). The principle of TPA consists of measuring the pressure change with temperature in a fixed volume of closed chamber associated with desorption and absorption of the substance during the gradual heating. Sometimes desorption of the sample is monitored

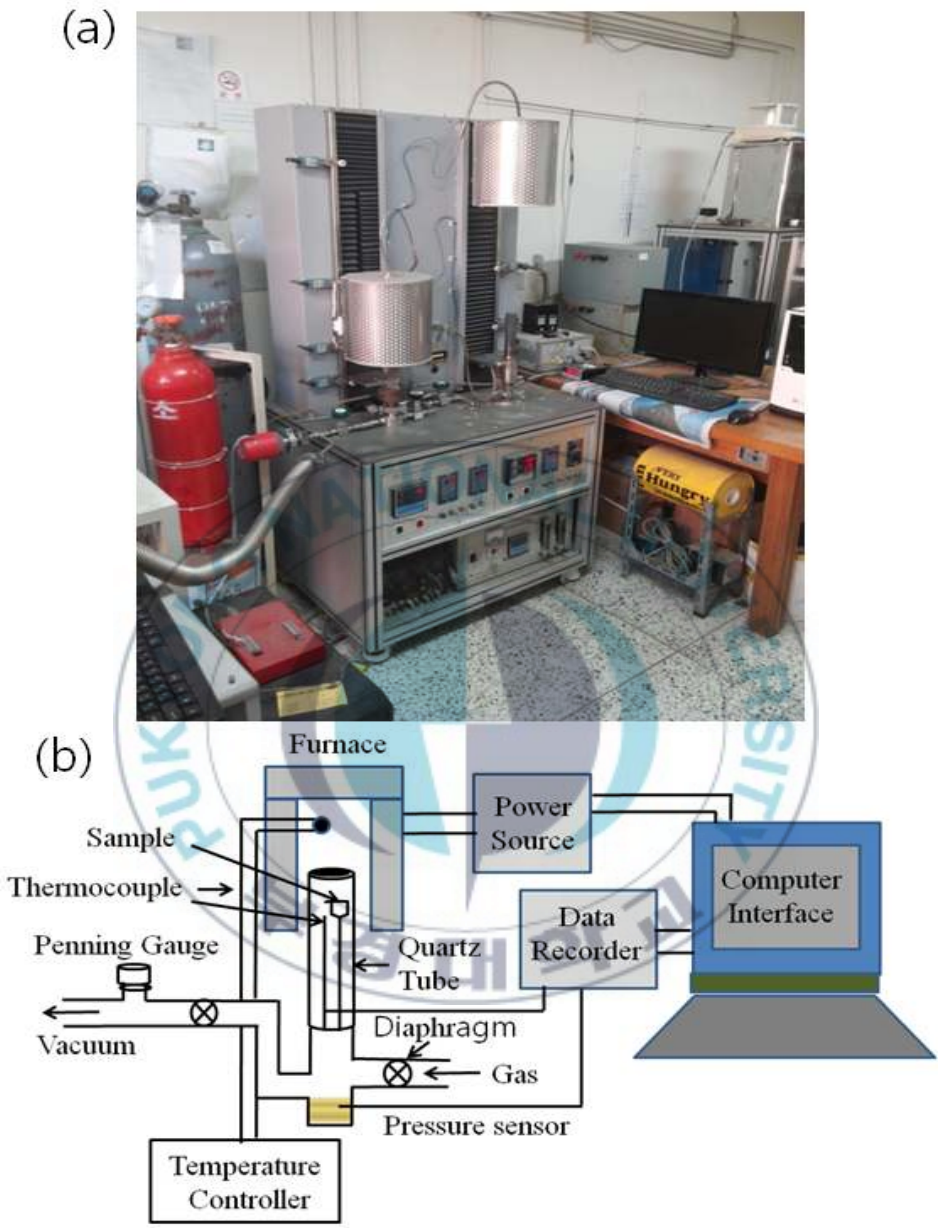

Fig. 3.12 (a) Real set-up and (b) schematic diagram of thermopiezic analyser (TPA).

continuously with vacuum gauge not closing vacuum outlet of the chamber on heating. The real set-up and schematic diagram of TPA consisting of basic parts are shown in Fig. 3.12 (a) and (b) respectively. There is one quartz tube covering the sample holder, thermocouple and pressure sensor. The tube is also connected to gas inlet along with diaphragm valve and vacuum outlet to make the necessary atmosphere and pressure inside the chamber. The sample is placed into the sample holder. The thermocouple and pressure sensor are connected to the programmed computer. An electric furnace is used to heat the sample chamber which is connected to the temperature controller via thermocouple to obtain required temperature and heating rate. Software of the computer plots pressure on y-axis against time or temperature on x-axis.

3.9 References

1. D. Book and I.R. Harris, J. Alloy Comp., vol. 221, pp. 187-192, 1995.
2. H. W. Kwon and J. H. Yu, Journal of Magnetics, vol. 14(4), pp.150 154, 2009.
3. http://www. shodhganga.inflibnet.ac.in/bitstream/10603/710/8/08...
4. http://www.hk-phy.org/atomic_world/tem/tem02_e.html

Chapter Four

A STUDY OF RESIDUAL HYDROGEN IN Nd-Fe-B-TYPE HDDR-TREATED MATERIAL

Abstract

Residual hydrogen in the $Nd_{12.5}Fe_{80.6}B_{6.4}Ga_{0.3}Nb_{0.2}$ HDDR-treated powder was investigated by hydrogen analysis and thermopeizic analyser (TPA). In spite of optimum HDDR treatment, HDDR-treated material contained significant amount of residual hydrogen (approx 1500 ppm). Desorption traces were also studied of the identical alloy ingot with no history of hydrogen and hydrogen decrepitated (HD) alloy with full hydrogen pick-up for comparison. Desorption trace for HDDR-treated material was in quite good agreement with HD materials although no desorption was traced for identical alloy ingot with no history of hydrogen. The HDDR-treated material was degassed by vacuum heating at different temperatures. It was found to decrease the value of hydrogen content with increasing the degassing temperature. Hydrogen content in the HDDR-treated material and pre-degassed material were determined by Hydrogen Determinator (LECO, RH-600). Desorption of residual hydrogen in the HDDR-treated material was also verified by the lattice shrinkage studied by XRD. Lattice parameters derived from the XRD patterns of HDDR-treated material were significantly higher than that of the tetragonal $Nd_2Fe_{14}B$ phase due to inclusion of hydrogen in $Nd_2Fe_{14}B$ phases.

Keywords:

HDDR, residual hydrogen, thermopeizic analyser (TPA), coercivity.

4.1 Introduction

Since the discovery in 1983, the $R_2Fe_{14}B$ (R stands rare earths) compounds had been extensively studied for their fundamentals aspects and their applications. Many studies had also been devoted to the analysis of the $R_2Fe_{14}B$-hydrogen systems because of easy accommodation of hydrogen in the $R_2Fe_{14}B$ structure to modify the physical properties of $R_2Fe_{14}B$. Alloys and inter-metallic compounds absorb large quantities of hydrogen for which hydrogen-metal system has become a very potential route for many practical applications [1-3]. One of the most important $R_2Fe_{14}B$-hydrogen system is the hydrogenation, disproportionation, desorption and recombination (HDDR) process developed by Takeshita and Nakyama in 1989 [4]. The HDDR process has received much attention over the last few years in the field of permanent magnets research. The HDDR process is an effective means of obtaining the ultrafine grain structure consisting of close to a single domain grain size (~300 nm for $Nd_2Fe_{14}B$) [5-7]. The HDDR process is in principle a strikingly simple method by utilizing a fully reversible hydrogen gas induced chemical reaction. The HDDR process consists of two steps, first one is hydrogenation-disproportionation (HD) treatment (typically described as $Nd_2Fe_{14}B + 2H_2 \rightarrow 2NdH_2 + 12Fe + Fe_2B$) and second one is desorption-recombination (DR) treatment (typically described as $2NdH_2 + 12Fe + Fe_2B \rightarrow Nd_2Fe_{14}B + 2H_2$) [8-10]. Nishiuchi et al. [10] reported that the hydrogen content did not come down to zero after the completion of optimum HDDR process. Afterwards, there are no detailed reports about the residual hydrogen in HDDR treated material and its consequences on magnetic performance on thermal processing the HDDR material. In this chapter, residual hydrogen in the HDDR-treated material and it's desorption in the course of heating are detailed to be discussed.

4.2 Experimental Work

Small alloy slabs with composition of $Nd_{12.5}Fe_{80.6}B_{6.4}Ga_{0.3}Nb_{0.2}$ in the form of (approx. 5 x 5 x 5 mm^3) were exposed to hydrogen (P_{H_2} = 1 bar) from room temperature, disproportionation was accomplished at 740 ℃ in hydrogen (P_{H_2} = 0.35 bar) for 3 hr. Desorption and recombination was accomplished at 820 ℃ for 40 min under vacuum. This HDDR-treated material (iHc =13.5 kOe, 100-150 μm) was used as a starting material for the present study. HDDR treatment is described in details in the third chapter namely apparatus and experimental procedure. Desorption behavior of the residual hydrogen in the HDDR-treated material was examined by vacuum gauge and TPA (thermopiezic analyser) hooked up pre-programmed computer software. 1.8 gm HDDR material was placed into an approximate fixed volume of 160 cm^3 TPA chamber and then heated up to 800°C at the rate of 7 °C /min. Desorption tests were also studied of identical alloy ingot with no history of hydrogen and with fully hydrogen decrepitated (HD) alloy for comparison. For full hydrogenation, the bulk alloy was heated up to 500 °C in 1 bar hydrogen. The HDDR-treated initial material was degassed by heating up to different temperatures in vacuum, and subsequently a hydrogen desorption was examined for the previously degassed material using vacuum gauge. Hydrogen content in the HDDR-treated initial material and pre-degassed material were determined by Hydrogen Determinator (LECO, RH-600). X-ray diffractometer (XRD) (Cu Kα radiation) was used to examine the lattice parameters in the HDDR-treated initial material and degassed material.

4.3 Results and Discussion

Desorption of residual hydrogen in the $Nd_{12.5}Fe_{80.6}B_{6.4}Ga_{0.3}Nb_{0.2}$ HDDR-treated material was studied by vacuum gauge and TPA, and the desorption trace was shown in Fig. 4.1. Also included in Fig. 4.1 is the hydrogen desorption trace for the identical composition of alloy ingot with fully hydrogenated and no history of hydrogen for comparison. For full hydrogenation, the bulk alloy was heated up to 500 °C in 1 bar hydrogen. It appears that the HDDR material showed similar hydrogen desorption pattern with that of the fully hydrogenated alloy except that the amount of desorbed hydrogen was much smaller. The residual hydrogen in the HDDR material was desorbed through three steps at specific temperatures around 200 °C, 300 °C, and 700 °C, respectively.

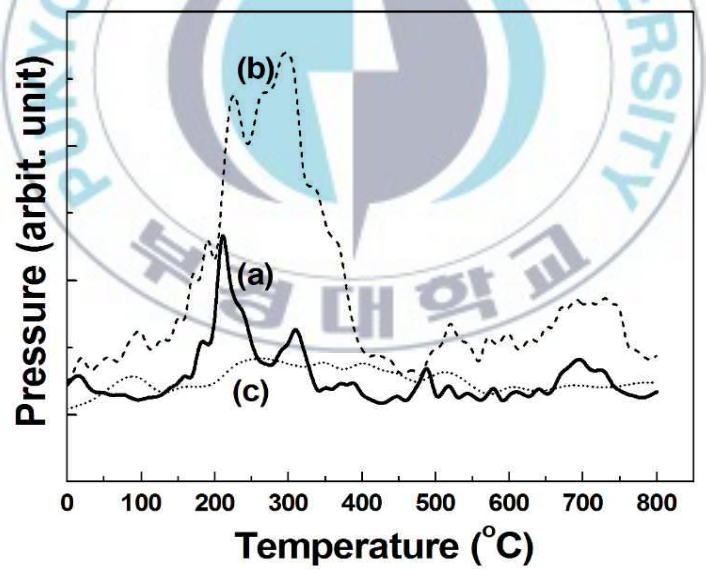

Fig. 4.1 Hydrogen desorption traces for $Nd_{12.5}Fe_{80.6}B_{6.4}Ga_{0.3}Nb_{0.2}$ (a) HDDR-treated material, (b) fully hydrogenated alloy ingot, and (c) alloy ingot no history of hydrogen.

Desorption at around 200 °C was corresponding to the hydrogen desorption due to the transition from $Nd_2Fe_{14}BH_x$ to $Nd_2Fe_{14}B$. The desorption events at 300 °C and 700 °C were corresponding to the hydrogen desorption due to the transition from $NdH_{2.7}$ to NdH_2, and NdH_2 to Nd, respectively [11, 12]. These results clearly indicated that the HDDR material contained a significant amount of hydrogen. The residual hydrogen is considered to be a common feature of Nd-Fe-B-type HDDR-treated material. Nishiuchi et al. [10] also reported previously that the hydrogen content did not come down to zero after the completion of optimum HDDR process.

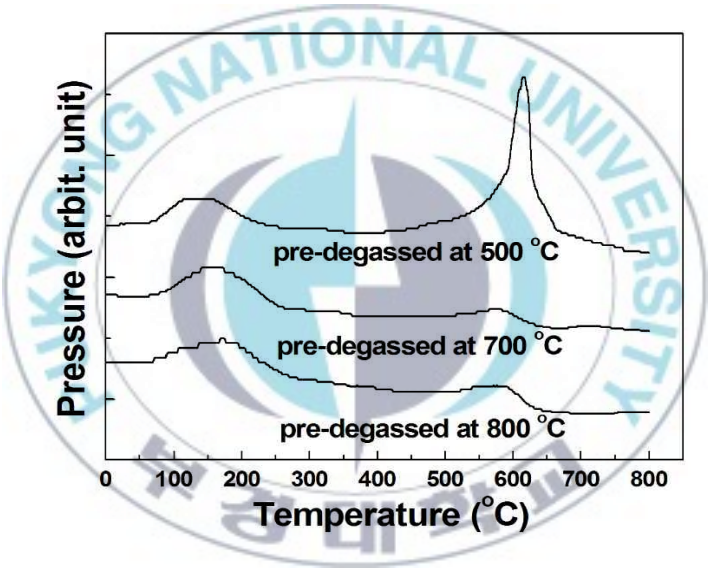

Fig. 4.2 Hydrogen desorption behavior of the $Nd_{12.5}Fe_{80.6}B_{6.4}Ga_{0.3}Nb_{0.2}$ HDDR-treated material pre-degassed at different temperatures.

The amount of Nd-rich phase in the present alloy is considered to be fairly small due to the slightly over stoichiometric composition. Therefore, it is more or less reasonable to assume that most of the hydrogen in the HDDR-treated material may exist in the $Nd_2Fe_{14}B$-type magnetic phase as form of $Nd_2Fe_{14}BH_x$. The HDDR-treated initial material was degassed by heating up

to different temperatures in vacuum, and subsequently a hydrogen desorption was examined for the previously degassed material up to 800 °C using vacuum gauge and results are shown in Fig. 4.2. The residual hydrogen was degassed markedly by heating above 700 °C, but it seems that complete removal of the residual hydrogen is impossible even after heating up to 800 °C in vacuum.

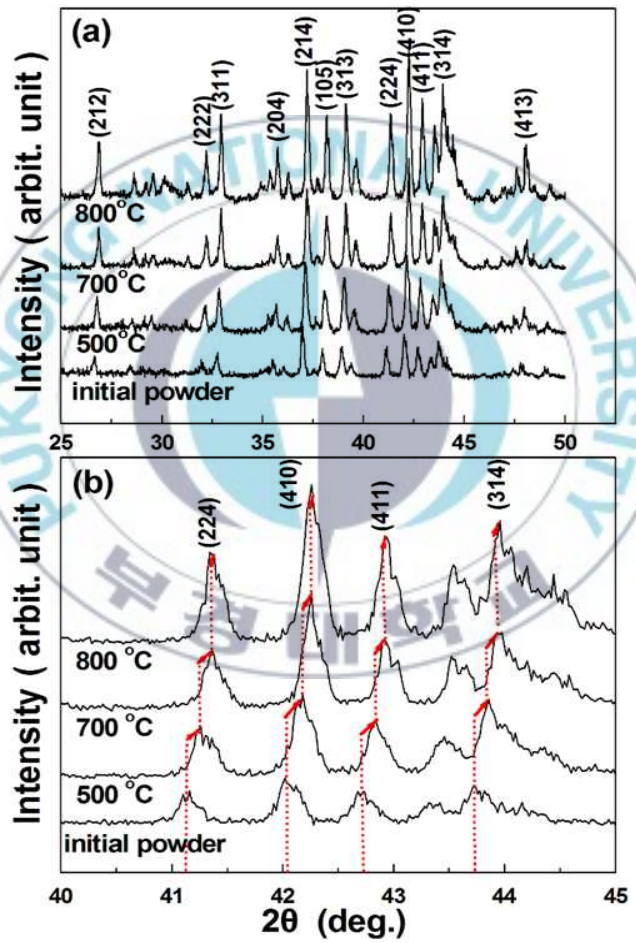

Fig. 4.3 (a) XRD patterns of $Nd_{12.5}Fe_{80.6}B_{6.4}Ga_{0.3}Nb_{0.2}$ HDDR-treated material degassed at different temperatures and (b) close-up highlighting the angle shift.

Degassing of the residual hydrogen was verified by the lattice shrinkage studied by XRD. Fig. 4.3 shows XRD patterns of the materials degassed at different conditions. It can be seen that diffraction peaks were shifted toward higher angle as the degassing temperature increases, indicating that the expanded lattice of the tetragonal $Nd_2Fe_{14}B$-type phase in the initial material was shrunk by the degassing.

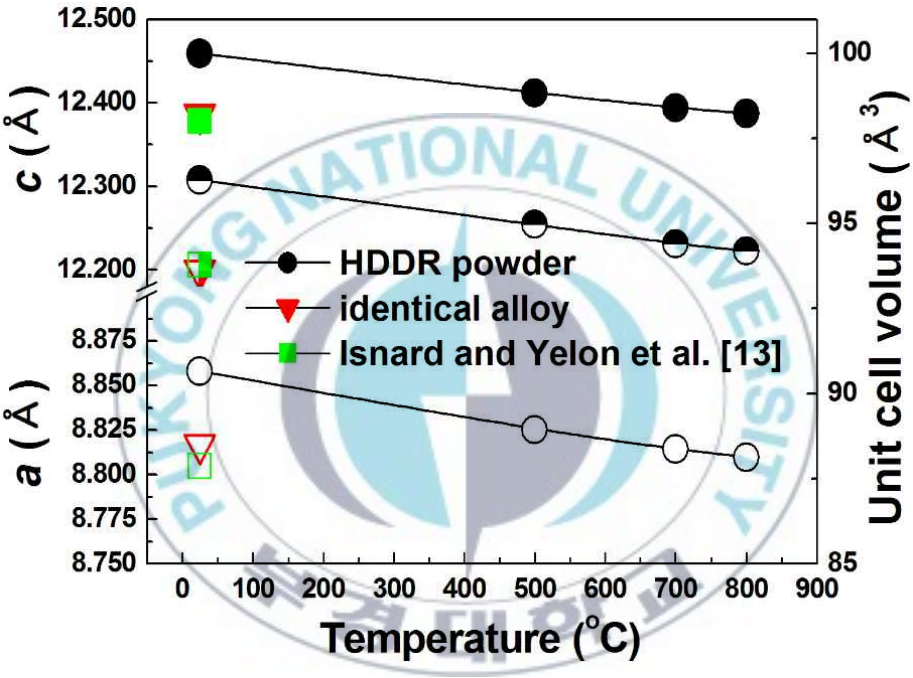

Fig. 4.4 Variation of lattice parameters *a* (blank symbol) and *c* (half filled symbol) with unit cell volume (filled symbol) of Nd-Fe-B-type HDDR-treated material as a function of dehydrogenation temperature also included identical arc-melted annealed alloy and the values obtained by Isnard and Yelon et al. of $Nd_2Fe_{14}B$ phase as Ref. [13].

It was also found that lattice parameters derived from the XRD patterns of HDDR-treated material *a* (8.858 Å) and *c* (12.3076 Å) were significantly

higher than the values of tetragonal $Nd_2Fe_{14}B$ phase *a* (8.805 Å) and *c* (12.2050 Å) due to inclusion of hydrogen in $Nd_2Fe_{14}B$ phases. The lattice parameters *a* and *c* with unit cell volume of the HDDR-treated material also decreased with increasing dehydrogenation temperature shown in Fig. 4.4. Also included in Fig. 4.4 are the lattice constants of identical arc-melted annealed alloy with no history of hydrogen and the values of $Nd_2Fe_{14}B$ obtained by Isnard and Yelon et al. [13] as a Ref. It was seen that lattice parameters of identical alloy and the values of Isnard and Yelon et al. were almost similar with little higher value of lattice *a* (8.8168 Å) of identical alloy than lattice *a* (8.805 Å) of Isnard and Yelon et al. The variations of lattice parameter suggest that HDDR-treated material contained significant amount of residual hydrogen and the material was remarkably degassed with the desorption temperature.

The values of lattice constants of $Nd_{12.5}Fe_{80.6}B_{6.4}Ga_{0.3}Nb_{0.2}$-type HDDR material treated in different conditions are also shown in the Table 4.1. Lattice constant variations for the materials treated in different conditions were due largely to the inclusion and desorption of residual hydrogen in the HDDR-treated material. Finally, the amount of the residual hydrogen in the HDDR powder was measured to be approximately 1500 ppm. It was found that the hydrogen content decreased with increasing the degassing temperature. The hydrogen analysis results determined by Hydrogen Determinator (LECO, RH-600) are shown in Table 4.2. The results show that hydrogen content decreased from 1500 ppm to 1200 ppm with the degassing temperature up to 750 °C. As it was mentioned earlier that most of the hydrogen in the HDDR-treated material may exist in the $Nd_2Fe_{14}B$-type magnetic phase as form of $Nd_2Fe_{14}BH_x$. Based on this assumption the

stoichiometry of the $Nd_2Fe_{14}BH_x$ was calculated and also shown in the Table 4.2.

Table 4.1. Lattice parameters variations of $Nd_{12.5}Fe_{80.6}B_{6.4}Ga_{0.3}Nb_{0.2}$ materials in different conditions.

MATERIALS CONDITIONS	LATTICE a (Å)	LATTICE c (Å)	UINIT CELL VOLUME V $(Å)^3$
$Nd_{12.5}Fe_{80.6}B_{6.4}Ga_{0.3}Nb_{0.2}$ HDDR-treated powder	8.8580	12.3076	965.71
HDDR-treated powder degassed up to 500 °C	8.8253	12.2547	954.47
HDDR-treated powder degassed up to 700 °C	8.8144	12.2317	950.23
HDDR-treated powder degassed up to 800 °C	8.8098	12.2226	948.63
$Nd_{12.5}Fe_{80.6}B_{6.4}Ga_{0.3}Nb_{0.2}$ Alloy	8.8168	12.1999	948.37
$Nd_2Fe_{14}B$ (Ref. Prof. Yelon)	8.8050	12.2060	946.307

Table 4.2. Hydrogen content and stoichiometry of the HDDR-treated materials in different conditions.

MATERIALS CONDITIONS	HYDROGEN CONTENT (ppm)	STOICHIOMETRY
$Nd_{12.5}Fe_{80.6}B_{6.4}Ga_{0.3}Nb_{0.2}$ HDDR-treated powder	1500	$Nd_2Fe_{14}BH_{1.6}$
HDDR-treated powder degassed up to 600 °C	1100	$Nd_2Fe_{14}BH_{1.2}$

The present study suggests that the HDDR-treated material contained significant amount of residual hydrogen after optimum HDDR process. The residual hydrogen can be degassed by heating in vacuum but complete removal of the residual hydrogen was almost impossible maintaining the magnetic performance of the powder.

4.4 Conclusion

$Nd_{12.5}Fe_{80.6}B_{6.4}Ga_{0.3}Nb_{0.2}$ HDDR powder contained significant amount of residual hydrogen (approximately 1500 ppm). The amount of Nd-rich phase in the present alloy is considered to be fairly small due to the slightly over stoichiometric composition. Therefore, it is more or less reasonable to assume that most of the hydrogen in the HDDR-treated material may exist in the $Nd_2Fe_{14}B$-type magnetic phase as form of $Nd_2Fe_{14}BH_x$. The HDDR-treated initial powder was degassed by vacuum heating at different temperatures. It was found that the residual hydrogen was degassed markedly by heating above 700 °C, but complete removal of the residual hydrogen was impossible keeping the magnetic performance.

4.5 References

1. O Gutfleisch, J. Phys. D: Appl. Phys., vol. 33, pp. 157-172, 2000.
2. Durst K-D, Kronmu¨ller H. “Proceedings of the 4th International Symposium on Magnetic Anisotropy and Coercivity in RETM alloys,” Dayton, OHIO: University of Dayton; 1985, pp. 725–35.
3. Adler E, Hamann P. “Proceedings of the 4th International Symposium on Magnetic Anisotropy and Coercivity in RETM alloys,” Dayton, OHIO: University of Dayton; 1985, pp. 747-60.

4. T. Takeshita and R. Nakayama, “Proceedings 10th International Workshop on RE Magnets and Their Applications,” Kyoto, 1989, unpublished, vol. 1, p. 551.
5. O. M. Ragg, I. R. Harris, H. Nagel and P. Bohm, IEEE Trans. Magn., vol. 32 (5), pp. 4395-4397, 1996.
6. W. F. Li, T. Ohkubo, K. Hono, T. Nishiuchi, and S. Hirosawa, Appl. Phys. Lett., vol. 93, p. 052505, 2008.
7. N. Nozawa, H. Sepehri-Amin, T. Ohkubo, K. Hono, T. Nishiuchi and S. Hirosawa, J. Magn. Magn. Mater., vol. 323, pp. 115-121, 2011.
8. P. J. McGuiness, X. J. Zhang, X. J. Yin and I. R. Harris, J. Less-Common Metals, vol. 158, pp. 359-365, 1990.
9. T. Takeshita, J. Alloys Comp., vol. 231, pp. 51-59, 1995.
10. Takeshi Nishiuchi, Satoshi Hirosawa, Masaki Nakamura, Masatoshi Kakimoto, Takeshi Kawabayashi, Hideki Araki and Yasuharu Shirai, IEEE, IEEJ Trans., vol. 3, pp. 390-393, 2008.
11. D. Book and I.R Harris, J. Alloy Comp., vol. 221, pp. 187-192, 1995.
12. M. Zakotnik, I. R. Harris and A. J. Williams, J. Alloy Comp., vol. 450, pp. 525-531, 2008.
13 O. Isnard, W. B. Yelon, S. Miraglia, and D. Fruchart, J. Appl. Phys., vol. 78, p. 1892, 1995.

Chapter Five

EFFECT OF RESIDUAL HYDROGEN ON COERCIVITY OF HEATED Nd-Fe-B-TYPE HDDR-TREATED MATERIAL

Abstract

The effect of residual hydrogen on coercivity of the $Nd_{12.5}Fe_{80.6}B_{6.4}Ga_{0.3}Nb_{0.2}$ HDDR-treated material was studied on heating. The HDDR-treated initial and pre-degassed materials were heated in Ar or in vacuum with distinctively different pumping out speed. In spite of no significant coercivity variation on heating the HDDR-treated initial material in a high pumping speed vacuum, coercivity was radically reduced at around or above 650 °C in a low pumping speed vacuum or in Ar atmosphere. The markedly different coercivity deterioration particularly at an elevated temperature in Ar or in vacuum with different pumping speed was due largely to the residual hydrogen in the HDDR-treated material. On the contrary, the coercivity variations for pre-degassed HDDR material were almost identical regardless of atmosphere or pumping speed of the heating chamber. The coercivity of the HDDR-treated material was profoundly influenced by the residual hydrogen and how it was evacuated on heating. The radical coercivity reduction above 650 °C is believed to be attributed to the disproportionation of the $Nd_2Fe_{14}BH_x$ caused by the residual hydrogen in the HDDR-treated material.

Keywords:

HDDR, residual hydrogen, desorption, disproportionation, coercivity.

5.1 Introduction

The key feature of Nd-Fe-B-type HDDR (hydrogenation, disproportionation, desorption and recombination)-treated material is the unique microstructure consisting of ultra fine $Nd_2F_{14}B$ grains, of which size is close to a single domain size (~300 nm for $Nd_2F_{14}B$) [1-6]. This fine grain structure can be exploited for achieving high performance, in particular high coercivity in permanent magnet [7-11]. But the poor thermal stability is the great concern for the HDDR-treated material [12, 13]. The Nd-Fe-B-type HDDR-treated powder lost the coercivity radically on heating to an elevated temperature. Coercivity loss in the HDDR-treated material was profound by heating in Ar or in a less effective vacuum system. Coercivity of the HDDR-treated material was influenced significantly by many factors, such as temperature, heating rate, evacuating speed, environment, and others. This radical coercivity reduction is considered to be one of the technical barriers for thermal processing of the HDDR-treated material without losing the permanent magnetic performance. It is important in technological point of view, therefore, to fully understand the cause of radical coercivity reduction on heating of HDDR-treated material. The Nd-Fe-B-type HDDR-treated material contained significant amount of residual hydrogen (1500 ppm). This residual hydrogen may exist in the form of $Nd_2Fe_{14}BH_x$ hydride in the powder which might have disproportionated into α-Fe, Fe_2B and NdH_2 phases particularly in a system where hydrogen is not desorbed effectively on heating. The effect of the residual hydrogen on coercivity of the HDDR-treated material during heating is to be discussed details in this chapter.

5.2 Experimental Work

The starting material used in the present study is the $Nd_{12.5}Fe_{80.6}B_{6.4}Ga_{0.3}Nb_{0.2}$ HDDR-treated material (iHc =13.5 kOe). The HDDR-treated material was heated over a temperature range from 500 °C to 800 °C with heating rate 25 °C/min in Ar atmosphere or in vacuum with different pumping speed. The heating apparatus were shown in the chapter three (Fig. 3.4 and 3.5). The HDDR-treated powder was also degassed by vacuum heating up to 800 °C. Previously degassed HDDR-treated materials were also subjected to the heating in Ar or in vacuum with different pumping speed. The out-gassing speed from the heating chamber was controlled by adjusting the pumping out-let diameter in the vacuum system. Magnetic characterization of the materials was undertaken by means of vibrating sample magnetometer (VSM) with a maximum field of 12 kOe. Prior to the VSM measurement, the samples were wax bonded and then magnetized in 4.5 T pulsing field. X-ray diffraction (XRD) (Cu-K_α radiation) was used for studying the phase change due to the disproportionation of $Nd_2Fe_{14}BH_x$ in HDDR-treated powder during heating in various conditions. Desorption and absorption behavior of the HDDR-treated material was examined by TPA (thermopiezic analyser) up to 800 °C. Differential thermal analysis (DTA) was carried out to investigate the phase change in the material during heating under different atmospheres. Morphology of the heated specimens was observed by SEM.

5.3 Results and Discussion

The $Nd_{12.5}Fe_{80.6}B_{6.4}Ga_{0.3}Nb_{0.2}$HDDR-treated initial material was heated over the temperature range from 500°C to 800°C under vacuum. It is noted that

the vacuum system used in the present study had distinctively different pumping out speed. The coercivity was measured of the heated specimens and results were shown in Fig. 5.1.

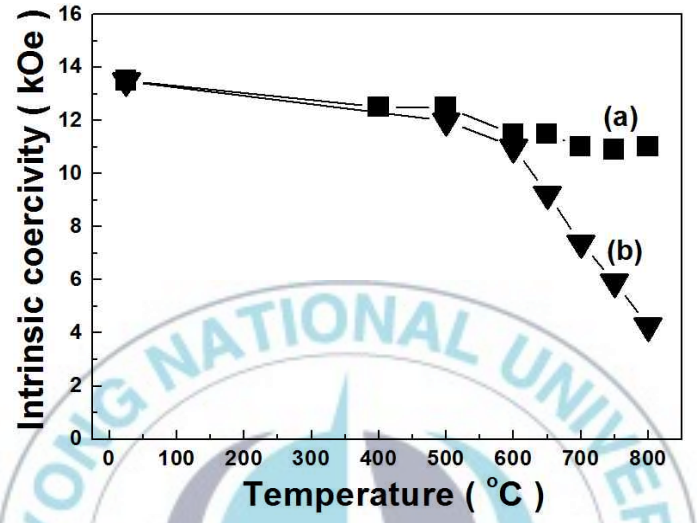

Fig. 5.1 Coercivity variation of $Nd_{12.5}Fe_{80.6}B_{6.4}Ga_{0.3}Nb_{0.2}$ HDDR-treated initial material (a) heated in high pumping speed (b) heated in low pumping speed vacuum.

It was noticed that the pumping speed of vacuum influenced the coercivity of the heated HDDR-treated material profoundly. As can be seen in Fig. 5.1, the HDDR-treated material showed quite different coercivity reduction behavior depending on the pumping speed in the course of heating. The material heated in the high pumping speed system showed gradual and inconsiderable decrease the coercivity. On the contrary, the material heated in the slow pumping speed system showed a radical coercivity reduction in the temperature range over 650 °C.

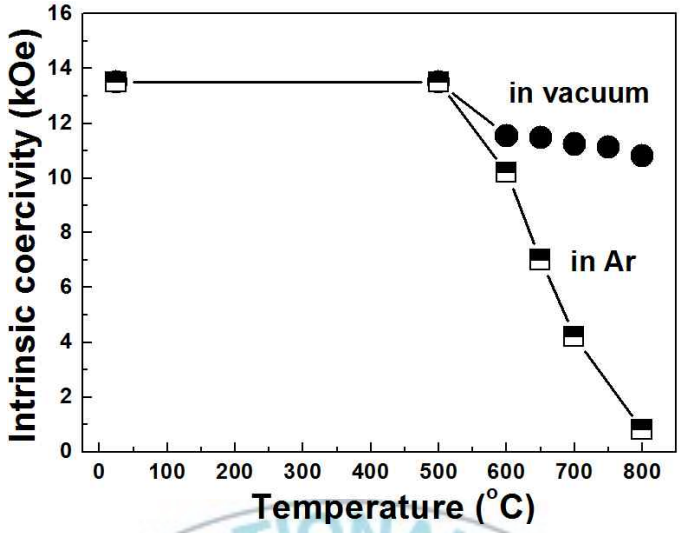

Fig. 5.2 Coercivity variation of $Nd_{12.5}Fe_{80.6}B_{6.4}Ga_{0.3}Nb_{0.2}$ HDDR-treated material heated under vacuum or Ar atmosphere.

The $Nd_{12.5}Fe_{80.6}B_{6.4}Ga_{0.3}Nb_{0.2}$ HDDR-treated material was also heated in vacuum and Ar atmosphere over the temperature range from 500 °C to 800 °C. The coercivity was measured at room temperature after heat treatment, and results were shown in Fig. 5.2. It appears that coercivity of the powder was reduced significantly above 600 °C, and interestingly, the coercivity reduction was much more profound for the material heated in Ar atmosphere than in vacuum.

One of the possible reasons for coercivity reduction would be an excessive grain growth caused by the heating at elevated temperature. However, this is not the case. The microstructure of the HDDR-treated materials heated up to 800 °C in Ar or vacuum with different pumping speed showed no appreciable difference in overall grain structure. Microstructure observed by SEM was shown in Fig. 5.3. It is natural to see no appreciable difference in

grain structure into the materials because the material were subjected to the same thermal profile regardless the atmosphere or pumping speed of vacuum system.

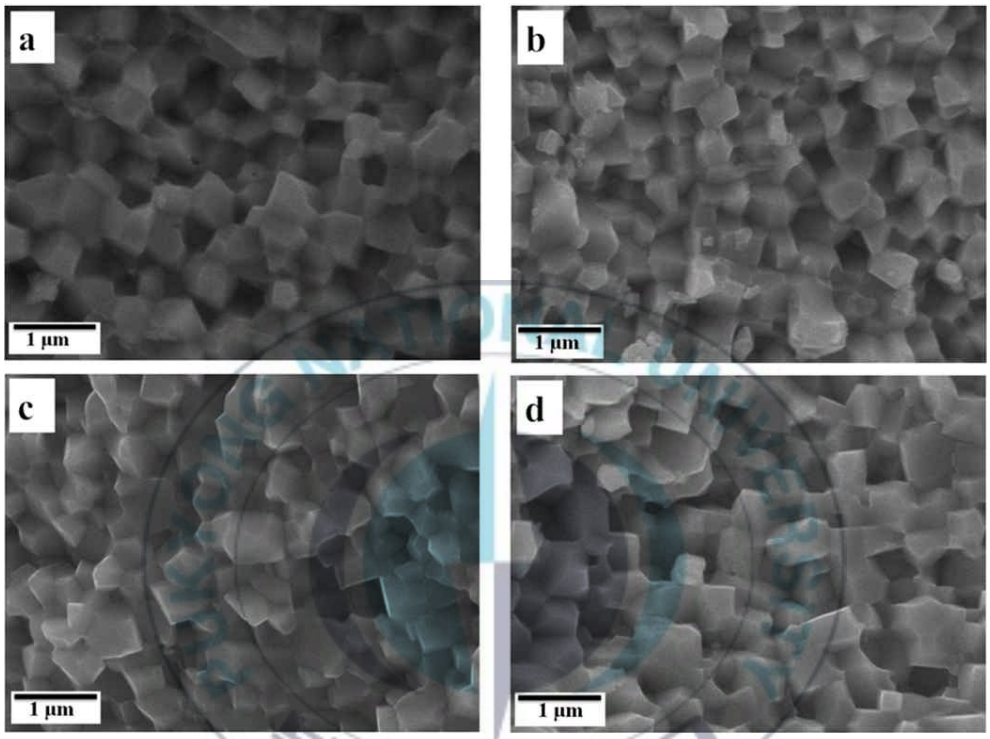

Fig. 5.3 SEM micrographs showing the grain structure of $Nd_{12.5}Fe_{80.6}B_{6.4}Ga_{0.3}Nb_{0.2}$ HDDR treated (a) initial material, (b) heated up to 800 °C in high pumping speed vacuum, (c) heated up to 800 °C in slow pumping speed vacuum, and (d) heated up to 800 °C in Ar atmosphere.

It is quite certain that grain coarsening was not the cause for the radical coercivity reduction on heating in Ar atmosphere or in vacuum with a slow pumping speed. The markedly different coercivity deterioration particularly at an elevated temperature in Ar or in vacuum system with different pumping

speed implies that the coercivity was affected profoundly by the residual hydrogen and how it was evacuated during heating. It was reported that the hydrogen from the HDDR-treated material was not fully removed after optimum HDDR process [14]. The HDDR-treated material contained significant amount of residual hydrogen [12]. The residual hydrogen may be desorbed more effectively in the course of heating in a high pumping speed than Ar atmosphere or slow pumping speed vacuum chamber. It is thought that residual hydrogen may exist in the form of $Nd_2Fe_{14}BH_x$ in the powder. This hydride might have disproportionated into α-Fe, Fe_2B and NdH_2 phases due to complexity of the residual hydrogen desorption in Ar or slow pumping speed vacuum system. Because the coercivity started to decrease at around 650 °C for both the cases which is the typical onset disproportionation temperature (650 °C) of the $Nd_2Fe_{14}BH_x$ hydride [15, 16].

Desorption and disproportionation of $Nd_2Fe_{14}BH_x$ hydride in HDDR-treated material during heating was simulated using TPA. The HDDR-treated material (1.8 gm) was placed in the TPA reaction chamber with a small fixed volume of 160 cm^3. The reaction chamber was evacuated and then back-filled with Ar gas to 15 mbar. Pressure change with temperature in the chamber was monitored, and the result was shown in Fig. 5.4. The pressure presented in Fig. 5.4 indicates genuine hydrogen partial pressure after subtracting the pressure increase due to thermal expansion of the back-filled Ar gas. It appears that the pressure increased up to 630 °C with slight flat around 250 °C (a), and then it was followed by radical pressure decrease up to 750 °C (b). Eventually, the pressure again started to increase above 750 °C (c). As the material was heated in small closed chamber in vacuum, the residual hydrogen was released and confined in the chamber. The confined hydrogen may, therefore, react again as the temperature increases.

The pressure increase and the flat up to 630 °C may be due to dehydrogenation of the HDDR powder and slight rehydrogenation of the desorbed hydrogen with the powder. The pressure drop from 630 °C to 750 °C may be due to partial disproportionation of the $Nd_2Fe_{14}BH_x$ phase, which absorbs additional hydrogen. This disproportionation temperature seems to be significantly higher than the usual disproportionation temperature (around 650 °C) of the $Nd_2Fe_{14}BH_x$ hydride. This may be due to lower hydrogen pressure in the TPA reaction chamber. Because disproportionation temperature is greatly influenced by many factors, hydrogen pressure is one of them [16-18]. The pressure increase above 750 °C may be due to partial recombination of the disproportionated phases, releasing hydrogen.

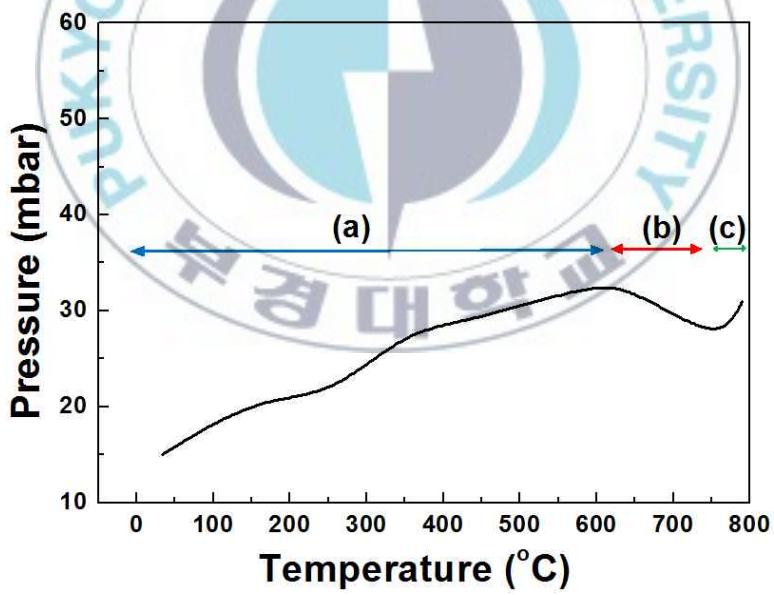

Fig. 5.4 TPA trace showing the hydrogen desorption and absorption of $Nd_{12.5}Fe_{80.6}B_{6.4}Ga_{0.3}Nb_{0.2}$ HDDR-treated material in closed system.

Disproportionation of the $Nd_2Fe_{14}BH_x$ hydride in the sample heated in Ar was verified by XRD phase analysis. Fig. 5.5 shows XRD patterns of initial HDDR powder and powder heated up to 800 °C in Ar atmosphere. Patterns were almost similar except that Fe_2B and α-Fe phases existed along with

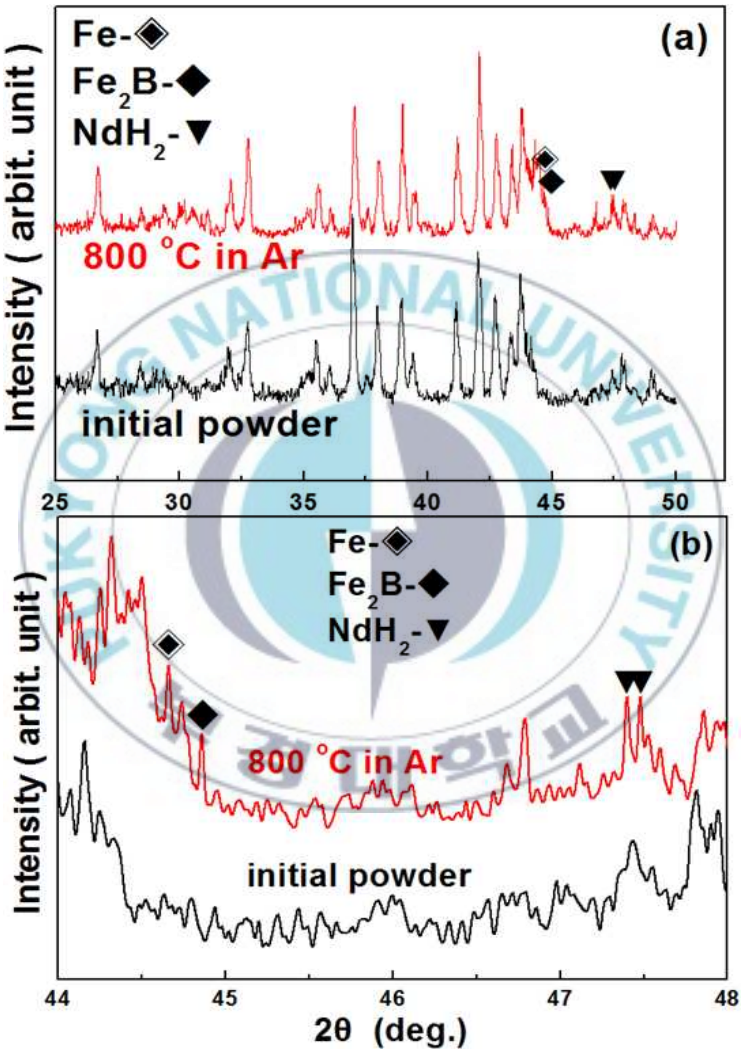

Fig. 5.5 (a) XRD patterns of initial $Nd_{12.5}Fe_{80.6}B_{6.4}Ga_{0.3}Nb_{0.2}$ HDDR-treated material and material heated up to 800 °C in Ar atmosphere, and (b) close-up highlighting the presence of disproportionated NdH_2, α-Fe and Fe_2B phases.

NdH_2 in the powder heated in Ar. It is believed that the radical coercivity reduction in Ar atmosphere heating above 600 °C is attributed to the presence of the soft magnetic phases, α-Fe and Fe_2B formed via disproportionation of the $Nd_2Fe_{14}BH_x$ caused by the residual hydrogen in the HDDR-treated material.

DTA also verified the disproportionation of the $Nd_2Fe_{14}BH_x$ hydride in the sample heated in Ar. As can be seen in Fig. 5.6, while no thermal event was found in the course of heating in vacuum, a noticeable exothermic event occurred at the temperature range of 620 °C - 655 °C in the course of heating in Ar atmosphere. This exothermic event is believed to be corresponding to the disproportionation of the $Nd_2Fe_{14}BH_x$ hydride in the HDDR-treated material.

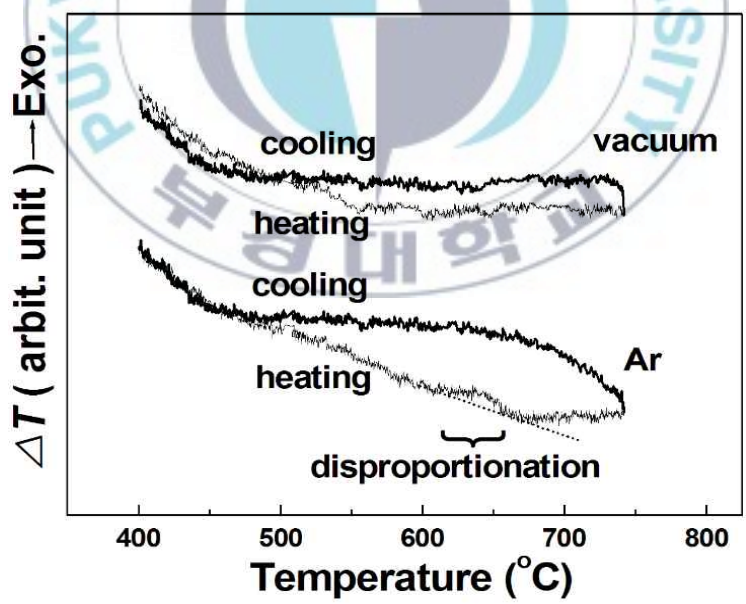

Fig. 5.6 DTA results for the $Nd_{12.5}Fe_{80.6}B_{6.4}Ga_{0.3}Nb_{0.2}$ HDDR-treated material in different atmospheres.

The present study suggests that the radical coercivity reduction of the HDDR-treated material during heating in Ar or in vacuum with slow pumping speed system is due largely to the residual hydrogen. It was found that coercivity reduction was less profound and inconsiderable where residual hydrogen is desorbed effectively on heating particularly in vacuum with high pumping out speed system. Then, it would be expected that the HDDR-treated material may show similar coercivity variation during heating regardless of the atmosphere or pumping speed of vacuum system if the residual hydrogen is degassed previously.

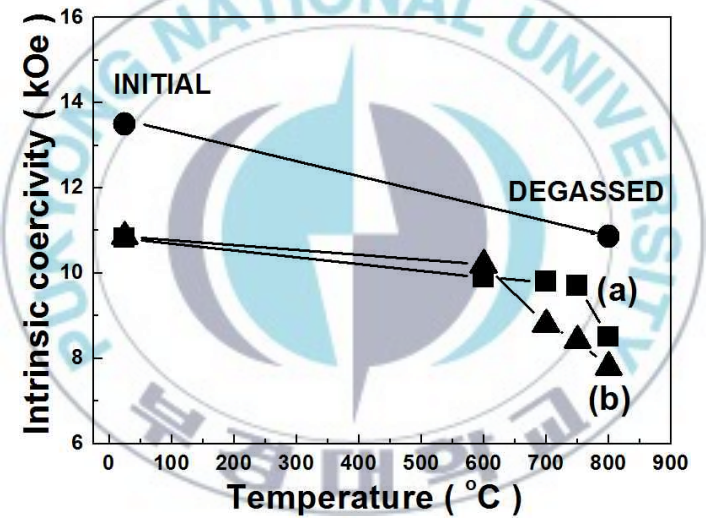

Fig. 5.7 Coercivity variations of the $Nd_{12.5}Fe_{80.6}B_{6.4}Ga_{0.3}Nb_{0.2}$ HDDR-treated material previously degassed by heating up to 800 °C (a) heated in high pumping speed, and (b) heated in slow pumping speed vacuum.

In order to see whether the previously degassed powder show similar coercivity variation during heating regardless of the pumping speed of the vacuum system, the degassed material (by heating up to 800 °C under

vacuum) was heated in vacuum with different pumping speed, and the coercivity variations were shown in Fig. 5.7. Also included in Fig. 5.7 are the coercivity values in initial HDDR-treated material and in degassed state for comparison.

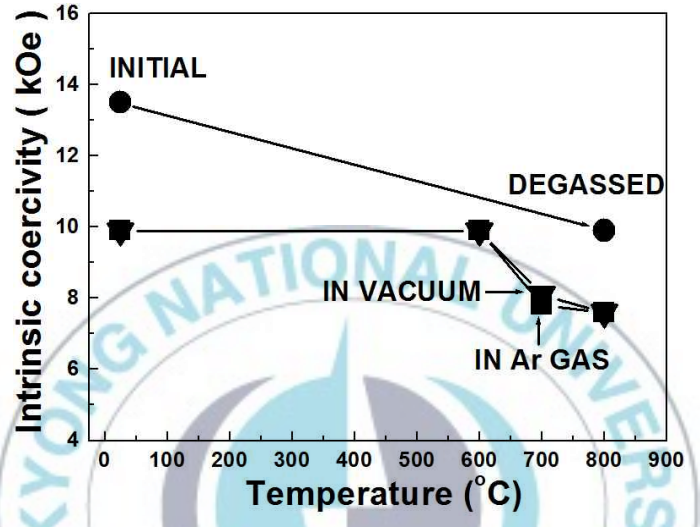

Fig. 5.8 Coercivity variations of the $Nd_{12.5}Fe_{80.6}B_{6.4}Ga_{0.3}Nb_{0.2}$ HDDR-treated material previously degassed by heating up to 800 °C.

It can be seen that coercivity variation of the previously degassed material in the course of heating is almost identical regardless of the pumping speed of vacuum system. Considering the radical coercivity reduction in the initial powder heated in slow pumping speed vacuum (Fig.5.1), the identical coercivity variation of the previously degassed material regardless of the pumping speed of the vacuum is somewhat striking. The coercivity variations of the previously degassed material were also verified in the course of heating in Ar or in vacuum. The results were shown in the Fig. 5.8. The coercivity variations were almost similar regardless of the atmosphere.

Although, HDDR-treated initial powder lost the coercivity radically in Ar atmosphere compared to the vacuum heating (Fig.5.2).

The above findings suggest that residual hydrogen was somehow associated with the radical coercivity reduction on heating of the HDDR-treated material. The pre-degassed HDDR-treated material contained less amount of residual hydrogen compared to the HDDR-treated initial material. That's why coercivity variations were almost identical for the pre-degassed HDDR-treated material regardless of the atmosphere or vacuum system of heating chamber. On the other hand, markedly different coercivity deterioration was noticed for the HDDR-treated initial material depending on the effective desorption of residual hydrogen in the course of heating.

5.4 Conclusion

Coercivity of the $Nd_{12.5}Fe_{80.6}$ $B_{6.4}Ga_{0.3}Nb_{0.2}$ HDDR-treated material was reduced significantly by heating around 650 °C or above, in Ar atmosphere or in vacuum with a slow pumping speed system. On the contrary, coercivity variations were gradual and inconsiderable on heating in vacuum with high pumping speed system. This fact was due to the residual hydrogen in the HDDR-treated material. The residual hydrogen existed in the form of $Nd_2Fe_{14}BH_x$ hydride, and it was disproportionated into α-Fe, Fe_2B and NdH_2 phases at an elevated temperature particularly in a system where residual hydrogen is not desorbed effectively during heating. This residual hydrogen-related disproportionation was responsible for the coercivity reduction attributed to the magnetically soft α-Fe, Fe_2B phases. The coerecivity variations of the pre-degassed HDDR-treated material were almost identical regardless of the atmosphere or vacuum system of heating chamber. The

HDDR-treated initial material had more residual hydrogen than pre-degassed material. Hence, coercivity deterioration was markedly different for the initial HDDR-treated material compared to the degassed powder. The findings of the present study are closely associated with residual hydrogen which almost certainly affects the coercivity of HDDR-treated material during heating.

5.5 References

1. T. Takeshita and R. Nakayama, "Proceedings 10th Int. Workshop on RE Magnets and Their Applications," Kyoto, 1989, vol. 1, p. 551.
2. P. J. McGuiness, X. J. Zhang, X. J. Yin and I. R. Harris, J. Less-Common Metals, vol. 158, pp. 359-365, 1990.
3. W. F. Li, T. Ohkubo, K. Hono, T. Nishiuchi and S. Hirosawa, Appl. Phys. Lett., vol. 93, p. 052505, 2008.
4. O. Gutfleisch, M. Matzinger, J. Fidler, and I. R. Harris, J. Magn. Magn. Mater. vol. 147, pp. 320-330, 1995.
5. O. Gutfleisch, N. Martinez, M. Verdier, and I. R. Harris, J. Alloys Comp., vol. 215, pp. 227-233, 1994.
6. Takuo Takeshita, J. Alloys Comp., vol. 231, pp. 51-59, 1995.
7. O. M. Ragg, I. R. Harris, H. Nagel and P. Bohm, IEEE Trans. Magn., vol. 32 (5) pp. 4395-4397, 1996.
8. K. Morimoto, E. Niizuma, K. Igarashi, K. Mori, M. Watanabe and R. Nakayama, J. Magn. Magn.Mater., vol. 265, pp. 345-351, 2003.
9. N. Nozawa, H. Sepehri-Amin, T. Ohkubo, K. Hono, T. Nishiuchi and S. Hirosawa, J. Magn.Magn.Mater., vol. 323, pp. 115-121, 2011.
10. E. Estevez, J. Fidler, C. Short and I. R. Harris, J. Phys. D: Appl. Phys., vol. 29, pp. 951-956, 1996.

11. O. Gutfleisch, A. Kirchner, W. Grunberger, D. Hinz, H. Nagel, P. Thompson, J. N. Chapman, K. H. Muller, L. Schultz and I. R. Harris, J. Phys. D: Appl. Phys., vol. 31, pp. 807–811, 1998.
12. Md. Abdul Matin, Hae-Woong Kwon, Jung-Goo Lee, Ji-HunYu, Tae Hoon Kim , and Cheol-Woong Yang, IEEE Trans. Magn. vol. 49 (7), pp. 3398-3401, 2013.
13. Md. Abdul Matin, Hae-Woong Kwon, Jung-Goo Lee, and Ji-HunYu, IEEE Trans. Magn. vol. 50 (1), p. 2100504, 2014.
14. Takeshi Nishiuchi, Satoshi Hirosawa, Masaki Nakamura, Masatoshi Kakimoto, Takeshi Kawabayashi, Hideki Araki and Yasuharu Shirai, IEEE, IEEJ Trans., vol. 3, pp. 390-393, 2008.
15. D. Book, I.R Harris, A. Manaf, I. Ahmad and H. A. Davies, J. Alloy Comp., vol. 221, pp. 180-186, 1995.
16. H. W. Kwon and J. H. Yu, J. Alloys Comp., vol. 487, pp. 138-141, 2009.
17. V. A. Yartys, O. Gutfleisch, and I. R. Harris, J. Alloys Comp., vol. 253-254, pp. 134-139, 1997.
18. V. A. Yartys, O. Gutfleisch, V. V. Panasyuk and I. R. Harris, J. Alloys Comp., vol. 253-254, pp. 128-133, 1997.

Chapter Six

COERCIVITY OF HOT-PRESSED COMPACTS OF Nd-Fe-B-TYPE HDDR-TREATED MATERIAL

Abstract

The $Nd_{12.5}Fe_{80.6}B_{6.4}Ga_{0.3}Nb_{0.2}$ HDDR-treated material was compacted by hot-pressing under vacuum using different types of dies in terms of evacuation system. The coercivity variations in the compacts were studied emphasizing the effect of residual hydrogen in HDDR-treated material. The HDDR-treated material contained significant amount of residual hydrogen (approx.1500 ppm). The coercivity in the compacts was profoundly influenced by residual hydrogen and how it was desorbed on heating for hot-pressing. Coercivity was radically reduced around 650 °C or above in the compacts where residual hydrogen is not desorbed effectively on hot-pressing. In spite of identical hot-pressing temperature and heating rate, coercivity reduction was inconsiderable in the compacts prepared with effective evacuation system. The coercivity in the full dense compact prepared in the open die was 10.8 kOe. The value was only 3.8 kOe in the full dense compacts prepared in closed-type die. This fact was due largely to the different desorption behavior of residual hydrogen in the HDDR-treated material in the course of heating for hot-pressing.

Keywords:

HDDR, hot-pressing, residual hydrogen, disproportionation, **c**oercivity.

6.1 Introduction

The permanent magnet research communities are now pursuing high coercievity bulk magnet by consolidating the hydrogenation, disproportionation, desorption and recombination (HDDR)-treated material. It has been generally accepted that one of the potential requirements for achieving high coercivity in Nd-Fe-B-type magnet is having a fine $Nd_2Fe_{14}B$ grain structure [1-4]. The HDDR-treated material is usually in powder form, and it would be desirable if the material can be consolidated into a high density bulk magnet keeping the fine grain structure. Previous reports revealed that HDDR-treated material was consolidated into high density bulk magnet by approaching rapid hot-pressing technique [5-8]. An attempt was also made to consolidate the Nd-Fe-B-type HDDR-treated material in our laboratory by hot-pressing. It was found that coercivity of the HDDR-treated material was radically reduced around 650 °C or above on thermal processing of the HDDR-treated material [9, 10]. The coercivity reduction was more profound in HDDR-treated material where evacuation system is not worked effectively on heating for hot-pressing. It was also witnessed that coercivity reduction was inconsiderable and gradual for the case of effective evacuation system of heating chamber. HDDR-treated material contained significant amount of residual hydrogen (1500 ppm) in the form of $Nd_2Fe_{14}BH_x$ hydride. This $Nd_2Fe_{14}BH_x$ hydride was disproportionated into Fe_2B, α-Fe, and NdH_x phases at an elevated temperature which caused the radical coercivity reduction on thermal processing of the material. Then, it would be expected that the HDDR-treated material may be consolidated into high density bulk magnet without losing coercivity if the residual hydrogen is desorbed effectively on heating for consolidation. In this chapter,

coercivity of the compacts prepared approaching different hot-pressing techniques are to be discussed.

6.2 Experimental Work

$Nd_{12.5}Fe_{80.6}B_{6.4}Ga_{0.3}Nb_{0.2}$ HDDR-treated material (iHc =13.5 kOe, 100-150 μm) was used as a starting material for the present study. The powder was compacted by hot-pressing (1 Ton/cm^2) in vacuum (1.2 x 10^{-5} mbar at RT) at a temperature range from 500 to 800 °C using different heating rate. The hot-pressing of the HDDR-treated powder was performed using distinctively different die configurations in terms of evacuation system on heating. The dies are named closed or open-type depending on the easiness of removal desorbed hydrogen from HDDR-treated powder on heating for hot-pressing schematic shown in (Fig.3.3 and Fig.3.4. of the chapter 3). Magnetic characterization of the hot-pressed compacts prepared in different dies was undertaken by means of vibrating sample magnetometer (VSM) with a maximum field of 12 kOe. Prior to the VSM measurement, the samples were wax bonded and then magnetized in 4.5 T pulsing field. Microstructure of the compacts prepared at different dies was observed by SEM and TEM. In order to examine the residual hydrogen in the hot-pressed compacts prepared in different dies, TPA (thermopiezic analysis) equipped with vacuum gauge was performed schematic shown in (Fig.3.12 of the chapter 3). Sample was heated under vacuum in TPA chamber and the pressure change with temperature due to desorbed hydrogen was monitored by the vacuum gauge and pre-programmed computer software. X-ray diffraction (XRD) (Cu-K_α radiation) was used for studying phase evolution and the crystallographic lattice parameter change by angle shifting in the XRD patterns of the tetragonal $Nd_2Fe_{14}B$ matrix phases in the hot-pressed compacts.

6.3 Results and Discussion

The $Nd_{12.5}Fe_{80.6}B_{6.4}Ga_{0.3}Nb_{0.2}$ HDDR-treated material was compacted by hot-pressing under vacuum over the temperature range from 500 °C to 850 °C with rapid heating rate 200 °C/min in a closed-type die. The coercivity of the compacts was measured, and results were shown in Fig. 6.1. Coercivity of the compact was lower than that of the initial HDDR powder, and it decreased with increasing the hot-pressing temperature. It is worth noting that coercivity of the compact was radically reduced when the compaction was performed at the temperature above 650 °C.

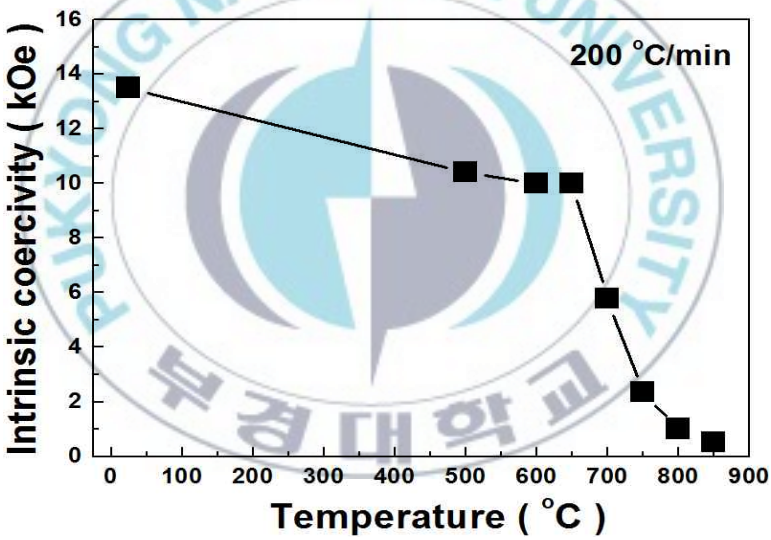

Fig. 6.1 Coercivity variation of the hot-pressed compact of $Nd_{12.5}Fe_{80.6}B_{6.4}Ga_{0.3}Nb_{0.2}$ HDDR-treated material as a function of hot-pressing temperature.

One of possible explanations for this radical coercivity reduction would be an excessive grain growth caused by the hot-pressing at higher temperature. However, this is not the case. Microstructure observation of the hot-pressed

compact showed that no significant difference in the grain size was noticed before and after hot-pressing at higher temperature as shown in Fig. 6.2.

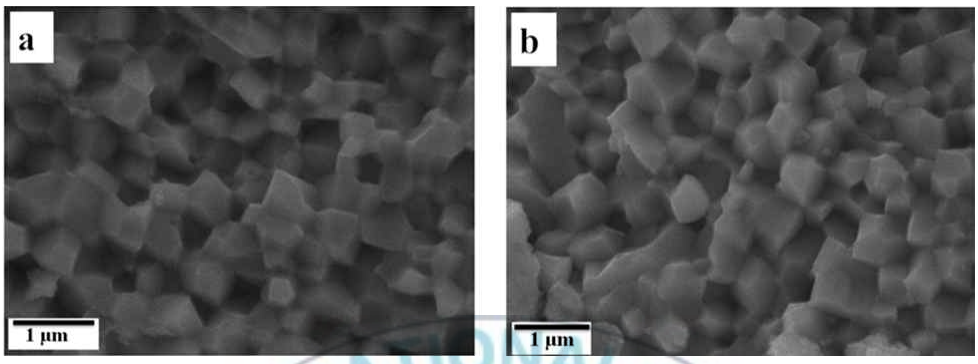

Fig. 6.2 SEM micrographs showing the grain structure of $Nd_{12.5}Fe_{80.6}B_{6.4}Ga_{0.3}Nb_{0.2}$ HDDR-treated (a) initial material, and (b) compact hot-pressed at 800 °C.

More detailed microstructural observation of the compact hot-pressed at higher temperature was carried out by TEM. Interestingly, in some local area in the compact hot-pressed at 800 °C, the α-Fe and Fe_2B phases were found as shown in Fig. 6.3. It is believed that these α-Fe and Fe_2B phases may have been formed by the disproportionation of the $Nd_2Fe_{14}BH_x$ hydride caused by the residual hydrogen in HDDR-treated material.

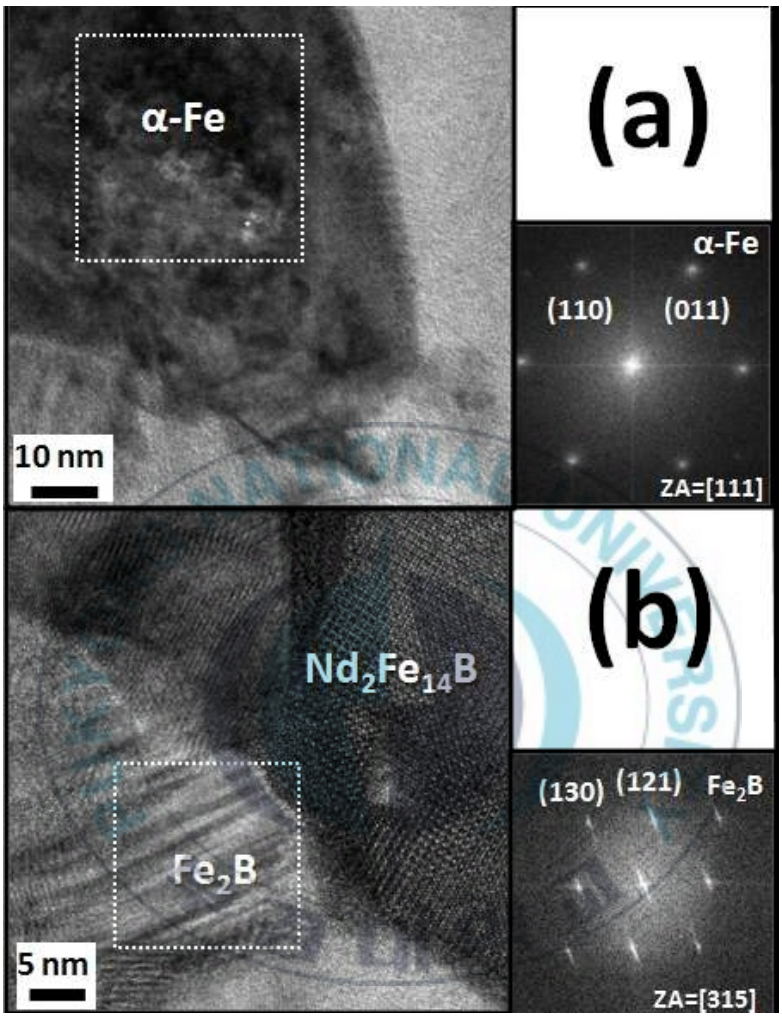

Fig. 6.3 TEM micrographs showing the presence of (a) α-Fe and (b) Fe_2B phases in the $Nd_{12.5}Fe_{80.6}B_{6.4}Ga_{0.3}Nb_{0.2}$ HDDR-treated material compacted at 800 °C.

Presence of the α-Fe and Fe_2B phases in the compact hot-pressed at higher temperature was also confirmed by XRD. Fig. 6.4 shows XRD patterns of the initial HDDR-treated material and compacts hot-pressed at 800 °C or

600 °C. Besides the $Nd_2Fe_{14}B$ major phase, Fe_2B and α-Fe phases existed along with Nd-hydride in the compact hot-pressed at 800 °C. Based upon the results of TEM observation and XRD, it is believed that the $Nd_2Fe_{14}BH_x$ hydride in the HDDR-treated material was disproportionated into Fe_2B, α-Fe, and NdH_x phases at an elevated temperature. The temperature above which coercivity started to decrease in the hot-pressed compact is the typical onset disproportionation temperature (650 °C) of $Nd_2Fe_{14}BH_x$ hydride [11-13]. It would be worth noting that there was no existence of the disproportionated Fe_2B, α-Fe, and NdH_x phases in the compact hot-pressed at 600 °C shown in XRD pattern of Fig. 6.4. This fact can be explained that radical coercivity reduction in the compacts at around or above 650 °C was almost certainly due to the disproportionation of $Nd_2Fe_{14}BH_x$ hydride in the HDDR-treated material.

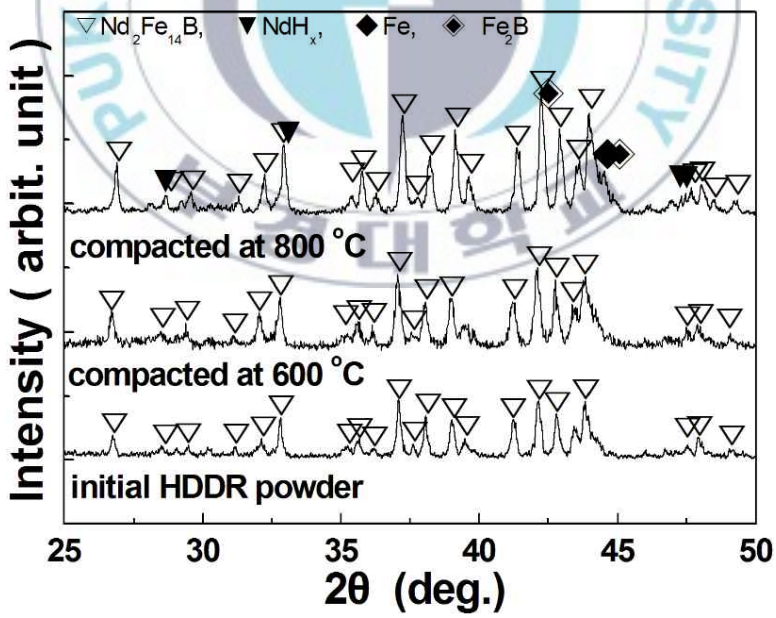

Fig. 6.4 XRD patterns of the initial $Nd_{12.5}Fe_{80.6}B_{6.4}Ga_{0.3}Nb_{0.2}$ HDDR-treated material and compacts hot-pressed at 600 °C and 800 °C.

The coercivity reduction in the compacts is believed to be largely attributed to the residual hydrogen in the HDDR-treated material. Then it would be expected that coercivity values of the compacts would be different depending on the heating rate due to vary the time allowances for desorbing the residual hydrogen in the course of heating for hot-pressing. The HDDR-treated material was hot-pressed at identical temperature 750 °C using different heating rate. The results were shown in the Fig. 6.5. The results showed that the compacts prepared with slow heating rate (40 °C /min) maintained better coercivity compared to the compacts prepared with high heating rate (200 °C /min). The fact can be explained that time allowance was much to be desorbed the residual hydrogen with slow heating rate than high heating rate in the course of heating for hot-pressing. Previous report revealed that HDDR-treated material was hot-pressed successfully without losing the coercivity with employing an extremely high heating rate (~750 °C/min) [8].

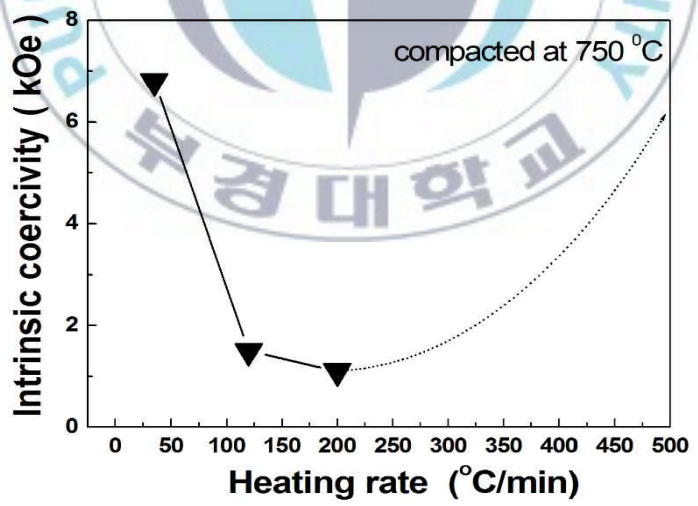

Fig. 6.5 Coercivity variations of $Nd_{12.5}Fe_{80.6}B_{6.4}Ga_{0.3}Nb_{0.2}$ HDDR-treated material compacted at 750 °C as a function of heating rate.

It is quite reasonable to assume that the extremely rapid heating was employed to avoid the harm associated with the residual hydrogen-related disproportionation. The dotted line in Fig. 6.5 showed the assumption of coercivity improvement trend in the compact by using extremely high heating rate which could suppress the disproportionation-related problem.

Actually extremely high heating rate is not convenient in practical aspects; rather slow heating rate was preferable. The $Nd_{12.5}Fe_{80.6}B_{6.4}Ga_{0.3}Nb_{0.2}$ HDDR-treated material was compacted by hot-pressing under vacuum in a closed-type die at a temperature range from 500 to 800 °C with heating rate 70 °C/min. The coercivity and density of the compacts were measured. The results were shown in Fig. 6.6. The results showed that the coercivity was reduced radically above 600 °C and temperature 750 °C was at least required to have full densification of the compacts with applying load 1 Ton/cm^2.

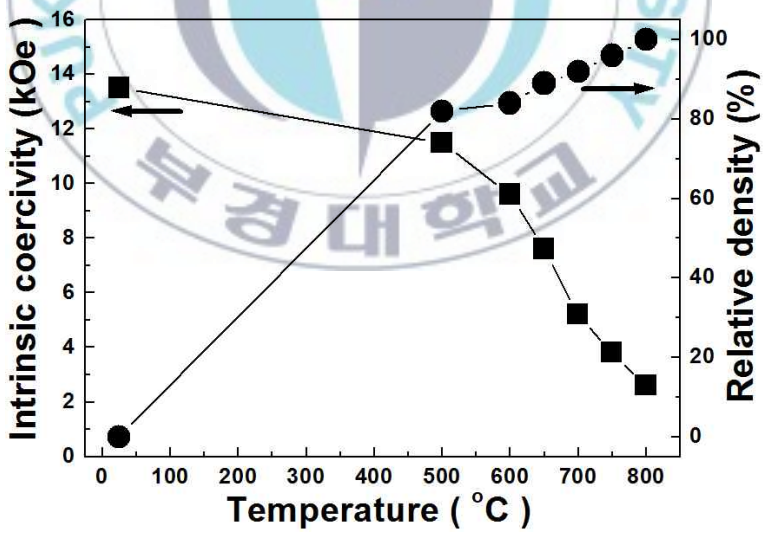

Fig. 6. 6 Variations of coercivity and relative density for the hot-pressed compact of $Nd_{12.5}Fe_{80.6}B_{6.4}Ga_{0.3}Nb_{0.2}$ HDDR-treated material prepared in closed die as a function of hot-pressing temperature.

The coercivity was radically reduced in the hot-pressed compact above 600 °C in spite of using rather slow heating rate 70 °C/min as it occurred in compacted material prepared with 200 °C /min [9]. It was witnessed that the coercivity loss in the heated HDDR-treated material was insignificant if the residual hydrogen is desorbed effectively on heating [10]. Then, it would be expected that HDDR powder could have been compacted without losing magnetic performance if the residual hydrogen is desorbed effectively in the course of heating for hot-pressing. In order to see whether the compacts show distinctive coercivity variations depending on the hot-pressing die configuration, the HDDR-treated powder was compacted by hot-pressing in the open-type effective evacuation system die.

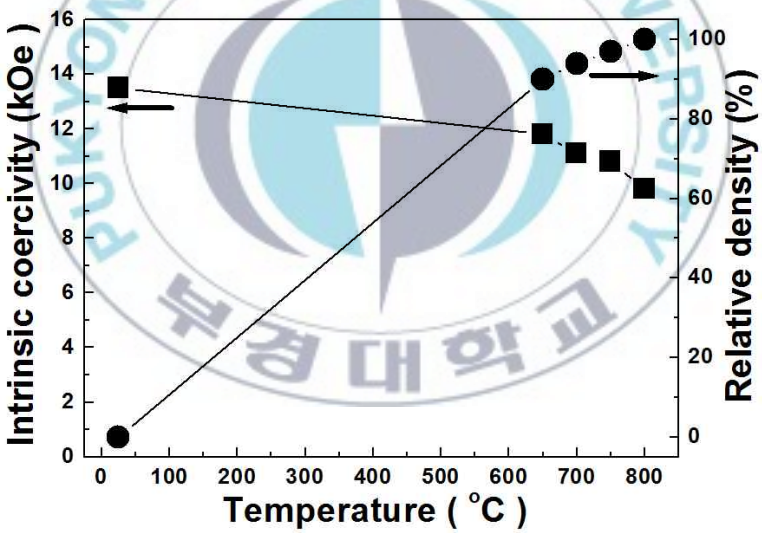

Fig. 6.7 Variations of coercivity and relative density for the hot-pressed compact of $Nd_{12.5}Fe_{80.6}B_{6.4}Ga_{0.3}Nb_{0.2}$ HDDR-treated material prepared in open die as a function of hot-pressing temperature.

Hot-pressing of HDDR-treated material was performed at a temperature range from 650 to 800 °C with heating rate 70 °C/min. The coercivity and relative density of the compacts were measured. The results were shown in Fig. 6.7. The results showed that the coercivity in the compacts prepared in the open die decreased gradually and full dense compact was achieved at 750 °C. The coercivity in the full dense compact prepared in the open die was 10.8 kOe (Fig. 6.7). The value was only 3.8 kOe (Fig. 6.6) in the compact prepared in the closed die. In spite of identical temperature and heating rate, the coercivity in the compact hot-pressed in the open die was significantly higher compared to the coercivity in the compact hot-pressed in closed-type die. The coercivity variations are believed to be attributed to the different evacuation system of hot-pressing die (Fig.3.3 and Fig.3.4 of chapter 3). This fact can be explained that residual hydrogen might be confined in a closed-type die in the course of heating for hot-pressing, hence resulting disproportionation in the HDDR-treated powder caused radical coercivity loss above 600 ℃ in the compacts. In an open die, residual hydrogen was desorbed effectively avoiding the detrimental effect of hydrogen-related disproportionation, hence retaining the significant coercivity in the hot-pressed compacts.

The coercivity variations of the compacts hot-pressed of HDDR-treated material in different dies are attributed to the distinctively different desorption behavior of residual hydrogen in the course of heating for hot-pressing. Then, it would be expected that hydrogen content may be different in the compact hot-pressed in closed and open die. Resulting hydrogen desorption of the compacts may show dissimilar patterns. The compacts hot-pressed in different die configurations were subjected for desorption tests by vacuum gauge and TPA (thermopiezic analyser). A bulk (0.5 gm) sample

was placed in a TPA small chamber. Then it was heated under vacuum and monitored the pressure change with temperature by vacuum gauge connected to the programmed computer. Desorption results were shown in Fig. 6.8. As can be seen in Fig. 6.8 that compacts hot-pressed in the closed die showed more hydrogen desorption than that of the compacts of the open die.

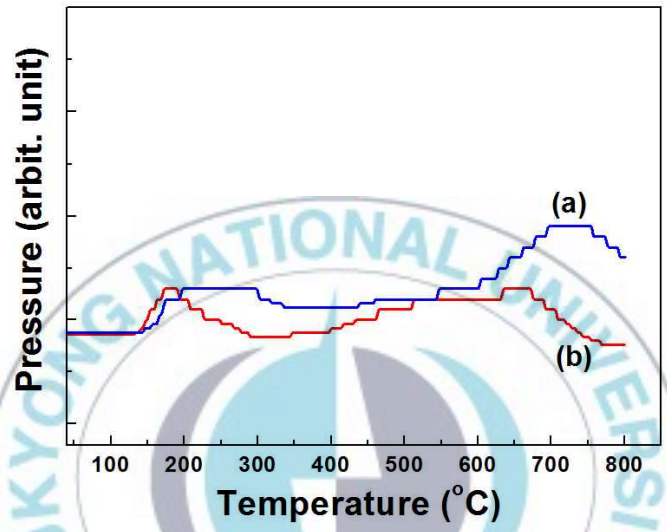

Fig. 6.8 Hydrogen desorption traces by TPA for the compacts of $Nd_{12.5}Fe_{80.6}B_{6.4}Ga_{0.3}Nb_{0.2}$ HDDR-treated powder prepared in (a) closed-type die, and (c) open-type die at 800 °C.

Residual hydrogen in the hot-pressed compacts was also verified by the lattice shrinkage studied by XRD. Fig. 6.9 shows the XRD patterns of the compacts prepared in closed and open die at 800 °C. Also included in Fig. 6.9 are the patterns of HDDR-treated initial material and the alloy before HDDR-treatment with no history of hydrogen for comparison. It was found that diffraction peaks were shifted toward higher angle as the hydrogen content decreased, indicating that the expanded lattice of the tetragonal

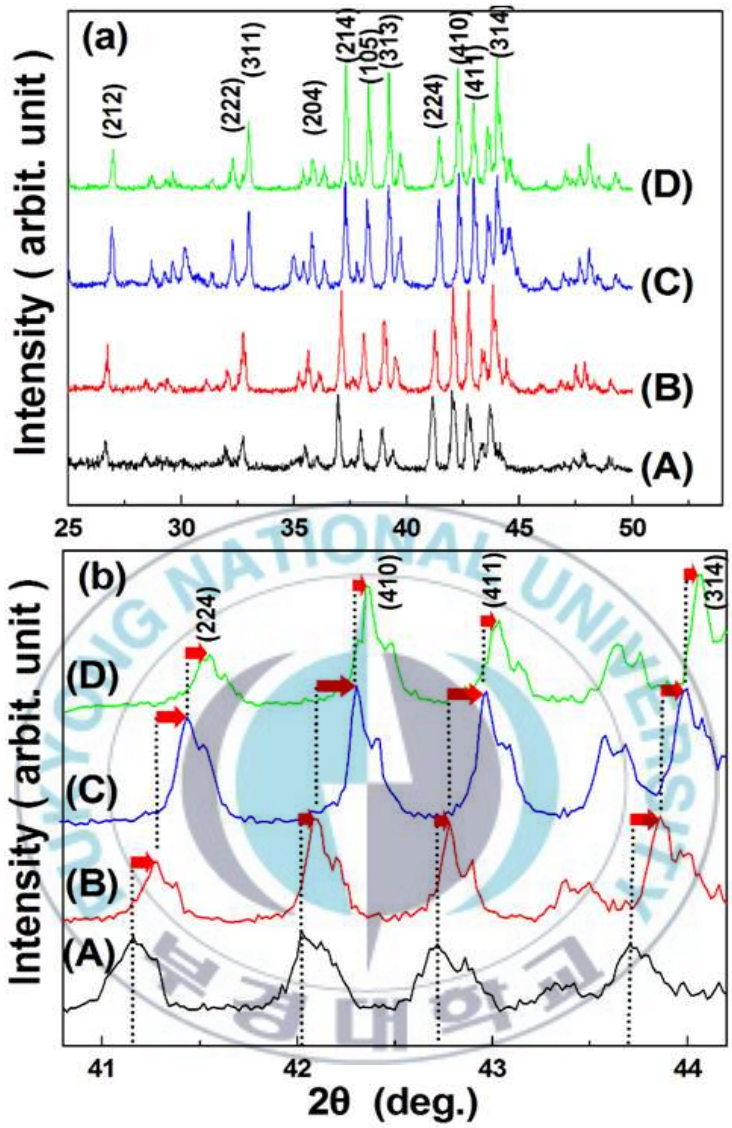

Fig. 6.9 (a) XRD patterns of $Nd_{12.5}Fe_{80.6}B_{6.4}Ga_{0.3}Nb_{0.2}$ alloy (A) after HDDR-treatment, (B) HDDR-treated material compacted at 800 °C in closed die, (C) HDDR- treated material compacted at 800 °C in open die, (D) before HDDR treatment, and (b) close-up highlighting the angle shift.

$Nd_2Fe_{14}B$-type phase in the materials was shrunk by dehydrogenation degree. It was also noticed that peaks for the compacts hot-pressed in the open die shifted more than that of the compacts hot-pressed in the closed die. It indicated that residual hydrogen was more in the compacts hot-pressed in a closed die than that of the compact in the open die. It was also witnessed by the lattice constants calculated from the corresponding XRD patterns, the values were found to decrease with increasing dehydrogenation shown in Table 6.1. It was seen that lattice parameters *a* (8.8580 Å) and *c* (12.3076 Å) of $Nd_{12.5}Fe_{80.6}B_{6.4}Ga_{0.3}Nb_{0.2}$ alloy after HDDR-treatment were significantly higher than that of the values *a* (8.8168 Å) and *c* (12.1999 Å) for the alloy before HDDR-treatment.

Table 6. 1. Lattice parameters variations of $Nd_{12.5}Fe_{80.6}B_{6.4}Ga_{0.3}Nb_{0.2}$ materials in different conditions.

MATERIALS CONDITIONS	LATTICE a	LATTICE c	UINIT CELL VOLUME v
$Nd_{12.5}Fe_{80.6}B_{6.4}Ga_{0.3}Nb_{0.2}$ HDDR-treated powder	8.8580	12.3076	965.7055
Hot-pressed compact of HDDR-treated powder prepared at 800 °C in closed die	8.8319	12.2562	956.0137
Hot-pressed compact of HDDR-treated powder prepared at 800 °C in open die	8.8181	12.2212	950.3069
$Nd_{12.5}Fe_{80.6}B_{6.4}Ga_{0.3}Nb_{0.2}$ Alloy	8.8168	12.1999	948.3710

However, lattice parameters *a* (8.8181 Å) and *c* (12.2212 Å) of the compacts prepared in open die decreased more than that of the values *a* (8.8319 Å) and *c* (12.256 Å) for the compacts hot-pressed in closed die. This fact can be

explained that lattice constant variations for the compacts hot-pressed in different dies were due largely to the effective desorption of residual hydrogen in the HDDR-treated material on heating for hot pressing. The coercivity of the compacts hot-pressed at 750 °C in the open die was 10.8 kOe which was only 3.8 kOe in the closed die. At the identical hot-pressing conditions, the radical coercivity reduction in the compacts hot-pressed in a closed die compared to the compacts in the open die was due to the different hot-pressing die configurations. The reality of this finding is closely associated with residual hydrogen which almost certainly strikes the coercivity of HDDR-treated material in the course of heating for hot-pressing.

6.4 Conclusion

The $Nd_{12.5}Fe_{80.6}B_{6.4}Ga_{0.3}Nb_{0.2}$ HDDR-treated material was compacted by using different types of dies in terms of evacuation of desorbed hydrogen on heating for hot-pressing. The coercivity in the compacts prepared in the closed-type less effective evacuation die reduced significantly around 650 °C or above compared to the compacts prepared in the open-type effective evacuation die. In spite of identical hot-pressing temperature and heating rate, the coercivity variations in the compacts prepared in different dies were due largely to the effective desorption of residual hydrogen in the HDDR-treated material in the course of heating for hot-pressing. Residual hydrogen in the HDDR-treated material is considered as a technical barrier for consolidation of the HDDR material by hot pressing without losing magnetic performance. The residual hydrogen existed in the form of $Nd_2Fe_{14}BH_x$ hydride, and it was disproportionated into α-Fe, Fe_2B and NdH_2 phases on hot-pressing in the closed-type die, hence reducing the coercivity significantly in the compacts. However, effective evacuation system from the sample area is an inevitable

prerequisite in the course of heating for hot-pressing of HDDR-treated material. The coercivity retaining rate in the compacts prepared in the open die was 80 % (10.8 kOe out of 13.5 kOe) which was only 28% (3.8 kOe out of 13.5 kOe) in the compact prepared in the closed die at 750 °C. It is almost quite certain that residual hydrogen in the HDDR-treated material should be desorbed effectively in the course of heating for hot-pressing to avoid its detrimental effect on coercivity of the compacts.

6.5 References

1. T. Takeshita and R. Nakayama, "Proceedings 10th Int. Workshop on RE Magnets and Their Applications," Kyoto, 1989, unpublished, vol. 1, p. 551.
2. P. J. McGuiness, X. J. Zhang, X. J. Yin and I. R. Harris, J. Less-Common Metals, vol. 158, p. 359, 1990.
3. T. Takeshita, J. Alloys Comp., vol. 231, p. 51, 1995.
4. W. F. Li, T. Ohkubo, K. Hono, T. Nishiuchi and S. Hirosawa, Appl. Phys. Lett., vol. 93, p. 052505, 2008.
5. O. M. Ragg, I. R. Harris, H. Nagel and P. Bohm, IEEE Trans. Magn., vol. 32 (5), p. 4395, 1996.
6. S. Liesert, A. Kirchner, W. Grunberger, A. Handstein, P. De Rango, D. Fruchart, L. Schultz and K. H. Muller, J. Alloys Comp., vol. 266, p. 260, 1998.
7. K. Morimoto, E. Niizuma, K. Igarashi, K. Mori, M. Watanabe and R. Nakayama, J. Magn. Magn. Mater., vol. 265, p. 345, 2003.
8. N. Nozawa, H. Sepehri-Amin, T. Ohkubo, K. Hono, T. Nishiuchi and S. Hirosawa, J. Magn. Magn. Mater., vol. 323, p. 115, 2011.

9. Md. Abdul Matin, Hae-Woong Kwon, Jung-Goo Lee, Ji-HunYu, Tae Hoon Kim , and Cheol-Woong Yang, IEEE Trans. Magn., vol. 49 (7), p. 3398, 2013.
10. M. A. Matin, H. W. Kwon, J. G. Lee, and J. H. Yu, IEEE Trans. Magn. vol. 50 (1), p. 2100504, 2014.
11. A. J. Williams, P. J. McGuiness and I. R. Harris, J. Less-Common Metals, vol. 171, pp. 149-155, 1991.
12. D. Book, I.R Harris, A. Manaf, I. Ahmad and H. A. Davies, J. Alloys Comp., vol. 221, p. 180, 1995.
13. H. W. Kwon and J. H. Yu, J. Alloys Comp., vol. 487, p.138, 2009.

Chapter Seven

SUMMERY

In this dissertation, the coercivity of Nd-Fe-B-type HDDR-treated material was studied on thermal processing. The work was categorized into three parts:

(i) A study of residual hydrogen in Nd-Fe-B-type HDDR-treated material,

(ii) Effect of residual hydrogen on coercivity of heated Nd-Fe-B-type HDDR-treated material, and

(iii) Coercivity of hot-pressed compacts of Nd-Fe-B-type HDDR-treated material

The first part was devoted to the investigation of residual hydrogen in the Nd-Fe-B-type HDDR-treated material by several means. The presence of hydrogen in the HDDR-treated material was verified by vacuum gauge and thermopeizic analyzer (TPA). The HDDR-treated material showed similar hydrogen desorption pattern with that of the fully hydrogenated alloy except that the amount of desorbed hydrogen was much smaller. The residual hydrogen in the HDDR material was desorbed through three steps at specific temperature around 200 °C, 300 °C, and 700 °C. Desorption at around 200 °C was corresponding to the hydrogen desorption due to the transition from $Nd_2Fe_{14}BH_x$ to $Nd_2Fe_{14}B$. The desorption events at 300 °C and 700 °C were corresponding to the hydrogen desorption due to the transition from $NdH_{2.7}$ to NdH_2, and NdH_2 to Nd, respectively. The material was also degassed by vacuum heating at different temperatures. It was found that the

residual hydrogen was degassed markedly by heating above 700 °C, but it appeared that complete removal of the residual hydrogen was impossible even after heating up to 800 °C in vacuum. The amount of the residual hydrogen in the HDDR-treated material was measured to be approximately 1500 ppm. The amount of Nd-rich phase in the studying alloy is considered to be fairly small due to the slightly over stoichiometric composition. Therefore, it is more or less reasonable to assume that most of the hydrogen in the HDDR-treated material may exist in the $Nd_2Fe_{14}B$-type magnetic phase as form of $Nd_2Fe_{14}BH_x$ hydride.

The second part was the effect of residual hydrogen on coercivity of the heated Nd-Fe-B-type HDDR-treated material without applying load. The powder was heated over the temperature range from 500 °C to 800 °C in Ar or in vacuum with a distinctively different evacuation system of the heating chamber. The coercivity was reduced significantly around 650 °C or above for the material heated in Ar atmosphere or in vacuum with slow pumping speed. The coercivity reduction was less profound and insignificant for the material heated in vacuum with high pumping speed. This fact was due largely to the residual hydrogen in the HDDR-treated material. The residual hydrogen was desorbed less effectively in the course of heating in Ar or slow pumping speed compared to the heating in vacuum with high pumping speed.

Afterwards, one of the possible reasons for the radical coercivity reduction would be an excessive grain growth caused by the heating at an elevated temperature. However, this is not the case. Microstructure observation of the heated specimens showed that no significant difference in the grain size was noticed before and after the heat treatment. It would be note worthy that the temperature at which coercivity started to decrease is the typical onset

disproportionation temperature (650 °C) of the $Nd_2Fe_{14}BH_x$ hydride. It is believed that radical coercivity reduction was largely attributed to the magnetically soft α-Fe and Fe_2B phases formed via disproportionation of $Nd_2Fe_{14}BH_x$ hydride caused by the residual hydrogen in the HDDR-treated material. The presence of disproportionated α-Fe, Fe_2B and NdH_2 phases in the material heated above 650 °C was verified by XRD. It is quite certain that residual hydrogen in the HDDR-treated material is a technical barrier on thermal processing without losing the permanent magnetic performance.

The third part was the coercivity of hot-pressed compacts of Nd-Fe-B-type HDDR-treated material. The Nd-Fe-B-type HDDR-treated material was compacted by hot-pressing under vacuum in the closed and in the open-type die. The die configurations were distinctively different in terms of evacuation system of desorbed hydrogen on heating for hot-pressing. The coercivity in the compact was radically reduced above 650 °C when the compaction was performed in the closed-type die. The coercivity reduction was inconsiderable in the compacts prepared in the open-type die. The coercivity retaining rate was 80 % (10.8 kOe out of 13.5 kOe) in the full dense compact prepared in the open die. The value was only 28 % (3.8 kOe out of 13.5 kOe) in the full dense compacts prepared in the closed-type die. The residual hydrogen could be desorbed effectively in the open-type die compared to the closed-type die. That's why compact prepared in the open die retains the appreciable coercivity avoiding the detrimental effect of hydrogen-related disproportionation in the HDDR-treated material.

Previous report revealed that HDDR-treated powder was hot-pressed successfully without losing the coercivity with employing an extremely high heating rate (~750 °C/min) and pressure (6 Ton/ cm^2). It can be assumed that extremely high heating rate and pressure was used to suppress the hydrogen-

related disproportionation in the HDDR-treated material. Our finding is that HDDR-treated material contains significant amount of residual hydrogen and this hydrogen is considered as a technical barrier for thermal processing of the HDDR-treated material. Hot-pressing technique can be approached successfully using rather slow heating rate and lower pressure than employed by other groups if residual hydrogen is desorbed effectively on heating for hot-pressing.

It can be concluded that the coercivity in the HDDR-treated material is affected profoundly by the residual hydrogen and how it is evacuated during heating for thermal processing. As discussed, our research work completed so far has provided guidance on the poor thermal stability in terms of coercivity of Nd-Fe-B-type HDDR-treated material. In this study, we only focused the residual hydrogen-related disproportionation affecting the coercivity of the HDDR-treated material on thermal processing.

APPENDIX

Publications:

1. Md. Abdul Matin , Hae-Woong Kwon , Jung-Goo Lee , Ji-Hun Yu ,Tae Hoon Kim , and Cheol-Woong Yang, "Residual Hydrogen in Nd-Fe-B HDDR Powder and Its Effect on Coercivity of Hot-Pressed Compact," IEEE Transactions on Magnetics, Vol. 49, No. 7, pp. 3398-3401, July 2013.

2. Md. Abdul Matin, Hae-Woong Kwon, Jung-Goo Lee , and Ji-Hun Yu "Origin of Poor Thermal Stability of HDDR-Treated Nd-Fe-B-Type Material," IEEE Transactions on Magnetics, Vol. 50, No.1, p. 2100504, January 2014.

Conference Proceedings:

1. Md. Abdul Matin , Hae-Woong Kwon , Jung-Goo Lee , Ji-Hun Yu ,Tae Hoon Kim , and Cheol-Woong Yang, "Magnetic properties of HDDR-treated Nd-Fe-B-type materials," 2012 년도 한국자기학회 자성 및 자성재료 국제학술대회 논문개요집, 평창, 보광휘닉스, (2012.11.29.-12.1), 86-87 (2012).

2. Md. Abdul Matin , Hae-Woong Kwon , Jung-Goo Lee , Ji-Hun Yu ,Tae Hoon Kim , and Cheol-Woong Yang, "Residual hydrogen in HDDR powder and Its effect on coercivity of hot-pressed compact," Abstract book of 12th Joint MMM–INTERMAG, Chicago. IL, USA, (January 14-18, 2013), 292 (Paper No. HX-02).

3. Md. Abdul Matin , Hae-Woong Kwon , Jung-Goo Lee , Ji-Hun Yu, "Thermal stability of HDDR-treated Nd-Fe-B-type material," 한국자기학회 2013 년도 하계 학술연구발표회 논문개요집, 안동, 리첼호텔, (2013. 5. 30-6.1), 52-53 (2013).

4. Md. Abdul Matin , Hae-Woong Kwon , Jung-Goo Lee , Ji-Hun Yu, “Thermal stability of HDDR-treated Nd-Fe-B-type material,” Proceedings of the International Symposium on Advanced Magnetic Materials and Applications (ISAMMA 2013), Taichung, Taiwan, July 21-25, 2013, p. 133.

5. Md. Abdul Matin , Hae-Woong Kwon , Jung-Goo Lee , Ji-Hun Yu, “Thermal stability of HDDR-treated Nd-Fe-B-type powder,” Abstract book of the 8th PACIFIC RIM, International Congress on Advanced Materials and Processing (PRICM8), Waikoloa, Hawaii, USA, August 4-9, 2013, p. 48.

6. Md. Abdul Matin , Hae-Woong Kwon , Jung-Goo Lee, and Ji-Hun Yu, “Coercivity of hot-pressed compacts of Nd-Fe-B-type HDDR-treated powder,” The International Symposium on Magnetism and Magnetic Materials 2013, The Korean Magnetic Society, S. Korea, (2013.12.5.-12.7), 44-45 (2013).